THE INSTABILITY OF SWIRLING FLOWS IN GAS TURBINE COMBUSTORS: THE ROLE OF RADIAL DENSITY VARIATION AND SURFACE TENSION

By

INSOO CHO

A DISSERTATION PRESENTED TO THE GRADUATE SCHOOL OF THE UNIVERSITY OF FLORIDA IN PARTIAL FULFILLMENT OF THE REQUIREMENTS FOR THE DEGREE OF DOCTOR OF PHILOSOPHY

UNIVERSITY OF FLORIDA

1996

TO my Wife and my Mother

ACKNOWLEDGMENTS

I wish to express my gratitude to Dr. Elmer C. Hansen for his guidance and counseling during the research and the preparation of this manuscript. His instruction has been a great help in broading my knowledge in physical theory. I also wish to thank Dr. U. H. Kurzweg for guiding the mathematical development to my research and providing articles related to my research. Dr. A. Green, Dr. W. Lear and Dr. J. Abbitt are acknowledged for their guidance and support and for serving on the graduate advisory committee.

I would like to acknowledge a deep debt of gratitude to Dr. Crane. He permitted me to use his Silicon Graphics Laboratory for my computational execution.

Also, I would like to express my deepest appreciation to my wife, Younghee, for her unselfish love, continuous encouragement and helpful assistance. My appreciation also goes to my mother and my father-in-law and my mother-in-law for their love, encouragement and patience. This work could not have been accomplished without their moral and emotional support.

Finally, I would like to thank National Science Foundation for grant (CTS-9500-44P) for use of a CRAY supercomputer to accomplish this research.

TABLE OF CONTENTS

LIST OF FIGURES

LIST OF SYMBOLS

(Arranged in alphabetical order)

D $\frac{d}{dr}$

D^* $D+\frac{1}{r}$

D_* $D-\frac{1}{r}$

d_* $\frac{\partial}{\partial t}+\Omega\frac{\partial}{\partial\theta}+W\frac{\partial}{\partial z}$

g gravitational constant

$I_m(\zeta)$ modified Bessel function of the first kind

$K_m(\zeta)$ modified Bessel function of the second kind

k axial wave number

m azimuthal wave number

N $kW+m\Omega-\omega$

n_j $\frac{N_j}{\Omega_j}$

P total pressure

P_0 steady - state pressure

p amplitude of $\hat{p}$

$\hat{p}$ pertubation pressure

q_j $\dfrac{\sqrt{n_j^{\,2}-4}}{n_j}$

R_j radial position

r radial coordinate in cylindrical coordinate system

t time

$\hat{u}$ radial component of perturbation velocity

u amplitude of $\hat{u}$

$\hat{v}$ tangential component of perturbation velocity

$\hat{w}$ axial component of perturbation velocity

w amplitude of $\hat{w}$

z axial coordinate of cylindrical coordinate system

T_{st} $\dfrac{\sigma}{\rho_s \Omega_s^{\,2} R_t^{\,3}}$: non-dimensional surface tension

R_1 inner radius

R_2 outer radius

Greek letters

α_{st} density ratio at interface, $\alpha = \dfrac{\rho_s}{\rho_t}$

β_{st} angular velocity ratio at interfaces, $\beta_{st} = \dfrac{\Omega_s}{\Omega_t}$

$\varepsilon = \dfrac{R_2 - R_1}{R_1}$

$\hat{\eta}$ radial perturbation displacement

η amplitude of $\hat{\eta}$

K kR

v amplitude of $\hat{v}$

θ azimuthal coordinate of cylindrical coordinate system

$\hat{\rho}$ perturbation density

ρ amplitude of $\hat{\rho}$

ρ_0 steady-state density

σ surface tension

Ω angular velocity component (steay-state)

ω complex amplication factor, $\omega = \omega_r + i\omega_i$

ζ_j $q_j kr$

Subscripts

i imaginary part

j, s, t index

r real part

Abstract of Dissertation Presented to the
Graduate School of the University of Florida in Partial Fulfillment
of the Requirements for the Degree of Doctor of Philosophy

THE INSTABILITY OF SWIRLING FLOWS IN GAS TURBINE COMBUSTORS:
THE ROLE OF RADIAL DENSITY VARIATION AND SURFACE TENSION

by

Insoo Cho

May 1996

Chairman : Dr. Elmer C. Hansen
Major Department : Mechanical Engineering

A general mathematical investigation of the instability prior to physical breakup of the annular liquid fuel flowing from the airblast nozzle using airswirlers in gas turbine combustors is presented. This investigation seeks to give a clear understanding of the growth of instabilities in an annular liquid fuel sheet. This understanding will help guide atomizer design efforts to achieve improved spray quality and emissions reductions.

The annular fuel sheet flow under consideration is assumed to be inviscid and incompressible. The mathematical formulation applied linearized theory to the Euler equation. The mathematical model derived is a single second order ordinary differential equation using modified Bessel functions of the first and second kind.

Experimental data necessary for the mathematical investigation are provided by the University of California, Irvine, Combustion Laboratory. The mathematical model is solved for the growth rate of a disturbance of helical fuel sheet using a computer code. Variable parameters are axial wave number, tangential wave number, surface tension, axial velocity, angular velocity, density and the radius at the interface in the mathematical model. The analytical solutions of axial, rotating, and helical flow annular jets were derived. When the growth rate for an axial flow annular jet was investigated, angular velocity and tangential wave number were not considered. The computer code was written in Fortran, linked to IMSL routines and executed on a CRAYC90.

The instability growth rate showed a difference between rotating flow annular jet and helical flow annular jet. The growth rate for a helical flow annular sheet is much larger at small axial wave numbers than that of the axial flow annular sheet. Also, the growth rate for the helical sheet increases with the angular wave number while the growth rate for the helical sheet increases only at very small axial wave numbers and then decreases. These results seem to be enough to explain the phenomenon of sudden fuel sheet breakup just after the nozzle tip. The effects of thickness decrease and angular velocity increase are relatively strong in comparison with other effects. They are the best candidates to be used in the design of atomizers.

CHAPTER 1
INTRODUCTION

1.1 Physical Considerations and Objectives

When liquid fuel is injected from the annular nozzle injector into a gas turbine burner section, the fuel swirls circumferentially as it proceeds downstream, in an annular sheet with air surrounding it. Figure 1 shows the location of the annular nozzle injector in the typical gas turbine engine. Figures 2 and 3 show the atomizer head cross section and atomizer head cutaway. Figure 4 shows an actual photograph of annular fuel sheet disintegration just after the nozzle tip in the experiment by McDonell and Samuelsen (1988).

Aerodynamic forces on the inside and outside of the fuel sheet produce instabilities that eventually cause breakup of the fuel sheet. Also, there are the instabilities due to different centrifugal forces of the liquid and the air. Since both the air and the fuel have high velocities in the axial direction and circumferential direction, even disturbances of very short wavelengths exist in both the axial direction and the circumferential direction. These instabilities are known as Kelvin-Helmholtz Instabilities. In addition, centrifugal instabilities occur because the liquid fuel is much denser than the air outside the fuel sheet. The outer air being much less dense moves radially inward while the denser fuel moves radially outward.

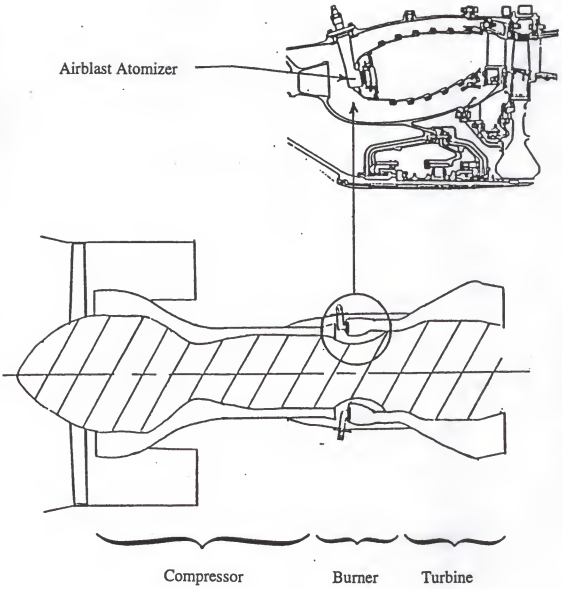

Figure 1. Typical Aircraft Gas Turbine Engine

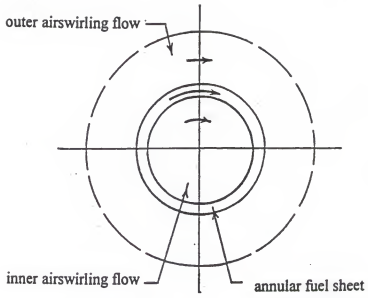

Figure 2. Atomizer Head Cross Section; Exit Plane

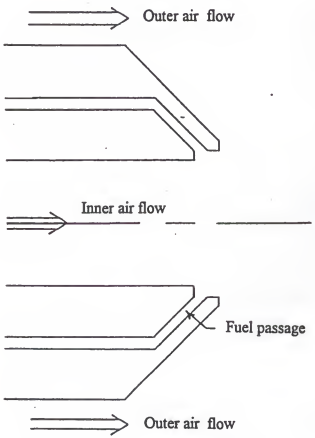

Figure 3. Atomizer Head Cutaway

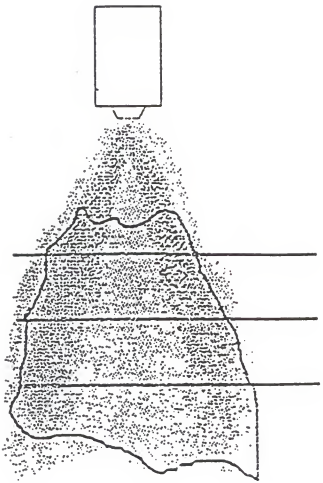

Figure 4. Schematic of spray structure in experiment at UCICL

The combination of Kelvin-Helmholtz Instability and centrifugal instability is expected to have an impact on the finely atomized liquid fuel just beyond the nozzle tip in the gas turbine combustor. Most importantly the centrifugal instability is expected to dominate the sudden breakup of the liquid jet. To validate the strong impact of centrifugal instability on the finely atomized annular liquid fuel, the mathematical formulation of the helical disturbance must be derived. The mathematical expression used to solve the problem of those instabilities actually consists of a system of nonlinear partial differential equations. The usual approach to an instability problem, assumes that for small disturbances the equations may be linearized. The terms quadratic or higher in the disturbances and their derivatives are neglected. The dispersion relationship will then be derived from the application of interfacial conditions and boundary conditions to the mathematically linearized equation.

Objectives of this research are 1) to describe the mathematical formulation which describes the growth of the instability for an annular sheet, 2) to solve the mathematical formulation using a computer code, 3) to validate the computer code by comparison to other known solutions, and 4) to study quantitatively all the effects of fuel surface tension, density, fuel sheet thickness and air swirling on the growth of instability.

1.2 Literature Review

The process of breaking up a liquid jet into droplets of diameters much smaller than the jet diameter is called jet atomization. This process has various applications,

including the liquid fuel injection in internal combustion engines and gas turbine engines. A good knowledge of the fundamental mechanism of atomization is essential for increasing combustion efficiency and reducing the formation of pollutants. Despite its practical importance, the mechanism of atomization is not yet well understood.

Advanced gas turbine engines are dependent upon the development of advanced fuel injector systems that will provide an efficient and very uniform combustion system over a wide operating range. Emissions of advanced gas turbine engines have been the subject of many studies and programs. Of particular importance are the oxides of nitrogen (NO_x) which are produced in advanced-cycle engines that operate at high pressures and temperatures.

For combustion to be effective and environmentally acceptable, the fuel must be atomized well. If good atomization is not obtained, nonuniform burning will occur. Localized hot spots at near-stoichiometric conditions cause the highest temperatures and produce the greatest amount of NO_x. Reducing the NO_x emissions by reducing the reaction temperature could adversely affect the combustion stability and could increase emissions of carbon monoxide(CO) and unburned hydrocarbons, especially at low-power operation. Therefore a means of controlling the reaction zone stoichiometry over the entire operating range is required to minimize NO_x production while maintaining good combustor efficiency. Uniform fuel injection and mixing are essential for achieving these conditions.

Soot formation is also associated with poor fuel atomization. Soot is not an equilibrium product of combustion, and therefore its formation is influenced as much by

the physical processes of atomization, evaporation, and fuel-air mixing as by reaction kinematics. Soot is generally produced anywhere that fuel-air mixing is inadequate. Problems of concern associated with soot formation are higher liner temperatures due to increased radiative heat transfer, impingement of carbon on metal surfaces resulting in erosion and reduced equipment lifetimes, and distortion of fuel spray distribution because of carbon deposits, leading to hot spots and increased NO_x formation.

The study for the atomization of liquid jet has a long history. Rayleigh(1879) first studied the phenomenon for the breakup of liquid jets into drops mathematically by treating the jet as a doubly infinite parallel flow and determining when that flow becomes unstable because of temporally growing instability waves. It was natural for the experimentalists to approach this problem by imposing controlled harmonic (usually acoustic) disturbances of a single frequency on their flows (either from within or from outside their nozzles) which then generate spatially amplifying waves that are closely related to the temporally growing instability waves of Rayleigh. Castleman (1931) did some of the early work in this area. He postulated that jet breakup is due to aerodynamic interaction between the liquid and gas phases on a moving jet. He argued that this interaction leads to the formation of ligaments or liquid columns which have one end still attached to the surface of the jet, and, once formed, these ligaments rupture according to Rayleigh's classical breakup theory. He proposed that the formation of the ligaments was due to the relative gas-liquid motion. He observed from the experimental results that the size of the ligaments, and hence their lifetimes, decreases producing smaller drops as the relative velocity is increased.

Schweitzer (1937) noted the existence of a radial component of velocity in turbulent pipe flow and argued that this radial flow could cause the disruption of the jet surface as soon as the jet emerged from the nozzle. He separated the effect of the surrounding gas in a series of experiments by injecting liquid jets into evacuated chambers. He found that jet atomization could not be achieved unless the jet was injected into a compressed gas. This led him to reason that the effect of turbulence in the liquid flow is to disturb the jet-gas interface and to augment the aerodynamic jet breakup effects. He proposed that if the emerging jet were truly laminar, no immediate breakup would occur and hence liquid turbulence is essential to the jet breakup mechanism.

Holroyd (1933) used dimensional reasoning to postulate that a balance between centrifugal forces (arising from angular turbulent velocity components) and the opposing surface tension may account for the jet breakup process. Liquid supply pressure oscillations have been noted by Giffen and Muraszew (1953) to have an effect on the outcome of the jet breakup process.

Ranz (1956) analyzed the forces involved and the energy expended in the ligament model of breakup. He considered the ligament to be stretched by the action of the relative motion of the gas and liquid flows and found that the surface energy creation rate was comparable to the viscous dissipation rate and that the surface tension forces and viscous forces opposing the stretching process were approximately equal. He postulated that the ligament diameters were related to the wavelengths of unstable aerodynamically induced surface waves growing on the core of the liquid jet. He proposed that the estimates of Taylor (1940), which were derived from considerations of the growth of

infinitesimal surface waves, could be used for a quantitative analysis of the jet breakup process.

Rupe (1962) observed that high velocity laminar liquid jets could be more unstable than fully developed turbulent jets. This was contrary to previous information in the literature. He believed that this behavior was due to changes in the fully developed laminar velocity profile within the liquid jet as the jet penetrates the chamber gas. This velocity profile relaxation process occurs by a mechanism of momentum transfer between adjacent liquid layers once the constraint of the nozzle wall is removed at the nozzle exit. The kinetic energy per unit mass of the discharged liquid is dependent on the details of the initial fluid velocity profile at the nozzle exit. In pipe flow, with a parabolic velocity profile, the kinetic energy of the fluid is twice what it would be if the fluid had a uniform velocity profile and had the same average velocity. In the course of the passage of the jet into the chamber gas, the profile relaxes to a nearly flat profile. He suggested that the excess kinetic energy is redistributed and converted into potential energy within the jet. He described that this produces a radial pressure gradient, and hence radial velocities within the jet since the kinetic energy is concentrated along the core of the jet. He postulated that these radial velocity components could disrupt the jet, lead to the formation of ligaments which could then be broken up by aerodynamic forces.

Generation of ripples by wind blowing over a viscous fluid was investigated by Batchelor (1963) with linear stability analysis.

Dombrowski, N. and Johns, W. R. (1963) derived the linearized formulations of the two-dimensional planar sheet nozzle. They considered a sheet which is thinning with

time and moving in the x-direction with a constant velocity through the stationary gas. They obtained the equation of motion of the neutral axis midway between the two gas / liquid interfaces by interrelating the forces caused by gas pressure surface tension, liquid inertia and dynamic instability and disintegration of viscous planar sheets produced by spray viscosity. They described that the displacement of the liquid sheet is proportional to the exponential growth with time. In their analysis, the disturbance of wave amplitude is higher in inviscid sheet than in viscous sheet. They described that the growth of disturbance is increased and then decreased as wave number is increased and the growth rate of disturbance is increased as the thickness of sheet is decreased. They derived the relation between sheet thickness and the diameter of the ligament which is formed when disintegration occurs through aerodynamic wave motion. They described that waves grow on the sheet until they reach a critical amplitude. He suggested that tears occur in the crests and troughs, and fragments of sheet, corresponding to one-half wavelength, are broken off. They also described that the fragments contract by surface tension into unstable ligaments which subsequently break down into drops.

Shkadov (1970) investigated the effect of changes in the interface tangential stresses in a stability analysis. He considered the planar problem and described the liquid flow by the Boundary Layer Equations, with a prescribed tangential stress at the interface such that a self similar problem could be obtained. He then employed the numerical solution to the Boundary Layer Equation in an inviscid Orr-Sommerfeld equation incorporating the effect of surface tension, and a stability analysis was performed. For the case of constant shear stress, his analysis revealed the existence of unstable short

wavelength surface waves; i.e., according to this theory the abrupt change of boundary conditions at the nozzle exit would indeed be responsible for the atomization of the jet.

Hanratty, T. J. (1983) tried to solve the linear momentum equations to determine whether small amplitude wavelike disturbances at the interface will grow or decay when air flows concurrently with a thin liquid film in an enclosed channel. In this framework the gas flow is found to affect the stability of the liquid film through the imposition of pressure and shear forces at the interface. He described that the prediction of the pressure and shear stress variation along a wavy surface over which a turbulent gas is flowing then becomes the central problem in predicting the stability of the liquid film. He also described that a slight increase of the gas velocity above that required to produce two-dimensional waves causes the interface to break into a pebbled structure with a distance between crests.

The two-dimensional waves are found to be more stable on liquids of larger viscosity than water; i.e., they exist over a wider range of gas velocities. He described that for very high gas velocities wave-induced pressure variations in phase with the wave height can be so large that they overcome the stabilizing influence of surface tension. He described that under these circumstances small wavelets riding on top of the roll waves are atomized and these waves are generated because wave-induced pressure variations in the gas that are in phase with the wave slope transfer energy from the air to the liquid through velocity fluctuations normal to the interface. He described that an instability is predicted when the rate of this energy input exceeds the rate of dissipation in the liquid.

However, for very thin film, according to Hanratty, wave-induced velocity fluctuations in the liquid have much larger components in the tangential direction than in the normal direction. Consequently, the shear stress amplitude can be an important mechanism for transferring energy from the air to the liquid. The capillary ripples appear on thin liquid films at high gas velocities. For very high gas velocities for all film flow rates, the destabilizing influence of wave-induced pressure variations is found to be greater than the stabilizing influence of gravity and surface tension; very rapid wave growth is found to occur.

Sattelmayer, T. and Wittig, S. (1986) showed through their experiment for the airblast film disintegration that the film disintegration becomes more uniform with increasing air velocity or with reduced viscosity and surface tension. They described that the disintegration of the liquid film always takes place close to the atomizing edge, regardless of the liquid properties. They described that small liquid ligaments are formed in the main flow direction while string-like structures are observed only at very high viscosities and low air velocities. At high liquid viscosity, the air is found to be unable to atomize the liquid immediately after separation due to the high damping capacity. Ligaments, therefore, are formed which can be observed. At high air velocities, the liquid disintegration is found to take place in a very small zone near the atomizing edge. Immediately after separating from the atomizing edge, the liquid is forced to move with a strong component normal to the main flow direction of the air. Subsequently, the liquid is deflected in the opposite direction by the aerodynamic forces. The atomization of the liquid begins simultaneously.

Lin, S. P. and Kang, D. J. (1987) investigated the stability of an axisymmetric liquid jet issued into an ambient gas with respect to spatially growing disturbances. They assumed that the liquid is an incompressible Newtonian fluid and the gas is assumed to be an incompressible inviscid fluid. After the corresponding linearized boundary conditions are applied, they obtained normal mode solutions which contain the modified Bessel functions. From their mathematical approach, Lin and Kang showed that the onset of atomization is due to the pressure fluctuation which causes the resonant oscillation of capillary waves at the liquid-gas interface. The initial disturbance amplitude at the nozzle exit must be larger than a threshold amplitude for the atomization to take place immediately at the nozzle exit. Otherwise, atomization may also be caused by shear waves, which tend to produce droplets of a size several orders larger than the capillary length.

Reitz (1987) first extended the stability analysis of the atomization of fuel jet injected from fuel injector in internal combustion engine. He investigated the stability of a cylindrical liquid surface to perturbations using a first order linear theory. He imposed an infinitesimal axisymmetric displacement on the liquid surface and ultimately derived a dispersion equation from the linearized hydrodynamical equations for the liquid and gas.

This equation relates the growth rate of an initial perturbation of infinitesimal amplitude to its wavelength. The relationship also includes the physical and dynamical parameters of the liquid jet and the surrounding gas and modified Bessel functions. He predicted that the presence of finely atomized drops is seen at the spray edge near the nozzle in high- pressure sprays and a short intact(unbroken) region of the jet is still seen

close to the nozzle exit in high pressure sprays. Later, the investigation for jet atomization in case that both the gas phase and the liquid phase velocities are non-zero had been done.

Chuech, S. G. and Singhal, A. K. (1991) proposed the numerical model for primary atomization. They formulated for the one-dimensional mean flow equations for axisymmetric jets. They assumed that the gas phase flowfield is in a uniform or constant-velocity profile and the liquid phase flowfield in another uniform or constant velocity profile. They called different velocities in different layers as step-varying velocity profile. They derived the surface-wave dispersion equations with two types of wave-models, namely linear and approximate nonlinear models. From the calculation with the liquid surface and jet equations, they concluded that for low speed jets, only the large waves grow and drops are formed at the tail of the jet; and for high speed jets, small waves grow at the liquid gas interface and provide continuous liquid stripping. They also commented that the wave-dispersion equation is based on the linear small perturbation theory and cannot predict jet breakup due to larger (e.g., turbulence generated) perturbations. Further study of liquid breakup criteria is needed.

Lefebvre, A. H. (1992) experimented with jet atomization for two-dimensional gas phase flow. He assumed that the liquid phase flow field is one-dimensional, and, the atomizing air impinges on the liquid sheet at small angle. This method of air impaction prevents the wavy-sheet formation that in classical theories of liquid sheet disintegration is generally regarded as an essential first step in the atomization process. Before any waves have time to develop, the liquid sheet emerging from the nozzle is completely

disrupted by the atomizing air. The changes in the angle at which the atomizing air impacts the liquid sheet would be expected to affect the efficiency of the atomization process.

Samuelsen, G. S. and Stapper, B. E. (1992) experimented with the breakup of a two-dimensional liquid sheet in the presence of co-flow air with emphasis on the extent to which liquid properties affect breakup. The liquid (lower surface tension compared to water) displays smaller scale structures on the sheet, and a greater tendency to breakup into droplets rather than form streamwise ligaments. On the other hand, the liquid (higher viscosity than water) stretches farther before breakup, which results in the streamwise ligaments reaching smaller diameters. The breakup time of the sheet is dependent on liquid properties and relative velocity of the liquid and air. The liquid (lower surface tension and density) demonstrates decreased breakup time, while the liquid (higher viscosity and density) exhibits increased breakup time relative to water.

However, the physical breakup of fuel in gas turbine combustors actually occurs three-dimensionally. The pressure atomizer and airblast atomizer have predominantly been used to atomize the liquid fuel in gas turbine engines.

The superior combustion and reduced emissions of the airblast fuel injector relative to the conventional pressure atomizer is well established by Lefebvre (1972). Unlike pressure atomizers that are also used quite extensively, airblast nozzles feature a significant control range as a result of the decoupling of atomization quality and the fuel mass flow. In addition, it is easier to control the spatial distribution of droplets. This superior performance has led to the widespread adoption of the airblast fuel injector in

modern high-pressure ratio gas turbine engines. The airblast fuel injector produces a finer spray because of the thorough mixing of the fuel and air. This yields a flame of low luminosity and soot, thus resulting in relatively cooler liner walls, a minimum of exhaust smoke, and lower NO_x emissions. Furthermore, the placement of the fuel droplets in the burning zone is mainly dictated by the airflow pattern being almost insensitive to fuel flow variations. Thus airblast fuel injectors exhibit lower pattern factors and therefore offer an important practical advantage in terms of turbine nozzle guide vane durability.

Increasing use is being made of airblast atomizers in stationary combustion processes and for fuel preparation, particularly in gas turbine combustion chambers. An almost ideal combination results in cases where the atomization performance can be matched to the required operating parameters. These are mainly the mass flow provided for the combustion at a given load point and the pressure loss in the primary air needed to stabilize the flame. For this, it is advantageous to swirl the primary air used for flame stabilization before atomization of the fuel.

Aigner, M. and Wittig, S. (1987) experimented with the atomization of the liquid film exposed to the surrounding air coming out from the inner airswirler and the outer airswirler in gas turbine combustor. They observed that the velocity profiles of the atomization air and the properties of the liquid are the dominant parameters that determine the drop-size distribution generated at the atomizer edge. They also observed that the shear flow at the nozzle exit depends largely on the swirl and counterswirl of the exiting air and the swirl naturally has a considerable effect on the flow field and the droplet path downstream from the nozzle. As explained above, the sizes of the droplets

produced are not only inversely proportional to the air velocity but the breakdown is also strongly affected by the flow profile of the atomization air at the atomization edge. An increase in the swirl velocity produces a clear reduction in axial velocity.

At the same time, the pressure loss across the nozzle increases. With an identical pressure loss, however, a finer atomization would have been attainable only by utilizing counterswirl because the high additional turbulence intensity is generated in the shear zone downstream of the atomization edge. The volumetric flow and the viscosity of the liquid do not show a direct effect on the droplet size produced at the atomization edge. With a proper selection of swirl elements, and particularly with counterswirl, the shear stresses effective on the atomization edge can increase, resulting in a finer atomization. Particularly the size of the largest droplet classes is reduced. In all cases, the amount of air required by the atomizer to produce a constant quality of atomization is significantly reduced employing swirl. Swirling the atomization air in order to stabilize the flame can be achieved without reducing the atomization efficiency. Flow stall at the atomization edge should be avoided by reducing the swirl angle.

McDonell, V. G. and Samuelson, S. (1990) utilized a two-component phase Doppler interferometry to investigate the two-phase flow produced by a gas turbine air-blast atomizer. The atomizer is operated at an air-to-fuel ratio of 1.0, with a fuel mass flow of 0.00203 kg/s. Methanol was employed as liquid fuel at ambient condition. For the relatively low-pressure drops of the present study, the air flow is approximately incompressible. The fuel is injected through a swirl chamber to form a sheet that is immediately exposed to air on both sides. The outer air flows through a swirler, while the

inner air passes through a number of tangential slots to the central passage. The helical vanes of 55 degrees for swirling are used to atomize the liquid fuel and form the recirculation zone. The complete breakup of the annular fuel sheet into drops had occurred at the atomization edge.

Rizk, N. K. and Mongia, H. C. (1991) used data from McDonell, V. G. and Samuelson, S. (1990) to verify the performance of a numerical model for the initial atomization in a gas turbine combustor. That model was applied to an airblast atomizer that incorporated a short prefilming device and was formulated to include the numerical simulation of the airflow through and exiting from the atomizer passages, fuel filming and breakup. According to Rizk and Mongia, the fundamental processes of the fuel atomization include liquid formation into a sheet, its subsequent disintegration into ligaments and drops. The prefilmer geometry, fuel and air properties, and operating parameters are the main factors controlling the film thickness. The breakup of the liquid sheet into ligaments and drops involves the instability of the liquid stream and its tendency to form waves as the result of the interaction with the air. Being unstable, the wave amplitude rapidly increases to a critical value at which the liquid disintegrates into ligaments, which in turn break up into drops.

Rizk, N. K. (1977) shows that, with an increase in air velocity, the liquid sheet disintegrates earlier so that ligaments are formed nearer the lip. These ligaments tend to be thinner and shorter and disintegrate into smaller drops. The balance of forces caused by gas pressure, surface tension, liquid inertia, and viscosity controls the breakup mechanism of the sheet. It is shown that the breakup of planar liquid sheets due to the

wave growth concept occurs as the total growth of the wave, which is given by the natural logarithm of the ratio of wave amplitude to amplitude of initial disturbance.

However, there is no evidence of ligaments existing in the photograph of the spray structure by McDonell and Samuelsen (1990).

The mathematical investigation for annular layers with density variation and swirling flows has been made by a few researchers. Reshotko, E and Monnin, C. F. (1965) studied the stability of an incompressible two-fluid wheel flow to infinitesimal helical disturbances. In their analysis, Reshotko and Monnin found that as the density ratio of inner to outer fluid increases, the calculated growth rates increase and approach a limiting value as the density ratio becomes infinite and growth rates also increase with increasing axial as well as azimuthal wave number.

Fung, Y. T. (1974) investigated the instability growth rate for three regions of fluids with the cylindrical interfaces in a constant angular and axial velocity field and step type density distribution. He derived the dispersion equations by asymptotic form of Bessel functions by matching the kinematic and dynamic boundary conditions at both the interfaces. He observed that the growth rate increases when the density in middle region is larger than those in other regions and those in other regions are the same.

Fung, Y. T. and Kurzweg, U. H. (1975) investigated the inviscid instability of heterogeneous swirling flows with radial-dependent density and obtained the secular relations for the instability growth rates for several different flow configurations. They observed that very stable flows occur when the angular and axial velocity components

have no radial variation and simultaneously the density increases with radius as is the case in a typical centrifuge.

Fung, Y. T. (1983) also derived the mathematical formulation for rotating flow for three annular layers with density variation. Only azimuthal modes are considered. Angular velocity in a layer is not same as that in another layer.

Meyer, J. and Weihs, D. (1987) investigated the capillary instability of an annular liquid sheet. In their analysis, the researchers suggested that the annular jet behaves like a two-dimensional liquid sheet. The most unstable perturbations are antisymmetric and their growth rate increases as the jet thickness decreases. Therefore, an annular liquid jet with a sufficiently small ring thickness will disintegrate into spherical shells much faster than a full liquid jet disintegrates into drops.

Lin, S. P. and Zhou, Z. W. (1992) investigated the atomization of a liquid jet emanating from a hole nozzle into the ambient gas for the application to internal combustion engines. They used the linear stability analysis. They assumed that the fluid is inviscid, incompressible with surface tension. Only axial velocity components were considered in their analysis. They showed the spatial growth of the disturbance amplitude in the flow direction when the instability occurred. They proposed that the relation between the radius of droplet a and the wavelength of disturbance λ is $\pi R^2 \lambda = 4\pi a^3 / 3$ where R is the radius of a circular cylindrical nozzle. They showed that the surface tension has an impact on damping of growth of the disturbance amplitude.

In summary, the fuel sheet moves axially and circumferentially against the surrounding gas which is moving axially and tangentially with a different speed in the gas

turbine combustor. That means that the fuel sheet moves helically just after the tip nozzle in the gas turbine combustor. To investigate the instability of the fuel sheet, both the instability of the axial flow annular jet and the instability of the rotating flow annular jet must be investigated in advance in order to investigate and understand the helical flow annular jet. To understand the physical phenomena of instabilities, the investigation of Meyer, J. and Weihs, D. (1987) is helpful for the axial flow annular jet, and the Reshotko and Monnin (1965) investigation is helpful for the rotating flow annular jet. The investigation of Kurzweg (1970) is especially helpful in understanding the physical phenomena for the helical mode of instability in swirling flow between concentric cylinders. Also, the investigation of Fung (1983) is helpful in understanding the physical phenomena for the instability of three rotating annular layers. The extension of linear instability analysis by Reitz (1987) and Lin, S. P. and Zhou, Z. W. (1992) into the application of internal combustion engine has brought the idea of the extension of linear instability analysis in gas turbine combustors.

CHAPTER 2
MATHEMATICAL FORMULATION

The front view of the fuel atomizer is shown in figure 2 and side view of the fuel atomizer is shown in figure 3. The fuel leaves the nozzle as an approximate annular sheet surrounded inside and out by air. The schematic of the spray structure in the experiment is shown in figure 4.

The fuel injection into gas turbine combustor was modelled in this dissertation as a helical disturbance of the annular liquid fuel sheet exposed to the air. The fluids are assumed incompressible and inviscid. Wheel flow is applied to the air and the liquid fuel. However, each has a different angular velocity. The axial velocities of the inner air, liquid fuel and outer air are different from one another.

The experimental data used in mathematical formulation are provided by McDonell and Samuelsen (1990) at the University of California, Irvine Combustion Laboratory. From the experimental data, the following data for investigating the instability of an annular fuel sheet are calculated:

1. axial velocity components of both the surrounding gas and fuel sheet at atomizer exit
2. swirling velocity components of both the surrounding gas and fuel sheet at atomizer exit
3. fuel sheet thickness

4. density of fuel, density of air
5. surface tension
6. inner radius and outer radius at interfaces between the annular fuel sheet and surrounding gas

To understand the behavior of the instability mechanism in swirling flows, it is necessary to consider the mathematics of the Navier-Stokes equations, the continuity equation, and incompressibility and solve these governing differential equations. The onset of instability can be determined by assuming temporal or spatial disturbances whose behavior is governed by the linearized forms of the governing nonlinear equations. It has been accepted that the method of normal modes is complete and well explains the linear wave behavior in fluid mechanics. The linearized partial differential equations under consideration are cyclic with respect to time and to two spatial variables. This strongly suggests they be solved by Laplace (time) and Fourier (space) transform methods. The differential equations after transformation are ordinary and in general complex both with respect to the temporal and spatial parameters.

The solution to the governing equations has as a complex eigen growth rate $\omega = \omega_r + i\omega_i$. Whenever ω_i is positive, instability occurs. The breakup of the annular fuel sheet is caused by the increase of growth rate (ω_i). We wish to derive the instability mechanism at the interface between the surrounding air and the annular fuel sheet exposed to the surrounding air. Both the surrounding air and the annular fuel sheet are swirling and proceeding downstream just after the nozzle. Therefore, they have the steady-state radially dependent velocity field $\vec{V}\left[0, r\Omega(r), W(r)\right]$. The fluid under

consideration is assumed inviscid, incompressible and non-heat-conducting but has a radially dependent density $\rho_0(r)$. Euler's equations of motion, the incompressibility condition and the continuity equation governing such a swirling flow in cylindrical coordinates (r, θ, z) are, respectively,

$$(\frac{\partial \vec{V}}{\partial t} + \vec{V} \cdot \nabla \vec{V}) = -\frac{1}{\rho} \nabla \vec{V} + \vec{g} \tag{2.1}$$

or

$$\frac{\partial V_r}{\partial t} + V_r \frac{\partial V_r}{\partial r} + \frac{V_\theta}{r} \frac{\partial V_r}{\partial \theta} - \frac{V_\theta^2}{r} + V_z \frac{\partial V_r}{\partial z} = -\frac{1}{\rho} \frac{\partial p}{\partial r} + g_r$$

$$\frac{\partial V_\theta}{\partial t} + V_r \frac{\partial V_\theta}{\partial r} + \frac{V_\theta}{r} \frac{\partial V_\theta}{\partial \theta} + \frac{V_r V_\theta}{r} + V_z \frac{\partial V_\theta}{\partial z} = -\frac{1}{\rho} \frac{\partial p}{\partial \theta} + g_\theta$$

$$\frac{\partial V_z}{\partial t} + V_r \frac{\partial V_z}{\partial r} + \frac{V_\theta}{r} \frac{\partial V_z}{\partial \theta} + V_z \frac{\partial V_z}{\partial z} + g_z$$

$$\frac{\partial \rho}{\partial t} + \vec{V} \cdot (\nabla \rho) = 0 \tag{2.2}$$

or $\frac{\partial \rho}{\partial t} + V_r \frac{\partial \rho}{\partial r} + \frac{V_\theta}{r} \frac{\partial \rho}{\partial \theta} + V_z \frac{\partial \rho}{\partial z} = 0$

$$\nabla \cdot \vec{V} = 0 \tag{2.3}$$

or $\frac{1}{r} \frac{\partial}{\partial r}(r V_r) + \frac{1}{r} \frac{\partial V_\theta}{\partial \theta} + \frac{\partial V_z}{\partial z} = 0$

To derive the instability of two phase flow, we postulate an initial set of solutions based on the summation of the steady-state flow and infinitesimal time-dependent fluctuations, namely,

$$V_r = \hat{u}(r,\theta,z;t)$$

$$V_\theta = r\Omega(r) + \hat{v}(r,\theta,z;t)$$

$$V_z = W(r) + \hat{w}(r,\theta,z;t) \tag{2.4}$$

$$\rho = \rho_0(r) + \hat{\rho}(r,\theta,z;t)$$

$$P = P_0(r) + \hat{p}(r,\theta,z;t)$$

Substituting equations (2.4) into equations (2.1), (2.2) and (2.3), neglecting the gravitational effects, and following the normal linearization procedure of dropping second and higher order terms in the assumed infinitesimal perturbations lead to the linearized differential equations

$$\frac{\partial \hat{u}}{\partial r} + \frac{\hat{u}}{r} + \frac{1}{r}\frac{\partial \hat{v}}{\partial \theta} + \frac{\partial \hat{w}}{\partial z} = 0 \tag{2.5a}$$

$$d_*\hat{\rho} + (D\rho_0)\hat{u} = 0 \tag{2.5b}$$

$$\frac{\partial \hat{p}}{\partial r} + \rho_0(d_*\hat{u} - 2\Omega\hat{v}) - \hat{\rho}r\Omega^2 = 0 \tag{2.5c}$$

$$\frac{\partial \hat{p}}{\partial \theta} + r\rho_0\left[d_*\hat{v} + D^*(r\Omega)\hat{u}\right] = 0 \tag{2.5d}$$

$$\frac{\partial \tilde{p}}{\partial z} + \rho_0 \left[d_* \hat{w} + (DW)\hat{u} \right] = 0 \qquad (2.5e)$$

where

$$D = \frac{d}{dr}, D^* = D + \frac{1}{r} \quad \text{and} \quad d_* = \frac{\partial}{\partial t} + \Omega \frac{\partial}{\partial \theta} + W \frac{\partial}{\partial z}$$

To reduce the number of perturbation variables, it is desirable to eliminate $\hat{v}, \hat{w}$ and $\hat{\rho}$ because $\hat{u}$ and $\hat{p}$ are primarily related to boundary conditions and interfacial conditions.

To eliminate $\hat{v}, \hat{w}$ and $\hat{\rho}$ from eq. (2.5a) to (2.5e), we convert eq. (2.5c) into the terms including d_* , then we obtain

$$d_* \frac{\partial \tilde{p}}{\partial r} + d_* \left[\rho_0 (d_* \hat{u} - 2\Omega \hat{v}) \right] - d_* (\hat{\rho} r \Omega^2) = 0$$

or

$$d_* \frac{\partial \tilde{p}}{\partial r} + \rho_0 d_*^2 \hat{u} - 2\rho_0 \Omega d_* \hat{v} - r\Omega^2 d_* \hat{\rho} = 0 . \qquad (2.5c.1)$$

We multiply $\frac{2\Omega}{r}$ into eq. (2.5d), then we obtain

$$\frac{2\Omega}{r}\frac{\partial \hat{p}}{\partial \theta} + 2\Omega\rho_0[d_*\hat{v}] + \rho_0[4\Omega^2 + 2\Omega r\frac{d\Omega}{dr}]\hat{u} = 0. \qquad (2.5d.1)$$

From eq. (2.5b), $d_*\hat{\rho} = -(D\rho_0)\hat{u}$ is derived and this equation is substituted into (2.5c.1) and we obtain

$d_*\frac{\partial \hat{p}}{\partial r} + \rho_0 d_*^2\hat{u} - 2\rho\Omega d_*\hat{v} + r\Omega^2(D\rho_0)\hat{u} = 0$. Once this equation is added into (2.5d.1), we obtain

$$d_*\frac{\partial \hat{p}}{\partial r} + \frac{2\Omega}{r}\frac{\partial \hat{p}}{\partial \theta} + \rho_0 d_*^2\hat{u} + \Phi\hat{u} = 0 \qquad (2.6)$$

where $\Phi = \frac{1}{\rho_0}[r\Omega^2\frac{d\rho_0}{dr} + 4\rho_0\Omega^2 + 2\rho_0 r\Omega\frac{d\Omega}{dr}]$

We differentiate eq.(2.5d) with respect to θ and multiply $\frac{1}{r^2}$, then obtain

$$\frac{1}{r^2}\frac{\partial^2 p}{\partial \theta^2} + \rho_0\left[d_*(\frac{1}{r}\frac{\partial \hat{v}}{\partial \theta}) + \frac{1}{r}D^*(r\Omega)\frac{\partial \hat{u}}{\partial \theta}\right] = 0 \qquad (2.5d.2)$$

We differentiate eq.(2.5e) with respect to z, then obtain

$$\frac{\partial^2 \hat{p}}{\partial z^2} + \rho_0[d_*\frac{\partial \hat{w}}{\partial z} + (DW)\frac{\partial \hat{u}}{\partial z}] = 0 \qquad (2.5e.1)$$

Once (2.5d.2) and (2.5e.1) are added, then we obtain

$$\frac{1}{r^2}\frac{\partial^2 p}{\partial\theta^2}+\frac{\partial^2 \hat{p}}{\partial z^2}+\rho_0[d_*(\frac{1}{r}\frac{\partial \hat{v}}{\partial\theta}+\frac{\partial \hat{w}}{\partial z})+\frac{D^*}{r}(r\Omega)\frac{\partial \hat{u}}{\partial\theta}+(DW)\frac{\partial \hat{u}}{\partial z}]=0\,. \tag{2.5f.1}$$

From eq. (2.5a), we obtain

$$\frac{1}{r}\frac{\partial \hat{v}}{\partial\theta}+\frac{\partial \hat{w}}{\partial z}=-\frac{\partial \hat{u}}{\partial r}-\frac{\hat{u}}{r} \quad \text{or} \quad -\left[\frac{1}{r}\frac{\partial}{\partial r}(r\hat{u})\right]. \tag{2.5f.2}$$

Adding eq. (2.5f.1) to eq. (2.5f.2), we obtain

$$\frac{1}{r^2}\frac{\partial^2 p}{\partial\theta^2}+\frac{\partial^2 \hat{p}}{\partial z^2}+\rho_0[-d_*\{\frac{1}{r}\frac{\partial}{\partial r}(r\hat{u})\}+\frac{D^*}{r}(r\Omega)\frac{\partial \hat{u}}{\partial\theta}+(DW)\frac{\partial \hat{u}}{\partial z}]=0 \tag{2.7}$$

The coefficients from eq. (2.5a) to eq.(2.7) depend only on the radial coordinate r, while the remaining independent variables θ, z and t enter only in the partial derivatives.

This allows one to assume that (2.5),- (2.6) and (2.7) admit solutions having an exponential behavior in z, θ and t. This assumption reduces all these partial differential equations to ordinary differential equations. Following the normal analysis indicated in Chapter 1, we apply the Laplace transform with respect to time t and the Fourier transform with respect to the spatial variables (z, θ). The transforms have the form

$$\{u,p\}(k,m,\omega;r)=\int_0^\infty\int_{-\infty}^{\infty}\int_0^{2\pi}\{\hat{u},\hat{p}\}(r,\theta,z;t)e^{i(kz+m\theta-\omega t)}d\theta dz dt \tag{2.8}$$

which is equivalent to the standard transformation of assuming

$$\{\tilde{p}, \tilde{u}\} = \{p(r), u(r)\}e^{i(kz+m\theta-\omega t)}$$

We are here considering only temporal disturbances so that the axial wave number k is real while the amplification factor $\omega = \omega_r + i\omega_i$ is complex; m represents the azimuthal wave number and takes on only integer values because of the periodicity of the solution in the θ direction. Using transform (2.8) in equations (2.6) and (2.7) leads to the two ordinary differential equations

$$NDp + \frac{2m\Omega}{r} p = i(\Phi - \rho_0 N^2)u \tag{2.9}$$

$$(k^2 + \frac{m^2}{r^2})p = i\rho_0\{[k(DW) + \frac{mD*(r\Omega)}{r}]u - N(D*u)\} \tag{2.10}$$

where

$$d_* = \frac{\partial}{\partial t} + \Omega\frac{\partial}{\partial\theta} + W\frac{\partial}{\partial z}, D = \frac{d}{dr}, \quad D_* = D + \frac{1}{r} \text{ and}$$

$$N = kW + m\Omega - \omega$$

CHAPTER 3
BOUNDARY CONDITIONS

3.1 Inlet Conditions

The boundary conditions for the airblast atomizer delivering swirling airflows on either side of an annular fuel sheet are described in this chapter. Inner and outer counter clockwise swirled airstreams atomize and distribute fuel of a thin swirling annular sheet. Since the effect of the viscosity is regarded negligible, the flow field consists of three layers as seen in figure 2. The layers have discontinuous densities and velocities since the effect of the viscosity is regarded as negligible. The inner layer air stream core includes the axis. Next is the fuel sheet layer. Beyond the fuel sheet is the outer air stream layer.

The nozzle tip imparted a radial-inflow component to the outer swirled stream by forming an angle with the axis of the nozzle. The front view of the nozzle section surrounded by the air is shown in figure 2. The side view of the atomizer head section is shown in figure 3. The effect of the certain angle with which the outer swirled stream intersects the annular fuel sheet is not considered in this dissertation. Therefore, it is assumed that the nozzle tip is parallel to the axis of the nozzle.

The mean axial velocities and circumferential velocities are calculated in accordance with the dimensions and configurations of the airblast atomizer. The data

from the experimental setup is used to calculate the axial velocities of both airstream and fuel sheet. The pressure drop for both fuel ΔP_{fuel} and inner air ΔP_{air} given from the experimental setup are used to calculate the axial velocities of both airstream and fuel sheet. From the Bernoulli equation, $\Delta P_{fuel} = \frac{1}{2}\rho_{fuel} W_{fuel}^{\ 2}$, the fuel velocity, $W_{fuel} = \sqrt{\frac{2\Delta P_{fuel}}{\rho_{fuel}}}$ is obtained. ρ_{fuel} is known. The helical vane angle of 55^0 is used to determine the fuel swirl $V_{\theta(fuel)} = W_{fuel} * \tan(55^0)$. $\Omega_{fuel} = \frac{V_{\theta(fuel)}}{r_{fuel}}$ is obtained where r_{fuel} is the radial distance from the axis to the centerline of the fuel layer.

Similarly, $V_{air(inner)} = \sqrt{\frac{2\Delta P_{air}}{\rho_{air}}}$ is obtained and used to calculate $V_{\theta(air)_{inner}}$ and $W_{air\ (inner)}$. $V_{air(inner)} = \sqrt{V^2_{\theta(inner)} + W^2_{air(inner)}}$ and $V_{\theta(air)} = W_{air} * \tan(55^0)$ due to helical vane angle of 55^0 $W_{air} = V_{air} \frac{1}{\sqrt{1+\tan(55^0)^2}}$.

$\Omega_{air} = \frac{V_{\theta(inner)}}{r_{inner}} = \frac{V_{\theta(outer)}}{r_{outer}}$, where r_{inner} and r_{outer} are the radial distances from the axis to the centerline of the inner air layer and the outer air layer, respectively. $V_{\theta(outer)}$ is obtained from $V_{\theta(outer)} = \frac{r_{outer}}{r_{inner}} V_{\theta(inner)}$. $W_{air(outer)}$ is calculated from $\frac{V_{\theta(outer)}}{\tan(55^0)}$. ρ_{air} is approximately regarded as 10 times density at atmospheric pressure in gas turbine combustor inlet. ρ_{fuel} is the standard value at room temperature.

In summary, axial velocity components ($W_{air(inner)}, W_{fuel}, W_{air(outer)}$) and angular velocity components ($\Omega_{air}, \Omega_{fuel}$) and ($\rho_{air}$, ρ_{fuel}) are now setup. The values are as follows:

$\rho_{air(inner)} = 0.0122\ g/cm^3$

$W_{air(inner)} = 1.5010E+03\ cm/s$

$\Omega_{air(inner)} = 22.8664E+03\ /s$

$\rho_{fuel} = 0.787\ g/cm^3$

$W_{fuel} = 1.4567E+03\ cm/s$

$\Omega_{fuel} = 9.5649E+03\ /s$

$\rho_{air(outer)} = 0.0122\ g/cm^3$

$W_{air(outer)} = 5.0836E+03\ cm/s$

$\Omega_{air(outer)} = 22.8664E+03\ /s$

In this study, $W_{fuel} > W_{air(outer)}$ and $W_{air(inner)}$ is only considered since the known solutions which have $W_2 > W_3$ and W_1 are available to investigate the validation of the computational results of the mathematical development. $\Omega_{air(outer)}$ is set equal to zero since the radius is much longer to the combustor wall than to the outer interface between the annular fuel sheet and the surrounding outer air and the region affected by $\Omega_{air(outer)}$ is

is negligible in comparison with the region which is not affected by $\Omega_{air(outer)}$ in combustor.

3.2 Interfacial Conditions

u, the radial perturbation velocity, is finite at both the axis and the outerwall of the combustor.

The use of non-smoothly varying profiles can be sometimes justified as an approximation to related smoothly varying ones. The analysis of the instability for discontinuous velocity and density distributions allows simple solutions to the governing differential equation in the individual regions which each possess continuous simple varying velocity and density distributions.

3.2.1 Kinetic Interfacial Condition

The fluid regions are three circular rings or regions; inner air region, annular fuel sheet region and outer air region. Consider region 1 (inner air) and region 2 (annular fuel sheet) with an interface at r = R. Integrating (2.10) from R - ε to R + ε in the adjoining subintervals of the interface at r = R and assuming that the mean value exists for all the quantities of the flow and that their derivatives should be bounded at the interface. We obtain

$$\int_{R-\varepsilon}^{R+\varepsilon} i\rho_0[k(DW)+\frac{mD^*(r\Omega)}{r}-ND^*]udr=0. \qquad (3.2.1)$$

where

$$\varepsilon=\frac{thickness\ \ of\ \ sheet}{R}$$

When eq. (3.2.1) is divided by N, we obtain

$$\int_{R-\varepsilon}^{R+\varepsilon} i\frac{\rho_0}{N}[k(DW)+\frac{mD^*(r\Omega)}{r}-ND^*]udr=0. \qquad (3.2.2)$$

When eq. (3.2.2) is divided by $i\rho_0$, we obtain

$$\int_{R-\varepsilon}^{R+\varepsilon}\frac{u}{N}[k(DW)+\frac{mD^*(r\Omega)}{r}]dr-\int_{R+\varepsilon}^{R-\varepsilon}D^*u=0.$$

Here,

$$\int_{R-\varepsilon}^{R+\varepsilon}\frac{u}{N}[\frac{2m\Omega}{r}]dr=0, \text{ and } \int_{R+\varepsilon}^{R-\varepsilon}\frac{u}{r}dr=0 \text{ are consistent.}$$

Therefore,

$$\lim_{\varepsilon\to 0}\frac{u}{N}\Big|_R\int_{R-\varepsilon}^{R+\varepsilon}[m(D\Omega)+k(Dw)]dr-\int_{R-\varepsilon}^{R+\varepsilon}(Du)dr=0 \quad \text{or}$$

$$\frac{u}{N}\Big|_R[m(\Omega_2-\Omega_1)+k(W_2-W_1)]-[u_2-u_1]=0 \qquad (3.2.3)$$

where $\frac{u}{N}\Big|_R=\frac{1}{2}(\frac{u_1}{N_1}+\frac{u_2}{N_2})$. $\frac{u}{N}\Big|_R=\frac{u_2-u_1}{N_2-N_1}$ is also derived from eq. (3.1).

Ultimately, $\frac{1}{2}(\frac{u_1}{N_1}+\frac{u_2}{N_2}) = \frac{u_2-u_1}{N_2-N_1}$ leads to $\frac{u_1}{N_1}=\frac{u_2}{N_2}$. $\frac{u_1}{N_1}=\frac{u_2}{N_2}$ is defined as $\left\langle\frac{u}{N}\right\rangle = 0$ (3.2.4)

which is a jump condition at the interface. The quantity $\left\{\frac{u}{N}\right\}$, physically interpreted as a perturbation displacement, must be nowhere discontinuous at the interface or anywhere inside domain of the flow. Condition (3.2.4) is also obtainable by the following physical argument:

Let the radial perturbation displacement be $\hat{\eta}$. The analysis of the normal mode method allows the perturbation quantities to admit solutions with periodic behavior in z, θ and t and with radially dependent amplitudes. Hence we assume

$$\hat{\eta}(r,\theta,z;t) = \eta(r)e^{i(kz+m\theta-\omega t)} \tag{3.2.5}$$

According to the chain rule

$$\frac{d\hat{\eta}}{dt}=\frac{\partial\hat{\eta}}{\partial t}+\frac{\partial\hat{\eta}}{\partial r}\frac{dr}{dt}+\frac{\partial\hat{\eta}}{\partial\theta}\frac{d\theta}{dt}+\frac{\partial\hat{\eta}}{\partial z}\frac{dz}{dt}$$

$$\frac{d\hat{\eta}}{dt}=i(-\omega+m\Omega+kW)\eta(r)e^{i(kz+m\theta-\omega t)}$$

$$\frac{d\hat{\eta}}{dt}=iN\eta(r)e^{i(kz+m\theta-\omega t)} \tag{3.2.6}$$

By definition, the total derivative of the radial perturbation displacement is equal to the radial perturbation velocity which has the form

$$\hat{u} = u(r)e^{i(kz+m\theta-\omega t)} \tag{3.2.7}$$

Equating (3.2.6) and (3.2.7), one finds,

$$\eta = \frac{u}{iN} = -i\frac{u}{N} \tag{3.2.8}$$

Equation (3.2.4) then follows from the physical argument that the normal component of the perturbation displacement must be continuous across the material fluid interface inside the flow domain.

3.2.2 Dynamic Interfacial Condition

The general dynamic interfacial condition can be derived, using the integration technique across the interfaces in the similar way used for kinematic interfacial condition. When equation (2.9) is divided by N, it can be rearranged to the form

$$Dp + \frac{2m\Omega}{Nr} = i\{D(\rho_0 r\Omega^2) + \rho_0(3\Omega^2 - N^2)\}\left(\frac{u}{N}\right) \tag{3.2.9}$$

Applying the integration technique across the interface at r = R, we obtain

$$\int_{R-\varepsilon}^{R+\varepsilon}[Dp - i\{D(\rho_0 r\Omega^2)\left(\frac{u}{N}\right)\}]dr = 0 \tag{3.2.10}$$

Rearranging eq. (3.2.10), that becomes

$\int_{R-\varepsilon}^{R+\varepsilon}(Dp)dr - i\left(\frac{u}{N}\right)\int_{R-\varepsilon}^{R+\varepsilon}\{D(\rho_0 r\Omega^2)\}dr = 0$. When integrated becomes

$$\langle p\rangle - i\left(\frac{u}{N}\right)_R \langle \rho_0 r\Omega^2\rangle = 0 \tag{3.2.11}$$

3.2.3 Surface Tension

When we consider surface tension σ_j acting at the interface j located between two rings of fluids at r = R_j. The equation of motion for the mean flow in the radial direction is

$$\frac{dP_0}{dr} - \rho_0 r\Omega^2 = -\sum_{j=1}^{3} T_j(\frac{1}{R_j})\delta(r - R_j) \tag{3.2.12}$$

where $\delta(r - R_j)$ is a Delta function, R_j is the position as well as the principal radius of curvature for the disturbed interface.

Once the flow is disturbed, the principal radii of curvature on r-θ and r-z planes are specified as

$$\frac{1}{R_{r\theta}} + \frac{1}{R_{rz}} = \frac{1}{r} - \frac{1}{r^2}\frac{\partial^2 r}{\partial\theta^2} - \frac{\partial^2 r}{\partial z^2} \tag{3.2.13}$$

and the linearized perturbation equation of motion in the radial direction yields

$$\frac{dP_0}{dr} + \frac{\partial\hat{p}}{\partial r} + \rho_0(d_*\hat{u} - 2\Omega\hat{v}) - (\rho_0 + \hat{\rho})r\Omega^2 = -\sum_{j=1}^{3} T_j(\frac{1}{R_{r\theta}} + \frac{1}{R_{rz}})\delta(r - R_j) \tag{3.2.14}$$

Subtracting (3.2.12) from (3.2.14), one finds

$$\frac{\partial\hat{p}}{\partial r} + \rho_0(d_*\hat{u} - 2\Omega\hat{v}) - \hat{\rho}r\Omega^2 = \sum_{j=1}^{3} T_j[\frac{1}{R_j} - (\frac{1}{R_{r\theta}} + \frac{1}{R_{rz}})]\delta(r - R_j) \tag{3.2.15}$$

In the absence of surface tension, equation (3.2.15) becomes identically equal to equation (2.5c). Following the normal mode analysis and assuming infinitesimal disturbances, we let

$$r = R_j + \hat{\eta} = R_j + \eta(R_j)e^{i(kz+m\theta-\omega t)} \tag{3.2.16}$$

at the interface j. Equation (3.2.13) can be linearized by the rearrangement of each term in that equation. we simplify

$\frac{1}{r} = \frac{1}{R+\hat{\eta}} \approx \frac{1}{R}$ since $R >> \hat{\eta}$. With the following expressions,

$$\begin{aligned}
\frac{\partial r}{\partial \theta} &= im\eta(R_j)e^{i(kz+m\theta-\omega t)} \\
\frac{\partial^2 r}{\partial \theta^2} &= -m^2\eta(R_j)e^{i(kz+m\theta-\omega t)} \\
\frac{\partial^2 r}{\partial z^2} &= -k^2\eta(R_j)e^{i(kz+m\theta-\omega t)}
\end{aligned} \tag{3.2.17}$$

The bracket in eq. (3.2.15) becomes

$$\frac{1}{R_j} - \left(\frac{1}{R_{r\theta}} + \frac{1}{R_{rz}}\right) = \frac{1}{R_j} - \frac{1}{R_j^2}(1 - m^2 - K_j^2)\eta(R_j)e^{i(kz+m\theta-\omega t)}. \tag{3.2.18}$$

Here $\eta R_j)e^{i(kz+m\theta-\omega t)}$ can be expressed as $-i\left(\frac{u}{N}\right)_j$. When eq. (3.2.15) is transformed into ordinary differential equation and multiplied by N, eq. (3.2.15) becomes

$$NDp + \frac{2m\Omega}{r}p = i\{(\Phi - \rho_a N^2)u - N\sum_{j=1}^{3}\frac{T_j}{R_j^2}(1 - m^2 - K_j^2)\left(\frac{u}{N}\right)_j \delta(r - R_j)\} \tag{3.2.19}$$

Dividing eq. (3.2.19) by N and applying the integration technique across the interface at $r = R$, the first term in right hand side leads to

$$\int_{R-\varepsilon}^{R+\varepsilon} i\left(\Phi - \rho_0 N^2\right)\left(\frac{u}{N}\right) dr = \int_{R-\varepsilon}^{R+\varepsilon} i\{D(\rho_0 r\Omega^2) + \rho_0(3\Omega^2 - N^2)\}\left(\frac{u}{N}\right) dr =$$

$$\int_{R-\varepsilon}^{R+\varepsilon} i\{D(\rho_0 r\Omega^2)\}\left(\frac{u}{N}\right) dr$$

since $\int_{R-\varepsilon}^{R+\varepsilon} i\{\rho_0(3\Omega^2 - N^2)\}\left(\frac{u}{N}\right) dr = 0$. Ultimately eq. (3.2.19) becomes

$$\int_{R-\varepsilon}^{R+\varepsilon} [Dp - i\{D(\rho_0 r\Omega^2) - \frac{\sigma}{R^2}(1 - m^2 - K^2)\left(\frac{u}{N}\right)_R \delta(r - R)\}] dr = 0$$

or

$$\langle p\rangle - i\left(\frac{u}{N}\right)_R \{\langle \rho_0 r\Omega^2\rangle - \frac{\sigma}{R^2}(1 - m^2 - K^2)\} = 0 \qquad (3.2.20)$$

CHAPTER 4
ANALYTICAL SOLUTIONS

In Chapter 4, dispersion relationships are derived for both Reshotko's two wheel flows and for annular swirling flows with discontinuous velocity and density profiles subject to arbitrary infinitesimal perturbations. To derive the dispersion relationship, it is first necessary to solve the system of equations consisting of eq. (2.9) and eq. (2.10) with the boundary conditions. The type of dispersion relationship is $F(\frac{\omega}{\Omega}, m, kR, \frac{N}{\Omega}) = 0$. The growth rate ω depends on m and k. The growth rate (ω_i) indicates the strength of the instability. m is the circumferential wave number around the circular interface disturbed, while k is the axial wave number around the axisymmetric interface disturbed. The schematic diagram showing surface waves on an annular sheet and a full liquid jet is shown in figure 5. When a helical disturbance occurs on the infinite cylindrical core jet, the axisymmetric disturbance wave occurs in the axial direction and the tangential waves anti-symmetrically occur in the tangential direction at the same time. Similar phenomena occurs on the annular fuel sheet when a helical disturbance occurs on the infinite annular sheet.

Consider one ring of fluid with constant density ρ_j, constant angular velocity Ω_j and constant axial velocity W_j in region j. Φ becomes $4\Omega^2$. Eq. (2.9) and (2.10) are

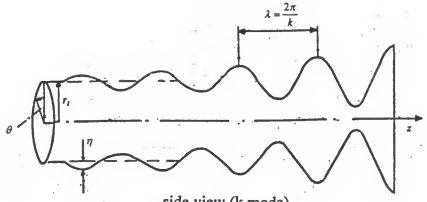

side view (k mode)

front view (m mode)

fully core jet

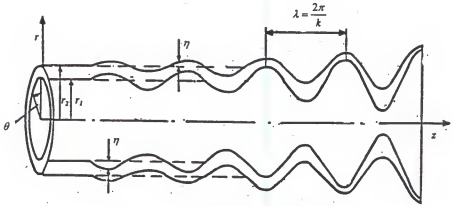

side view (k mode)

front view (m mode)
annular sheet

Figure 5. Schematic Diagram showing surface waves on an annular sheet and a fully core jet

repeatedly written as

$$NDp + \frac{2m\Omega}{r} p = i(\rho_0 \Phi - \rho_0 N^2)u \tag{4.1}$$

$$(\frac{m^2}{r^2} + k^2)p = i\rho_0[\{k(DW) + \frac{mD^*(r\Omega)}{r}\}u - N(D^*u)] \tag{4.2}$$

To eliminate all other quantities in favor of the pressure disturbance amplitude, eq. (4.1) can be reduced to

$$i\rho_j \Omega_j{}^2(4 - n_j{}^2)u = \Omega_j(n_j Dp + \frac{2m}{r} p) \quad \text{or}$$

$$i\rho_j \Omega_j(4 - n_j{}^2)u = (n_j Dp + \frac{2m}{r} p) \tag{4.3}$$

Eq. (4.2) can then be reduced to

$$(\frac{m^2}{r^2} + k^2)p = i\rho_0[\frac{2m\Omega}{r} u - N(D^*u)] \quad \text{or} \quad (\frac{m^2}{r^2} + k^2)p = i\rho_0\Omega_j[\frac{2m}{r} - n_j D^*]u \tag{4.4}$$

From (4.3), u is rearranged as

$$u = \frac{-in_j}{\rho_j \Omega_j(4 - n_j{}^2)} Dp - \frac{2mi}{r\rho_j \Omega_j(4 - n_j{}^2)} p \tag{4.5}$$

$D^*u = \frac{du}{dr} + \frac{u}{r}$ in eq. (4.4) is expressed as

$$D^*u = -\frac{i}{\rho_j \Omega_j(4 - n_j{}^2)}(\frac{2m}{r} Dp + n_j D^2 p + \frac{n_j}{r} Dp) \tag{4.6}$$

Therefore, eq. (4.4) is rearranged as

$$(k^2+\frac{m^2}{r^2})p=\frac{-n_j{}^2}{r(4-n_j{}^2)}D\ p-\frac{n_j{}^2}{(4-n_j{}^2)}D^2p+\frac{4m^2}{r^2(4-n_j{}^2)}p \text{ or}$$

$$D^2p+\frac{Dp}{r}-\{k^2(\frac{n_j{}^2-4}{n_j{}^2})+\frac{m^2}{r^2}\}p=0 \tag{4.7}$$

Here $\frac{n_j{}^2-4}{n_j{}^2}$ is defined as $q_j{}^2$. Once eq. (4.7) is multiplied by r^2, it becomes

$$r^2D^2p+rDp-(k^2q_j{}^2r^2+m^2)p=0 \tag{4.8}$$

It is called the disturbance equation.

Eq. (4.8) corresponds to modified Bessel function, where

$$p=c_1I_m(kq_jr)+c_2K_m(kq_jr) \tag{4.9}$$

where $q_j=\frac{\sqrt{n_j{}^2-4}}{n_j}$.

Alternatively, eq. (4.8) corresponds to any linear combination of Bessel functions of the first and second kind of the proper argument, ikq_jr where

$$p=eJ_m(ikq_jr)+fH_m{}^{(1)}(kq_jr) \tag{4.10}$$

where $q_j=-\frac{\sqrt{n_j{}^2-4}}{n_j}$.

Although eq. (4.10) is used less as a general solution than eq. (4.9), it was used by Reshotko (1965) for deriving the mathematical theory of two-wheel flows with different densities. Reshotko (1965)'s mathematical theory will be used in Chapter 5 to validate the numerical code. Therefore, the mathematical theory with eq. (4.10) for two-wheel

flows is derived. However, eq. (4.9) is preferably used to derive the mathematical expressions for the instability of the annular sheet exposed to the surrounding gas.

4.1 Reshotko's Solutions for Two-Wheel Flows

As shown in Figure 6, the wheel flow consisted of two immiscible and rotating fluids separated by a cylindrical interface. The flow was considered to be only azimuthal and solely a function of the radial coordinate. There is no axial velocity component and annular velocity in the inner fluid, Ω_1 is equal to the angular velocity in the outer fluid, Ω_2. And, ρ_1 in the inner core liquid is larger than ρ_2 in the outer liquid. In the inner liquid, the second term from eq. (4.10) is inadmissible so that

$$p_1 = e_1 J_m(iqkr) \tag{4.11}$$

In the outer fluid, the first term from eq. (4.10) is inadmissible so that

$$p_2 = f_2 H_m^{(1)}(iqkr) \tag{4.12}$$

e_1 and f_2 are unknowns. Two conditions are required to solve for those unknowns. The remaining conditions are that the radial displacement must be continuous at the interface and that the normal stress must be continuous at the interface. These conditions are treated consecutively. Eq. (3.2.4) for kinetic interfacial condition and eq. (3.2.11) for dynamic interfacial condition are applied to the interface between the inner core liquid and outer fluid. To the general solution for u, eq. (4.5) is used. Eq. (4.5) includes Dp and p. When the derivative term of eq. (4.10) with respect to r and eq. (4.10) are substituted into eq. (4.5), eq. (4.5) becomes

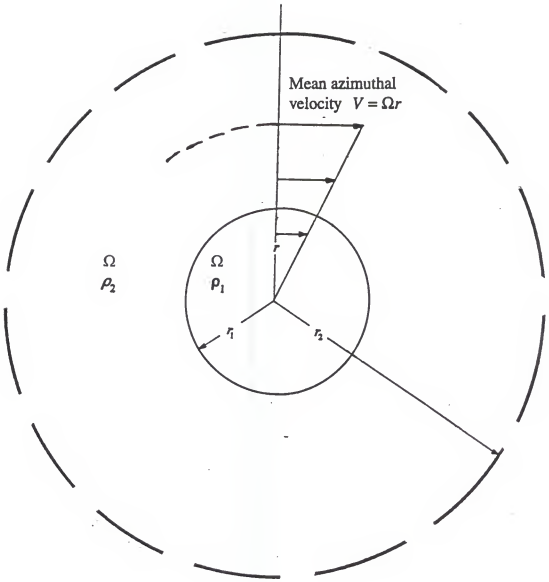

Figure 6. Geometry of two-fluid wheel flow

$$u = e\,[(\frac{\omega}{\Omega} - m)J_m{}'(iqkr) - \frac{2mR_1 J_m(iqkr)}{r}] + f\,[(\frac{\omega}{\Omega} - m)H_m{}'(iqkr) - \frac{2mR_1 H_m(iqkr)}{r}] \tag{4.13}$$

The interfacial conditions for eq. (3.2.4) and eq. (3.2.11) become

$$e_1[(\frac{\omega}{\Omega} - m)J_m{}'(iqkR_1) - 2mJ_m(iqkR_1)] - f_2[(\frac{\omega}{\Omega} - m)H_m{}'(iqkR_1) - 2mH_m(iqkR_1)] = 0 \tag{4.14}$$

and

$$\frac{i}{(\omega - m)}[e_1\{(\frac{\omega}{\Omega} - m)J_m{}'(iqkR_1) - 2mJ_m(iqkR_1)\}] + e_1 J_m(iqkR_1) - \frac{\rho_2}{\rho_1}[\, f_2\{(\frac{\omega}{\Omega} - m)H_m{}'(iqkR_1) - 2mH_m(iqkR_1)\}\,] = 0 \tag{4.15}$$

From eq. (4.14) and eq. (4.15), one dispersion relation is derived as

$$[\frac{1}{\alpha} - 1.]\{\frac{H_m{}'(iqK)}{H_m(iqK)} - \frac{2m}{(\frac{\omega}{\Omega} - m)}\}\{\frac{J_m{}'(iqK)}{J_m(iqK)} - \frac{2m}{(\frac{\omega}{\Omega} - m)}\} + \{(\frac{\omega}{\Omega} - m)^2 - 4\}[\frac{1}{\alpha}\{\frac{H_m{}'(iqK)}{H_m(iqK)} - \frac{2m}{(\frac{\omega}{\Omega} - m)}\} - \{\frac{J_m{}'(iqK)}{J_m(iqK)} - \frac{2m}{(\frac{\omega}{\Omega} - m)}\}] = 0 \tag{4.16}$$

where $\alpha = \frac{\rho_2}{\rho_1}$, $K = kR$, $q = \frac{\sqrt{(\frac{\omega}{\Omega} - m)^2 - 4}}{(\frac{\omega}{\Omega} - m)}$

R is the jet radius at the interface, J and H are general Bessel functions.

4.1.1 Axisymmetric Disturbances (m = 0)

Two dimensional disturbances are presented in r and z coordinate. The dispersion relationship from eq. (4.16) becomes

$$(\frac{1}{\alpha}-1.)\{\frac{1}{\left(\frac{\omega}{\Omega}\right)^2-4.}\}\{\frac{J_1(iqK)}{J_0(iqK)}\}\{-iKq\frac{H_1(iqK)}{H_0(iqK)}\}+\frac{1}{\alpha}\frac{H_1(iqK)}{H_0(iqK)} \tag{4.17}$$

$$-\frac{J_1(iqK)}{J_0(iqK)}=0$$

where $q=\dfrac{\sqrt{\left(\frac{\omega}{\Omega}\right)^2-4}}{\frac{\omega}{\Omega}}$.

The asymptotic form of dispersion relationship is reduced to

$$(\omega^2-4)\{1-\frac{1}{2qK}+\frac{1}{\alpha}(1+\frac{1}{2qK})\}+(\frac{1}{\alpha}-1)qK=0 \tag{4.18}$$

4.1.2 Non-axisymmetric Disturbances (m ≠ 0)

The dispersion relationship for $m\neq 0$ is eq. (4.16). There are two kinds of instabilities. One is two-dimensional disturbances in case of $K=0$. Another is three dimensional disturbances in case of $K\neq 0$. For $K=0$, two-dimensional disturbances (azimuthally periodic disturbances) are presented in r and θ coordinates. For $K\neq 0$, three dimensional disturbances (helical disturbances) are presented in r, θ and z coordinates. Although there is no axial velocity in two-wheel flows, these flows might be considered as infinite cylindrical flows for the disturbance in z coordinate.

For $K = 0$, the asymptotic form of the eq. (4.16) becomes

$$\begin{aligned}&(\frac{1}{\alpha}-1.)\{m-\frac{2m}{(\frac{\omega}{\Omega}-m)}\}\{m+\frac{2m}{(\frac{\omega}{\Omega}-m)}\}+\\&\{(\frac{\omega}{\Omega}-m)^2-4\}[\frac{1}{\alpha}\{m+\frac{2m}{(\frac{\omega}{\Omega}-m)}\}+\{m-\frac{2m}{(\frac{\omega}{\Omega}-m)}\}]=0\end{aligned} \tag{4.19}$$

For $K \neq 0$, the dispersion relationship in asymptotic form of eq. (4.16) becomes

$$\begin{aligned}&\{(\frac{\omega}{\Omega}-m)^2-4\}-[-\frac{qK}{(1+\alpha)}(1-\alpha)+\left(\frac{1-\alpha}{1+\alpha}\right)^2\{\frac{1}{2}+\frac{2m}{(\frac{\omega}{\Omega}-m)}\}\\&+\left(\frac{1-\alpha}{1+\alpha}\right)\frac{1}{qK}\{\frac{1}{4}+\frac{2m}{(\frac{\omega}{\Omega}-m)}+\frac{4m^2}{(\frac{\omega}{\Omega}-m)^2}\\&+\frac{1}{128}(32m^4-8m^2+18)\}-\frac{1}{(qK)^2}\left(\frac{1-\alpha}{1+\alpha}\right)^2\{\frac{1}{2}+\frac{2m}{(\frac{\omega}{\Omega}-m)}\}\\&\{\frac{1}{64}(32m^4-8m^2+18)+\frac{1}{4}+\frac{2m}{(\frac{\omega}{\Omega}-m)}+\frac{4m^2}{(\frac{\omega}{\Omega}-m)^2}\}]=0\end{aligned} \tag{4.20}$$

4.1.3 The Effects of Surface Tension

In Reshotko and Monnin's mathematical theory, there is no consideration of surface tension. This work extended Reshotko and Monnin's theory to include the effect of surface tension. When we consider the effects of surface tension, the dispersion relationship for m = 0 becomes

$$\frac{1}{\alpha}[\{1+T(1-K^2)\}-\alpha]\{\frac{1}{\left(\frac{\omega}{\Omega}\right)^2-4.}\}\{\frac{J_1(iqK)}{J_0(iqK)}\}\{-iKq\frac{H_1(iqK)}{H_0(iqK)}\}+\frac{1}{\alpha}\frac{H_1(iqK)}{H_0(iqK)}$$

$$-\frac{J_1(iqK)}{J_0(iqK)}=0 \tag{4.21}$$

The asymptotic forms of dispersion relationship for eq. (4.21) is reduced to

$$(\omega^2-4)\{1-\frac{1}{2qK}+\frac{1}{\alpha}(1+\frac{1}{2qK})\}+[\frac{1}{\alpha}\{1+T(1-K^2)\}-1]qK=0 \tag{4.22}$$

the general dispersion equation for m ≠ 0 becomes

$$[\frac{1}{\alpha}\{1+T(1-m^2-K^2)\}-1.]\{\frac{H_m'(iqK)}{H_m(iqK)}-\frac{2m}{(\frac{\omega}{\Omega}-m)}\}\{\frac{J_m'(iqK)}{J_m(iqK)}-\frac{2m}{(\frac{\omega}{\Omega}-m)}\}+$$
$$\{(\frac{\omega}{\Omega}-m)^2-4\}[\frac{1}{\alpha}\{\frac{H_m'(iqK)}{H_m(iqK)}-\frac{2m}{(\frac{\omega}{\Omega}-m)}\}-\{\frac{J_m'(iqK)}{J_m(iqK)}-\frac{2m}{(\frac{\omega}{\Omega}-m)}\}]=0 \tag{4.23}$$

For the asymptotic forms of dispersion relationship for $m \neq 0$ and $K = 0$ becomes

$$[\frac{1}{\alpha}\{1+T(1-m^2)\}-1.]\{m-\frac{2m}{(\frac{\omega}{\Omega}-m)}\}\{m+\frac{2m}{(\frac{\omega}{\Omega}-m)}\}+$$
$$\{(\frac{\omega}{\Omega}-m)^2-4\}[\frac{1}{\alpha}\{m+\frac{2m}{(\frac{\omega}{\Omega}-m)}\}+\{m-\frac{2m}{(\frac{\omega}{\Omega}-m)}\}]=0 \tag{4.24}$$

For the dispersion relationship for $m \neq 0$ and $K \neq 0$, the dispersion relationship in asymptotic form of eq. (4.23) becomes

$$\{(\frac{\omega}{\Omega}-m)^2-4\}-[1+\frac{T}{(1-\alpha)}(1-m^2-K^2)]-\frac{qK}{(1+\alpha)}(1-\alpha)+$$
$$\left(\frac{1-\alpha}{1+\alpha}\right)^2\{\frac{1}{2}+\frac{2m}{(\frac{\omega}{\Omega}-m)}\}+\left(\frac{1-\alpha}{1+\alpha}\right)\frac{1}{qK}\{\frac{1}{4}+\frac{2m}{(\frac{\omega}{\Omega}-m)}+\frac{4m^2}{(\frac{\omega}{\Omega}-m)^2}$$
$$+\frac{1}{128}(32m^4-8m^2+18)\}-\frac{1}{(qK)^2}\left(\frac{1-\alpha}{1+\alpha}\right)^2\{\frac{1}{2}+\frac{2m}{(\frac{\omega}{\Omega}-m)}$$
$$\{\frac{1}{64}(32m^4-8m^2+18)+\frac{1}{4}+\frac{2m}{(\frac{\omega}{\Omega}-m)}+\frac{4m^2}{(\frac{\omega}{\Omega}-m)^2}\}]=0 \qquad (4.25)$$

In Chapter 6, the special case of m = 0 will be presented.

4.2 Analytical Solutions for Annular Fuel Sheet Moving Axially and Rotating Tangentially

The modified Bessel function of eq. (4.9) is applied here. To obtain the radial disturbance amplitude u in terms of modified Bessel function, let

$c_1 = i\rho_j\Omega_j^2(4-n_j^2)Ak^{-m}$ and $c_2 = i\rho_j\Omega_j^2(4-n_j^2)Bk^m$ set. From Eq. (4.9), Dp is obtained as

$$Dp = c_1 I_m'(kq_j r) + c_2 K_m'(kq_j r) \qquad (4.26)$$

From eq. (4.5), u in terms of Dp and p is also expressed as the combination of the first and second kind of modified Bessel function. Therefore, u is expressed as

$$u = \frac{N_j}{r}Ak^{-m}\{r\frac{I_m'(kq_j r)}{I_m(kq_j r)}+\frac{2m}{n_j}\}I_m(kq_j r)+\frac{N_j}{r}Bk^m\{r\frac{K_m'(kq_j r)}{K_m(kq_j r)}+\frac{2m}{n_j}\}K_m(kq_j r) \text{ or}$$

$$u = kq_j N_j[Ak^{-m}\{\zeta_j\frac{I_m'(\zeta_j)}{I_m(\zeta_j)}+\frac{2m}{n_j}\}\frac{I_m(\zeta_j)}{\zeta_j}+Bk^m\{\zeta_j\frac{K_m'(\zeta_j)}{K_m(\zeta_j)}+\frac{2m}{n_j}\}\frac{K_m(\zeta_j)}{\zeta_j}]$$

where $\zeta_j = kq_j r$ (4.27)

The coefficients of A and B in eq. (4.27) are defined as A_0 and B_0 on the axis. Similarly, the coefficients of A and B are defined as A_1 and B_1 within inner air layer, A_2 and B_2 within fuel layer, A_3 and B_3 within the outer air layer.

u is finite at both the axis and the outerwall. When ζ_j is close to the axis, $K_m(\zeta_j)$ goes to ∞. Thus, B_1 should be 0 and A_1 will be unknown. On the other hand, $I_m(\zeta_j)$ goes to ∞ as ζ_j approaches to the outerwall. Therefore, A_3 should be 0 and B_3 will be unknown. Ultimately, there are 4 unknowns such as A_1, A_2, B_2 and B_3. To find the 4 unknowns, four equations are needed. Four equations are consisting of interfacial conditions for the displacement and pressure on the interface on both sides of annular fuel sheet. Thus, two equations are described at inner interface of fuel sheet and outer interface of fuel sheet, respectively. First, eq. (3.2.4) and eq. (3.2.11) are applied to the interface between the inner air and fuel sheet. The interfacial conditions become

$$A_1 k^{-m}\left[\frac{q_1 K_1 I_m'(q_1 K_1)}{I_m(q_1 K_1)} + \frac{2m}{n_1}\right] I_m(q_1 K_1) - A_2 k^{-m}\left[\frac{q_2 K_1 I_m'(q_2 K_1)}{I_m(q_2 K_1)} + \frac{2m}{n_2}\right] I_m(q_2 K_1) -$$
$$B_2 k^{m}\left[\frac{q_2 K_1 K_m'(q_2 K_1)}{K_m(q_2 K_1)} + \frac{2m}{n_2}\right] K_m(q_2 K_1) = 0 \qquad (4.28)$$

and

$$A_1 k^{-m}[(n_1^2-4)+\{\frac{q_1K_1I_m'(q_1K_1)}{I_m(q_1K_1)}+\frac{2m}{n_1}\}]I_m(q_1K_1)-$$

$$\alpha_{21}\beta_{21}^2A_2k^{-m}[(n_2^2-4)+\{\frac{q_2K_1I_m'(q_2K_1)}{I_m(q_2K_1)}+\frac{2m}{n_2}\}]I_m(q_2K_1)- \qquad (4.29)$$

$$\alpha_{21}\beta_{21}^2B_2k^{m}[(n_2^2-4)+\{\frac{q_2K_1K_m'(q_2K_1)}{K_m(q_2K_1)}+\frac{2m}{n_2}\}]K_m(q_2K_1)=0$$

where $K_1 = kR_1$, $\alpha_{21}=\dfrac{\rho_2}{\rho_1}$ and $\beta_{21}=\dfrac{\Omega_2}{\Omega_1}$.

When the surface tension is considered, eq. (4.29) becomes

$$A_1 k^{-m}[(n_1^2-4)+\{\frac{q_1K_1I_m'(q_1K_1)}{I_m(q_1K_1)}+\frac{2m}{n_1}\}]I_m(q_1K_1)-$$

$$\alpha_{21}\beta_{21}^2A_2k^{-m}[(n_2^2-4)+\{\frac{q_2K_1I_m'(q_2K_1)}{I_m(q_2K_1)}+\frac{2m}{n_2}\}\{1+T_{21}(1-m^2-K_1^2)\}]I_m(q_2K_1)-$$

$$\alpha_{21}\beta_{21}^2B_2k^{m}[(n_2^2-4)+\{\frac{q_2K_1K_m'(q_2K_1)}{K_m(q_2K_1)}+\frac{2m}{n_2}\}\{1+T_{21}(1-m^2-K_1^2)\}]K_m(q_2K_1)=0 \qquad (4.30)$$

where $T_{21}=\dfrac{\sigma}{\rho_2\Omega_2^2R_1^3}$.

Second, eq. (3.2.4) and eq. (3.2.11) are also applied to the interface between the outer air and fuel sheet. The interfacial conditions becomes

$$A_2k^{-m}[\frac{q_2K_2I_m'(q_2K_2)}{I_m(q_2K_2)}+\frac{2m}{n_2}]I_m(q_2K_2)+B_2k^{m}[\frac{q_2K_2K_m'(q_2K_2)}{K_m(q_2K_2)}+\frac{2m}{n_2}]K_m(q_2K_2)- \qquad (4.31)$$

$$B_3k^{m}[\frac{q_3K_2K_m'(q_3K_2)}{K_m(q_3K_2)}+\frac{2m}{n_3}]K_m(q_3K_2)=0$$

and

$$A_2 k^{-m}[(n_2^2-4)+\{\frac{q_2 K_2 I_m^{'}(q_2 K_2)}{I_m(q_2 K_2)}+\frac{2m}{n_2}\}]I_m(q_2 K_2)+$$

$$B_2 k^{m}[(n_2^2-4)+\{\frac{q_2 K_2 K_m^{'}(q_2 K_2)}{K_m(q_2 K_2)}+\frac{2m}{n_2}\}]K_m(q_2 K_2)-$$

$$\alpha_{32} B_3 k^{m}[(n_3^2-4)+\{\frac{q_3 K_2 K_m^{'}(q_3 K_2)}{K_m(q_3 K_2)}+\frac{2m}{n_3}\}]K_m(q_3 K_2)=0 \qquad (4.32)$$

where $K_2 = kR_2$

$$n_1 = \frac{N_1}{\Omega_1} = \frac{kW_1 + m\Omega_1 - \omega}{\Omega_1}$$

$$n_2 = \frac{N_2}{\Omega_2} = \frac{kW_2 + m\Omega_2 - \omega}{\Omega_2}$$

$$n_3 = \frac{N_3}{\Omega_3} = \frac{kW_3 + m\Omega_3 - \omega}{\Omega_3}$$

$$q_1 = \frac{\sqrt{n_1^2 - 4}}{n_1}$$

$$q_2 = \frac{\sqrt{n_2^2 - 4}}{n_2}$$

$$q_3 = \frac{\sqrt{n_3^2 - 4}}{n_3}$$

When the surface tension is considered, eq. (4.32) becomes

$$A_2 k^{-m}[(n_2^2-4)+\{\frac{q_2 K_2 I_m^{'}(q_2 K_2)}{I_m(q_2 K_2)}+\frac{2m}{n_2}\}\{1+T_{22}(1-m^2-K_2^2)\}]I_m(q_2 K_2)+$$

$$B_2 k^{m}[(n_2^2-4)+\{\frac{q_2 K_2 K_m^{'}(q_2 K_2)}{K_m(q_2 K_2)}+\frac{2m}{n_2}\}\{1+T_{22}(1-m^2-K_2^2)\}]K_m(q_2 K_2)- \qquad (4.33)$$

$$\alpha_{32}\beta_{32}^2 B_3 k^{m}[(n_3^2-4)+\{\frac{q_3 K_2 K_m^{'}(q_3 K_2)}{K_m(q_3 K_2)}+\frac{2m}{n_3}\}]K_m(q_3 K_2)=0$$

where $\alpha_{32} = \frac{\rho_3}{\rho_2}$, $\beta_{32} = \frac{\Omega_3}{\Omega_2}$ and $T_{22} = \frac{\sigma}{\rho_2 \Omega_2^{\ 2} R_2^{\ 3}}$.

From eq. (4.28) through eq. (4.33), there are four unknowns. The determinant should be zero to solve the equations.

$$\begin{bmatrix} I_{11} & -I_{21} & -K_{21} & \\ I_{11}^{*} & -I_{21}^{*} & -K_{21}^{*} & \\ & I_{22} & K_{22} & -K_{32} \\ & I_{22}^{*} & K_{22}^{*} & -K_{32}^{*} \end{bmatrix} \begin{bmatrix} X_1 \\ X_2 \\ X_3 \\ X_4 \end{bmatrix} = \begin{bmatrix} 0 \\ 0 \\ 0 \\ 0 \end{bmatrix} \tag{4.34}$$

where $X_1 = A_1 k^{-m}, X_2 = A_2 k^{-m}, X_3 = B_2 k^{m}, X_4 = B_3 k^{m}$ and

$$I_{11} = [\frac{q_1 K_1 I_m^{'}(q_1 K_1)}{I_m(q_1 K_1)} + \frac{2m}{n_1}] I_m(q_1 K_1)$$

$$I_{21} = [\frac{q_2 K_1 I_m^{'}(q_2 K_1)}{I_m(q_2 K_1)} + \frac{2m}{n_2}] I_m(q_2 K_1)$$

$$I_{22} = [\frac{q_2 K_2 I_m^{'}(q_2 K_2)}{I_m(q_2 K_2)} + \frac{2m}{n_2}] I_m(q_2 K_2)$$

$$K_{21} = [\frac{q_2 K_1 K_m^{'}(q_2 K_1)}{K_m(q_2 K_1)} + \frac{2m}{n_2}] K_m(q_2 K_1)$$

$$K_{22} = [\frac{q_2 K_2 K_m^{'}(q_2 K_2)}{K_m(q_2 K_2)} + \frac{2m}{n_2}] K_m(q_2 K_2)$$

$$K_{32} = [\frac{q_3 K_2 K_m^{'}(q_3 K_2)}{K_m(q_3 K_2)} + \frac{2m}{n_3}] K_m(q_3 K_2)$$

$$I_{11}^{*} = [(n_1^{\ 2} - 4) + \{\frac{q_1 K_1 I_m^{'}(q_1 K_1)}{I_m(q_1 K_1)} + \frac{2m}{n_1}\}] I_m(q_1 K_1)$$

$$I_{21}^{*} = \alpha_{21} \beta_{21}^{\ 2} [(n_2^{\ 2} - 4) + \{\frac{q_2 K_1 I_m^{'}(q_2 K_1)}{I_m(q_2 K_1)} + \frac{2m}{n_2}\}] I_m(q_2 K_1)$$

$$I_{22}^{*} = [(n_2^{\ 2} - 4) + \{\frac{q_2 K_2 I_m^{'}(q_2 K_2)}{I_m(q_2 K_2)} + \frac{2m}{n_1}\}] I_m(q_2 K_2)$$

$$K_{21}^{*} = \alpha_{21}\beta_{21}^{2}[(n_2^{2}-4)+\{\frac{q_2K_1K_m^{'}(q_2K_1)}{K_m(q_2K_1)}+\frac{2m}{n_2}\}]K_m(q_2K_1)$$

$$K_{22}^{*} = [(n_2^{2}-4)+\{\frac{q_2K_2K_m^{'}(q_2K_2)}{K_m(q_2K_2)}+\frac{2m}{n_2}\}]K_m(q_2K_2) \qquad (4.35)$$

$$K_{32}^{*} = \alpha_{32}\beta_{32}^{2}[(n_3^{2}-4)+\{\frac{q_3K_2K_m^{'}(q_3K_2)}{K_m(q_3K_2)}+\frac{2m}{n_3}\}]K_m(q_3K_2)$$

when the surface tension is considered, $I_{21}^{*}, I_{22}^{*}, K_{21}^{*}$ and K_{22}^{*} in eq. (4.35) become

$$I_{21}^{*} = \alpha_{21}\beta_{21}^{2}[(n_2^{2}-4)+\{\frac{q_2K_1I_m^{'}(q_2K_1)}{I_m(q_2K_1)}+\frac{2m}{n_2}\}\{1+T_{21}(1-m^{2}-K_1^{2})\}]I_m(q_2K_1)$$

$$I_{22}^{*} = [(n_2^{2}-4)+\{\frac{q_2K_2I_m^{'}(q_2K_2)}{I_m(q_2K_2)}+\frac{2m}{n_2}\}\{1+T_{22}(1-m^{2}-K_2^{2})\}]I_m(q_2K_2)$$

$$K_{21}^{*} = \alpha_{21}\beta_{21}^{2}[(n_2^{2}-4)+\{\frac{q_2K_1K_m^{'}(q_2K_1)}{K_m(q_2K_1)}+\frac{2m}{n_2}\}\{1+T_{21}(1-m^{2}-K_1^{2})\}]K_m(q_2K_1)$$

$$K_{22}^{*} = [(n_2^{2}-4)+\{\frac{q_2K_2K_m^{'}(q_2K_2)}{K_m(q_2K_2)}+\frac{2m}{n_2}\}\{1+T_{22}(1-m^{2}-K_2^{2})\}]K_m(q_2K_2)$$

(4.36)

where $\alpha_{21}=\left(\frac{\rho_2}{\rho_1}\right),\beta_{21}=\left(\frac{\Omega_2}{\Omega_1}\right)^{2},\alpha_{32}=\left(\frac{\rho_3}{\rho_2}\right),\beta_{32}=\left(\frac{\Omega_3}{\Omega_2}\right)^{2},T_{21}=\frac{\sigma}{\rho_2\Omega_2^{2}R_1^{3}}$ and

$T_{22}=\frac{\sigma}{\rho_2\Omega_2^{2}R_2^{3}}$

When the determinant of the coefficient matrix is set to zero, eq. (4.34) becomes

$$I_{11}K_{22}I_{21}^{*}K_{32}^{*}-I_{11}K_{32}I_{21}^{*}K_{22}^{*}-I_{11}K_{21}^{*}I_{22}K_{32}^{*}+I_{11}K_{32}I_{22}^{*}K_{21}^{*}- \\ I_{21}K_{22}I_{11}^{*}K_{32}^{*}+I_{21}K_{32}I_{11}^{*}K_{22}^{*}+I_{22}K_{21}I_{11}^{*}K_{32}^{*}-I_{11}^{*}K_{32}I_{22}^{*}K_{21}=0 \qquad (4.37)$$

Here the first derivatives of modified Bessel functions are expressed as

$$I_m'(q_jK_j) = I_{m+1}(q_jK_j) + \frac{m}{q_jK_j} I_m(q_jK_j)$$
$$K_m'(q_jK_j) = -K_{m+1}(q_jK_j) + \frac{m}{q_jK_j} K_m(q_jK_j) \qquad (4.38)$$

Eq. (4.37) is

the type of $F(\frac{\rho_1}{\rho_2}, \frac{\rho_2}{\rho_3}, \frac{\Omega_2}{\Omega_1}, \frac{\Omega_3}{\Omega_2}, q_1, q_2, q_3, n_1, n_2, n_3, K_1, K_2, m, \frac{\omega}{\Omega_2}, \frac{\omega}{\Omega_3}) = 0$ (4.39)

where ω is the only unknown parameter to be solved. Since the complex eigen amplification factor falls inside the arguments of the Bessel functions, general features of the system are difficult to see without the use of a computer. However, some important results can be obtained by using an analytical expansion for sufficiently large or small axial wave numbers. In those cases, the Bessel functions reduce to an exponential form or a power series.

Since eq. (4.34) consists of I and K of Bessel functions, I and K can be transformed into asymptotic expansions.

When ω is the conjugate, disturbances are growing or decaying according to whether ω_i is positive or negative, respectively. Since the fluids have been assumed to be inviscid, negative ω_i for damping the disturbance is not considered.

The physical phenomenon of fuel sheet breakup in gas turbine combustor is due to the instability of annular fuel sheet moving with axial and tangential velocity in the surrounding gas which has axial and tangential velocity. Helical flow annular jet includes the flow characteristics of both the axial flow annular jet and swirling flow annular jet.

Before investigating the physical phenomena of the annular fuel sheet axially moving and tangentially rotating exposed to the surrounding air axially moving and tangentially rotating, we first investigate independently two kinds of instability included in the physical phenomena of the annular fuel sheet. First kind is the instability for the annular sheet moving in axial direction in the surrounding gas moving in axial direction. Second kind is the instability for the annular sheet rotating in tangential direction in the surrounding gas rotating in tangential direction.

The degrees of these instabilities are basically influenced by the axisymmetric mode ($m = 0$ and $k \neq 0$) or many azimuthal modes ($m \neq 0$ and $k = 0$) or many helical modes ($m \neq 0$ and $k \neq 0$).

The axisymmetric mode for $m = 0$ is limited to two-dimensional disturbances in r and z coordinates. Therefore, this mode is independent of θ. But the component of perturbation velocity v is not equal to zero. The azimuthally periodic mode for $k = 0$ is limited to two-dimensional disturbances in r and θ. Therefore, this mode is independent of z. The helical disturbance mode for $m \neq 0$ and $k \neq 0$ is three-dimensional disturbances in r, θ and z. The properties of the instabilities to be investigated is as following:

Table 4.1 The special cases for which analytical solutions will be derived.

Axial flow annular jet Section 4.2.1	$m = 0$ and $k \neq 0$		
Rotating flow annular jet Section 4.2.2	$m = 0$ and $k \neq 0$ Section 4.2.2.1	$m \neq 0$ and $k = 0$ Section 4.2.2.2	$m \neq 0$ and $k \neq 0$ Section 4.2.2.3
Helical flow annular jet Section 4.2.3	$m = 0$ and $k \neq 0$ Section 4.2.3.1	$m \neq 0$ and $k = 0$ Section 4.2.3.2	$m \neq 0$ and $k \neq 0$ Section 4.2.3.3

4.2.1 The Axial Flow Annular Jet

There is no rotational velocity component in flow region. Therefore, Ω_1, Ω_2 and Ω_3 are all zeroes. Also, m, circumferential wave number is not considered. Eq. (4.35) becomes

$$I_{11} = 1$$

$$I_{21} = 1$$

$$I_{11}^{*} = K_{32} = 0$$

$$I_{21}^{*} = -1$$

$$K_{21} = \frac{K_0^{'}(K_1)}{I_0^{'}(K_1)}$$

$$K_{21}^{*} = -\frac{K_0^{'}(K_2)}{I_0^{'}(K_2)}$$

$$I_{22} = -\rho_2 N_2^{2}$$

$$I_{22}^{*} = \rho_2 N_2^{2}$$

$$K_{22} = -\rho_2 N_2^{2} \frac{K_0(K_1)}{I_0(K_1)}$$

$$K_{22}^{*} = \rho_2 N_2^{2} \frac{K_0(K_2)}{I_0(K_2)} \qquad (4.40)$$

$$I_{33} = \rho_1 N_1^{2}$$

$$K_{32}^{*} = \rho_3 N_3^{2}$$

When the surface tension is considered, $I_{22}, I_{22}^{*}, K_{22}, K_{22}^{*}$ and K_{32} * in eq. (4.35) becomes

$$I_{22} = -\rho_1 N_1^2 \{\frac{\rho_2 N_2^2}{\rho_1 N_1^2} + K_1 \frac{\sigma}{\rho_1 N_1^2 R_1^3}(1-K_1^2)\frac{I_0^{'}(K_1)}{I_0(K_1)}\}$$

$$I_{22}^{*} = \rho_2 N_2^2 \{1 + K_2 \frac{\sigma}{\rho_2 N_2^2 R_2^3}(1-K_2^2)\frac{I_0^{'}(K_2)}{I_0(K_2)}\}$$

$$K_{22} = -\rho_1 N_1^2 \{\frac{\rho_2 N_2^2}{\rho_1 N_1^2}\frac{K_0(K_1)}{I_0(K_1)} + K_1 \frac{\sigma}{\rho_1 N_1^2 R_1^3}(1-K_1^2)\frac{K_0^{'}(K_1)}{I_0(K_1)}\}$$

$$K_{22}^{*} = \rho_2 N_2^2 \{\frac{K_0(K_2)}{I_0(K_2)} + K_2 \frac{\sigma}{\rho_2 N_2^2 R_2^3}(1-K_2^2)\frac{K_0^{'}(K_2)}{I_0(K_2)}\} \qquad (4.41)$$

$$K_{32}^{*} = \rho_2 N_2^2 \{\frac{\rho_3 N_3^2}{\rho_2 N_2^2}\frac{K_0(K_2)}{I_0(K_2)} + K_2 \frac{\sigma}{\rho_2 N_2^2 R_2^3}(1-K_2^2)\frac{K_0^{'}(K_2)}{I_0(K_2)}$$

The asymptotic form of eq. (4.37) becomes

$$[\{\frac{\rho_2 N_2^2}{\rho_1 N_1^2} - 1\}\{1 - \frac{\rho_3 N_3^2}{\rho_2 N_2^2}\}] - \exp^{2K\varepsilon}[\{\frac{\rho_2 N_2^2}{\rho_1 N_1^2} + 1\}\{1 + \frac{\rho_3 N_3^2}{\rho_2 N_2^2}\}] = 0 \qquad (4.42)$$

where

$N_1 = kW_1 - \omega$

$N_2 = kW_2 - \omega$

$N_3 = kW_3 - \omega$

$K_1 = kR_1$

$$K_2 = kR_2$$

$$\varepsilon = \frac{R_2 - R_1}{R_1}$$

When the surface tension is considered, Equation (4.42) becomes

$$[\{Y_1 + \frac{\rho_2 N_2^{\,2}}{\rho_1 N_1^{\,2}} - 1\}\{1 - \frac{\rho_3 N_3^{\,2}}{\rho_2 N_2^{\,2}}\}] - \exp^{2K\varepsilon}[\{\frac{\rho_2 N_2^{\,2}}{\rho_1 N_1^{\,2}} + 1 - Y_1\}\{1 + \frac{\rho_3 N_3^{\,2}}{\rho_2 N_2^{\,2}}\}] = 0 \qquad (4.43)$$

where

$$Y_1 = K_1 \frac{\sigma}{\rho_1 N_1^{\,2} R_1^{\,3}}(1 - K_1^{\,2})$$

Equation (4.42) is called the dispersion relationship for annular axial jet.

When $\rho_1 = \rho_3$ and $N_1 = N_3$

eq. (4.42) becomes

$$[\{\frac{\rho_2 N_2^{\,2}}{\rho_1 N_1^{\,2}} - 1\}\{\frac{\rho_1 N_1^{\,2}}{\rho_2 N_2^{\,2}} - 1\}] - \exp^{2K\varepsilon}[\{\frac{\rho_2 N_2^{\,2}}{\rho_1 N_1^{\,2}} - 1\}\{1 + \frac{\rho_1 N_1^{\,2}}{\rho_2 N_2^{\,2}}\}] = 0 \qquad (4.44)$$

and eq. (4.43) for the effects of surface tension becomes

$$[\{Y_1 + \frac{\rho_2 N_2^{\,2}}{\rho_1 N_1^{\,2}} - 1\}\{\frac{\rho_1 N_1^{\,2}}{\rho_2 N_2^{\,2}} - 1\}] - \exp^{2K\varepsilon}[\{Y_1 - \frac{\rho_2 N_2^{\,2}}{\rho_1 N_1^{\,2}} - 1\}\{1 + \frac{\rho_1 N_1^{\,2}}{\rho_2 N_2^{\,2}}\}] = 0 \qquad (4.45)$$

4.2.2 Rotating Flow Annular Jet

There is no axial velocity component in flow region. Therefore, W_1, W_2 and W_3 are all zeroes. Equation (4.35) is applied. Therefore, each term in the coefficient matrix in eq. (4.34) becomes

$$I_{11} = [\frac{q_1 K_1 I_m^{'}(q_1 K_1)}{I_m(q_1 K_1)} + \frac{2m}{n_1}] I_m(q_1 K_1)$$

$$I_{21} = [\frac{q_2 K_1 I_m^{'}(q_2 K_1)}{I_m(q_2 K_1)} + \frac{2m}{n_2}] I_m(q_2 K_1)$$

$$I_{22} = [\frac{q_2 K_2 I_m^{'}(q_2 K_2)}{I_m(q_2 K_2)} + \frac{2m}{n_2}] I_m(q_2 K_2)$$

$$K_{21} = [\frac{q_2 K_1 K_m^{'}(q_2 K_1)}{K_m(q_2 K_1)} + \frac{2m}{n_2}] K_m(q_2 K_1)$$

$$K_{22} = [\frac{q_2 K_2 K_m^{'}(q_2 K_2)}{K_m(q_2 K_2)} + \frac{2m}{n_2}] K_m(q_2 K_2)$$

$$K_{32} = [\frac{q_3 K_2 K_m^{'}(q_3 K_2)}{K_m(q_3 K_2)} + \frac{2m}{n_3}] K_m(q_3 K_2)$$

$$I_{11}^{*} = [(n_1^2 - 4) + \{\frac{q_1 K_1 I_m^{'}(q_1 K_1)}{I_m(q_1 K_1)} + \frac{2m}{n_1}\}] I_m(q_1 K_1)$$

$$I_{21}^{*} = \alpha_{21}\beta_{21}^2[(n_2^2 - 4) + \{\frac{q_2 K_1 I_m^{'}(q_2 K_1)}{I_m(q_2 K_1)} + \frac{2m}{n_2}\}] I_m(q_2 K_1)$$

$$I_{22}^{*} = [(n_2^2 - 4) + \{\frac{q_2 K_2 I_m^{'}(q_2 K_2)}{I_m(q_2 K_2)} + \frac{2m}{n_1}\}] I_m(q_2 K_2)$$

$$K_{21}^{*} = \alpha_{21}\beta_{21}^2[(n_2^2 - 4) + \{\frac{q_2 K_1 K_m^{'}(q_2 K_1)}{K_m(q_2 K_1)} + \frac{2m}{n_2}\}] K_m(q_2 K_1)$$

$$K_{22}^{*} = [(n_2^2 - 4) + \{\frac{q_2 K_2 K_m^{'}(q_2 K_2)}{K_m(q_2 K_2)} + \frac{2m}{n_2}\}] K_m(q_2 K_2)$$

$$K_{21}^{*} = \alpha_{21}\beta_{21}^{2}[(n_2^{2}-4)+\{\frac{q_2K_1K_m^{'}(q_2K_1)}{K_m(q_2K_1)}+\frac{2m}{n_2}\}]K_m(q_2K_1)$$

$$K_{22}^{*} = [(n_2^{2}-4)+\{\frac{q_2K_2K_m^{'}(q_2K_2)}{K_m(q_2K_2)}+\frac{2m}{n_2}\}]K_m(q_2K_2) \qquad (4.46)$$

$$K_{32}^{*} = \alpha_{32}\beta_{32}^{2}[(n_3^{2}-4)+\{\frac{q_3K_2K_m^{'}(q_3K_2)}{K_m(q_3K_2)}+\frac{2m}{n_3}\}]K_m(q_3K_2)$$

where $\alpha_{21}=\left(\frac{\rho_2}{\rho_1}\right), \beta_{21}=\left(\frac{\Omega_2}{\Omega_1}\right)^2, \alpha_{32}=\left(\frac{\rho_3}{\rho_2}\right), \beta_{32}=\left(\frac{\Omega_3}{\Omega_2}\right)^2$

and

$$n_1=\frac{N_1}{\Omega_1}=\frac{m\Omega_1-\omega}{\Omega_1}$$

$$n_2=\frac{N_2}{\Omega_2}=\frac{m\Omega_2-\omega}{\Omega_2}$$

$$n_3=\frac{N_3}{\Omega_3}=\frac{m\Omega_3-\omega}{\Omega_3}$$

$$q_1=\frac{\sqrt{n_1^{2}-4}}{n_1}$$

$$q_2=\frac{\sqrt{n_2^{2}-4}}{n_2}$$

$$q_3=\frac{\sqrt{n_3^{2}-4}}{n_3}$$

when the surface tension is considered, $I_{21}^{*}, I_{22}^{*}, K_{21}^{*}$ and K_{22}^{*} in eq. (4.46) becomes

$$I_{21}^{*} = \alpha_{21}\beta_{21}^{2}[(n_2^{2}-4)+\{\frac{q_2K_1I_m^{'}(q_2K_1)}{I_m(q_2K_1)}+\frac{2m}{n_2}\}\{1+T_{21}(1-m^{2}-K_1^{2})\}]I_m(q_2K_1)$$

$$I_{22}^{*} = [(n_2^{2}-4)+\{\frac{q_2K_2I_m^{'}(q_2K_2)}{I_m(q_2K_2)}+\frac{2m}{n_2}\}\{1+T_{22}(1-m^{2}-K_2^{2})\}]I_m(q_2K_2)$$

$$K_{21}^{*} = \alpha_{21}\beta_{21}^{2}[(n_2^2 - 4) + \{\frac{q_2 K_1 K_m^{'}(q_2 K_1)}{K_m(q_2 K_1)} + \frac{2m}{n_2}\}\{1 + T_{21}(1 - m^2 - K_1^2)\}]K_m(q_2 K_1)$$

$$K_{22}^{*} = [(n_2^2 - 4) + \{\frac{q_2 K_2 K_m^{'}(q_2 K_2)}{K_m(q_2 K_2)} + \frac{2m}{n_2}\}\{1 + T_{22}(1 - m^2 - K_2^2)\}]K_m(q_2 K_2) \tag{4.47}$$

where

$$\alpha_{21} = \left(\frac{\rho_2}{\rho_1}\right), \beta_{21} = \left(\frac{\Omega_2}{\Omega_1}\right)^2, \alpha_{32} = \left(\frac{\rho_3}{\rho_2}\right), \beta_{32} = \left(\frac{\Omega_3}{\Omega_2}\right)^2, T_{21} = \frac{\sigma}{\rho_2 \Omega_2^{\,2} R_1^{\,3}} \text{ and}$$

$$T_{22} = \frac{\sigma}{\rho_2 \Omega_2^{\,2} R_2^{\,3}}$$

4.2.2.1 Axisymmetric disturbances(m = 0 and k ≠ 0)

When eq. (4.37) is expressed in asymptotic form, eq. (4.37) becomes

$$\begin{aligned}
&-\alpha_{21}\beta_{21}^{\,2}\alpha_{32}\beta_{32}^{\,2}\sqrt{q_1/q_3}\,\exp^{-q_2 K_1 \varepsilon}(n_2^2 - 4 + q_2 K_1)(n_3^2 - 4 - q_3 K_2)\\
&-\alpha_{21}\beta_{21}^{\,2}\alpha_{32}\beta_{32}^{\,2}\sqrt{q_1/q_3}\,\exp^{q_2 K_1 \varepsilon}(n_2^2 - 4 - q_2 K_1)(n_3^2 - 4 - q_3 K_2)\\
&+\alpha_{21}\beta_{21}^{\,2}\sqrt{q_1/q_2}\sqrt{q_3/q_2}\,\exp^{-q_2 K_1 \varepsilon}(n_2^2 - 4 + q_2 K_1)(n_2^2 - 4 - q_2 K_2)\\
&-\alpha_{21}\beta_{21}^{\,2}\sqrt{q_1/q_2}\sqrt{q_3/q_2}\,\exp^{q_2 K_1 \varepsilon}(n_2^2 - 4 + q_2 K_2)(n_2^2 - 4 - q_2 K_1)\\
&+\alpha_{32}\beta_{32}^{\,2}\sqrt{q_2/q_1}\sqrt{q_2/q_3}\,\exp^{-q_2 K_1 \varepsilon}(n_1^2 - 4 + q_1 K_1)(n_3^2 - 4 - q_3 K_2)\\
&-\alpha_{32}\beta_{32}^{\,2}\sqrt{q_2/q_1}\sqrt{q_2/q_3}\,\exp^{q_2 K_1 \varepsilon}(n_1^2 - 4 + q_1 K_1)(n_3^2 - 4 - q_3 K_2)\\
&-\sqrt{q_3/q_1}\,\exp^{-q_2 K_1 \varepsilon}(n_2^2 - 4 - q_2 K_2)(n_1^2 - 4 + q_1 K_1)\\
&-\sqrt{q_3/q_1}\,\exp^{q_2 K_1 \varepsilon}(n_2^2 - 4 + q_2 K_2)(n_1^2 - 4 + q_1 K_1) = 0
\end{aligned} \tag{4.48}$$

When the surface tension is considered, the asymptotic form of eq. (4.37) becomes

$$
\begin{aligned}
&-\alpha_{21}\beta_{21}{}^{2}\alpha_{32}\beta_{32}{}^{2}\sqrt{q_1/q_3}\,\exp^{-q_2K_1\varepsilon}\\
&[n_2{}^{2}-4+q_2K_1\{1+T_{21}(1-K_1{}^{2})\}](n_3{}^{2}-4-q_3K_2)\\
&-\alpha_{21}\beta_{21}{}^{2}\alpha_{32}\beta_{32}{}^{2}\sqrt{q_1/q_3}\,\exp^{q_2K_1\varepsilon}\\
&[n_2{}^{2}-4-q_2K_1\{1+T_{21}(1-K_1{}^{2})\}](n_3{}^{2}-4-q_3K_2)\\
&+\alpha_{21}\beta_{21}{}^{2}\sqrt{q_1/q_2}\sqrt{q_3/q_2}\,\exp^{-q_2K_1\varepsilon}\\
&[n_2{}^{2}-4+q_2K_1\{1+T_{21}(1-K_1{}^{2})\}][n_2{}^{2}-4-q_2K_2\{1+T_{22}(1-K_2{}^{2})\}]\\
&-\alpha_{21}\beta_{21}{}^{2}\sqrt{q_1/q_2}\sqrt{q_3/q_2}\,\exp^{q_2K_1\varepsilon}\\
&[n_2{}^{2}-4+q_2K_2\{1+T_{22}(1-K_2{}^{2})\}][n_2{}^{2}-4-q_2K_1\{1+T_{21}(1-K_1{}^{2})\}]\\
&+\alpha_{32}\beta_{32}{}^{2}\sqrt{q_2/q_1}\sqrt{q_2/q_3}\,\exp^{-q_2K_1\varepsilon}(n_1{}^{2}-4+q_1K_1)(n_3{}^{2}-4-q_3K_2)\\
&-\alpha_{32}\beta_{32}{}^{2}\sqrt{q_2/q_1}\sqrt{q_2/q_3}\,\exp^{q_2K_1\varepsilon}(n_1{}^{2}-4+q_1K_1)(n_3{}^{2}-4-q_3K_2)\\
&-\sqrt{q_3/q_1}\,\exp^{-q_2K_1\varepsilon}[n_2{}^{2}-4-q_2K_2\{1+T_{22}(1-K_2{}^{2})\}](n_1{}^{2}-4+q_1K_1)\\
&-\sqrt{q_3/q_1}\,\exp^{q_2K_1\varepsilon}[n_2{}^{2}-4+q_2K_2\{1+T_{22}(1-K_2{}^{2})\}](n_1{}^{2}-4+q_1K_1)=0
\end{aligned}
\tag{4.49}
$$

4.2.2.2 Azimuthally periodic disturbances (m ≠ 0 and k = 0)

The asymptotic form of eq. (4.37) becomes

$$
\left(\frac{n_1(n_1-2)-\alpha_{21}\beta_{21}{}^{2}n_2(n_2-2)+m(1-\alpha_{21}\beta_{21}{}^{2})}{n_1(n_1-2)+\alpha_{21}\beta_{21}{}^{2}n_2(n_2+2)+m(1-\alpha_{21}\beta_{21}{}^{2})}\left(\frac{R_1}{R_2}\right)^{2m}-\right.
\left.\frac{n_2(n_2-2)+\alpha_{32}\beta_{32}{}^{2}n_3(n_3+2)+m(1-\alpha_{32}\beta_{32}{}^{2})}{n_2(n_2+2)-\alpha_{32}\beta_{32}{}^{2}n_3(n_3+2)-m(1-\alpha_{32}\beta_{32}{}^{2})}\right)=0
\tag{4.50}
$$

When the surface tension is considered, the asymptotic form of eq. (4.37) becomes

$$\alpha_{21}\beta_{21}{}^{2}\alpha_{32}\beta_{32}{}^{2}(m+\frac{2m}{n_1})(-m+\frac{2m}{n_2})[n_2{}^{2}-4+(m+\frac{2m}{n_2})\{1.+T_{21}(1-m^2)\}]$$

$$(n_3{}^{2}-4-m+\frac{2m}{n_3})\left(\frac{R_1}{R_2}\right)^{2m}$$

$$-\alpha_{21}\beta_{21}{}^{2}\alpha_{32}\beta_{32}{}^{2}(m+\frac{2m}{n_1})(m+\frac{2m}{n_2})[n_2{}^{2}-4+(-m+\frac{2m}{n_2})\{1.+T_{21}(1-m^2)\}]$$

$$(n_3{}^{2}-4-m+\frac{2m}{n_3})$$

$$-\alpha_{21}\beta_{21}{}^{2}(m+\frac{2m}{n_1})(-m+\frac{2m}{n_3})[n_2{}^{2}-4+(m+\frac{2m}{n_2})\{1.+T_{21}(1-m^2)\}]$$

$$[n_2{}^{2}-4+(-m+\frac{2m}{n_2})\{1.+T_{22}(1-m^2)\}]\left(\frac{R_1}{R_2}\right)^{2m}$$

$$\alpha_{21}\beta_{21}{}^{2}(m+\frac{2m}{n_1})(-m+\frac{2m}{n_3})[n_2{}^{2}-4+(m+\frac{2m}{n_2})\{1.+T_{22}(1-m^2)\}]$$

$$[n_2{}^{2}-4+(-m+\frac{2m}{n_2})\{1.+T_{21}(1-m^2)\}]$$

$$-\alpha_{32}\beta_{32}{}^{2}(m+\frac{2m}{n_2})(-m+\frac{2m}{n_2})(n_1{}^{2}-4+m+\frac{2m}{n_1})$$

$$(n_3{}^{2}-4-m+\frac{2m}{n_3})\left(\frac{R_1}{R_2}\right)^{2m}$$

$$\alpha_{32}\beta_{32}{}^{2}(m+\frac{2m}{n_2})(-m+\frac{2m}{n_2})(n_1{}^{2}-4+m+\frac{2m}{n_1})$$

$$(n_3{}^{2}-4-m+\frac{2m}{n_3})$$

$$(m+\frac{2m}{n_2})(-m+\frac{2m}{n_3})(n_1{}^{2}-4+m+\frac{2m}{n_1})$$

$$[n_2{}^{2}-4+(-m+\frac{2m}{n_2})\{1.+T_{22}(1-m^2)\}]\left(\frac{R_1}{R_2}\right)^{2m} \qquad (4.51)$$

$$-(-m+\frac{2m}{n_2})(-m+\frac{2m}{n_3})(n_1{}^{2}-4+m+\frac{2m}{n_1})$$

$$[n_2{}^{2}-4+(m+\frac{2m}{n_2})\{1.+T_{22}(1-m^2)\}]$$

4.2.2.3 Helical disturbances ($m \neq 0$ and $k \neq 0$)

The asymptotic form of eq. (4.37) becomes

$$\alpha_{21}\beta_{21}{}^{2}\alpha_{32}\beta_{32}{}^{2}\exp^{(q_2K_1-q_1K_2)}(q_1K_1+\frac{2m}{n_1})(-q_2K_2+\frac{2m}{n_2})(n_3{}^{2}-4-q_3K_2+\frac{2m}{n_3})$$

$$[n_2{}^{2}-4+(q_2K_1+\frac{2m}{n_2})]$$

$$-\alpha_{21}\beta_{21}{}^{2}\alpha_{32}\beta_{32}{}^{2}\exp^{(q_2K_2-q_2K_1)}(q_1K_1+\frac{2m}{n_1})(q_2K_2+\frac{2m}{n_2})(n_3{}^{2}-4-q_3K_2+\frac{2m}{n_3})$$

$$[n_2{}^{2}-4+(-q_2K_1+\frac{2m}{n_2})]$$

$$-\alpha_{21}\beta_{21}{}^{2}\exp^{(q_2K_1-q_2K_2)}(q_1K_1+\frac{2m}{n_1})(-q_3K_2+\frac{2m}{n_3})[n_2{}^{2}-4+(q_2K_1+\frac{2m}{n_2})$$

$$[n_2{}^{2}-4+(-q_2K_2+\frac{2m}{n_2})]$$

$$\alpha_{21}\beta_{21}{}^{2}\exp^{(q_2K_2-q_2K_1)}(q_1K_1+\frac{2m}{n_1})(-q_3K_2+\frac{2m}{n_3})[n_2{}^{2}-4+(q_2K_2+\frac{2m}{n_2})$$

$$][n_2{}^{2}-4+(-q_2K_1+\frac{2m}{n_2})]$$

$$-\alpha_{32}\beta_{32}{}^{2}\exp^{(q_2K_1-q_2K_1)}(q_2K_1+\frac{2m}{n_2})(-q_2K_2+\frac{2m}{n_2})(n_1{}^{2}-4+q_1K_1+\frac{2m}{n_1})$$

$$(n_3{}^{2}-4-q_3K_2+\frac{2m}{n_3})$$

$$+\alpha_{32}\beta_{32}{}^{2}\exp^{(q_1K_2-q_1K_1)}(q_2K_2+\frac{2m}{n_2})(-q_2K_1+\frac{2m}{n_2})(n_1{}^{2}-4+q_1K_1+\frac{2m}{n_1})$$

$$(n_3{}^{2}-4-q_3K_2+\frac{2m}{n_3})$$

$$+\exp^{(q_2K_1-q_1K_2)}(q_2K_1+\frac{2m}{n_2})(-q_3K_2+\frac{2m}{n_3})(n_1{}^{2}-4+q_1K_1+\frac{2m}{n_1}) \qquad (4.52)$$

$$[n_2{}^{2}-4+(-q_2K_2+\frac{2m}{n_2})]$$

$$-\exp^{(q_2K_2-q_2K_1)}(-q_2K_1+\frac{2m}{n_2})(-q_3K_2+\frac{2m}{n_3})(n_1{}^{2}-4+q_1K_1+\frac{2m}{n_1})$$

$$[n_2{}^{2}-4+(q_2K_2+\frac{2m}{n_2})]=0$$

When the surface tension is considered, the asymptotic form of eq. (4.37) becomes

$$
\begin{aligned}
&\alpha_{21}\beta_{21}{}^{2}\alpha_{32}\beta_{32}{}^{2}\exp^{(q_2K_1-q_2K_2)}(q_1K_1+\frac{2m}{n_1})(-q_2K_2+\frac{2m}{n_2})(n_3{}^{2}-4-q_3K_2+\frac{2m}{n_3})\\
&[n_2{}^{2}-4+(q_2K_1+\frac{2m}{n_2})\{1+T_{21}(1-m^{2}-K_1{}^{2})\}]\\
&-\alpha_{21}\beta_{21}{}^{2}\alpha_{32}\beta_{32}{}^{2}\exp^{(q_2K_2-q_2K_1)}(q_1K_1+\frac{2m}{n_1})(q_2K_2+\frac{2m}{n_2})(n_3{}^{2}-4-q_3K_2+\frac{2m}{n_3})\\
&[n_2{}^{2}-4+(-q_2K_1+\frac{2m}{n_2})\{1+T_{21}(1-m^{2}-K_1{}^{2})\}]\\
&-\alpha_{21}\beta_{21}{}^{2}\exp^{(q_2K_1-q_2K_2)}(q_1K_1+\frac{2m}{n_1})(-q_3K_2+\frac{2m}{n_3})[n_2{}^{2}-4+(q_2K_1+\frac{2m}{n_2})\\
&\{1+T_{21}(1-m^{2}-K_1{}^{2})\}[n_2{}^{2}-4+(-q_2K_2+\frac{2m}{n_2})\{1+T_{22}(1-m^{2}-K_2{}^{2})\}]\\
&\alpha_{21}\beta_{21}{}^{2}\exp^{(q_2K_2-q_2K_1)}(q_1K_1+\frac{2m}{n_1})(-q_3K_2+\frac{2m}{n_3})[n_2{}^{2}-4+(q_2K_2+\frac{2m}{n_2})\\
&\{1+T_{22}(1-m^{2}-K_2{}^{2})\}][n_2{}^{2}-4+(-q_2K_1+\frac{2m}{n_2})\{1+T_{21}(1-m^{2}-K_1{}^{2})\}]\\
&-\alpha_{32}\beta_{32}{}^{2}\exp^{(q_2K_1-q_2K_2)}(q_2K_1+\frac{2m}{n_2})(-q_2K_2+\frac{2m}{n_2})(n_1{}^{2}-4+q_1K_1+\frac{2m}{n_1})\\
&(n_3{}^{2}-4-q_3K_2+\frac{2m}{n_3})\\
&+\alpha_{32}\beta_{32}{}^{2}\exp^{(q_2K_2-q_2K_1)}(q_2K_2+\frac{2m}{n_2})(-q_2K_1+\frac{2m}{n_2})(n_1{}^{2}-4+q_1K_1+\frac{2m}{n_1})\\
&(n_3{}^{2}-4-q_3K_2+\frac{2m}{n_3})\\
&+\exp^{(q_2K_1-q_2K_2)}(q_2K_1+\frac{2m}{n_2})(-q_3K_2+\frac{2m}{n_3})(n_1{}^{2}-4+q_1K_1+\frac{2m}{n_1})\\
&[n_2{}^{2}-4+(-q_2K_2+\frac{2m}{n_2})\{1+T_{22}(1-m^{2}-K_2{}^{2})\}]\\
&-\exp^{(q_2K_2-q_2K_1)}(-q_2K_1+\frac{2m}{n_2})(-q_3K_2+\frac{2m}{n_3})(n_1{}^{2}-4+q_1K_1+\frac{2m}{n_1})\\
&[n_2{}^{2}-4+(q_2K_2+\frac{2m}{n_2})\{1+T_{22}(1-m^{2}-K_2{}^{2})\}]=0
\end{aligned}
\tag{4.53}
$$

4.2.3 The Helical Flow Annular Jet

4.2.3.1 axisymmetric disturbances (m = 0 and k ≠ 0)

m, circumferential wave number is not considered. Each term in eq. (4.34) becomes

$$I_{11} = [\frac{q_1 K_1 I_0^{'}(q_1 K_1)}{I_0(q_1 K_1)}] I_0(q_1 K_1)$$

$$I_{21} = [\frac{q_2 K_1 I_0^{'}(q_2 K_1)}{I_0(q_2 K_1)}] I_0(q_2 K_1)$$

$$I_{22} = [\frac{q_2 K_2 I_0^{'}(q_2 K_2)}{I_0(q_2 K_2)}] I_0(q_2 K_2)$$

$$K_{21} = [\frac{q_2 K_1 K_0^{'}(q_2 K_1)}{K_0(q_2 K_1)}] K_0(q_2 K_1)$$

$$K_{22} = [\frac{q_2 K_2 K_0^{'}(q_2 K_2)}{K_0(q_2 K_2)}] K_0(q_2 K_2)$$

$$K_{32} = [\frac{q_3 K_2 K_0^{'}(q_3 K_2)}{K_0(q_3 K_2)}] K_0(q_3 K_2)$$

$$I_{11}^{*} = [(n_1^{2} - 4) + \{\frac{q_1 K_1 I_0^{'}(q_1 K_1)}{I_0(q_1 K_1)}\}] I_0(q_1 K_1)$$

$$I_{21}^{*} = \alpha_{21}\beta_{21}^{2}[(n_2^{2} - 4) + \{\frac{q_2 K_1 I_0^{'}(q_2 K_1)}{I_0(q_2 K_1)}\}] I_0(q_2 K_1)$$

$$I_{22}^{*} = [(n_2^{2} - 4) + \{\frac{q_2 K_2 I_0^{'}(q_2 K_2)}{I_0(q_2 K_2)}\}] I_0(q_2 K_2) \qquad (4.54)$$

$$K_{21}^{*} = \alpha_{21}\beta_{21}^{2}[(n_2^{2} - 4) + \{\frac{q_2 K_1 K_0^{'}(q_2 K_1)}{K_0(q_2 K_1)}\}] K_0(q_2 K_1)$$

$$K_{22}^{*} = [(n_2^{2} - 4) + \{\frac{q_2 K_2 K_0^{'}(q_2 K_2)}{K_0(q_2 K_2)}\}] K_0(q_2 K_2)$$

where

$$
\begin{aligned}
n_1 &= \frac{N_1}{\Omega_1} = \frac{kW_1 - \omega}{\Omega_1} \\
n_2 &= \frac{N_2}{\Omega_2} = \frac{kW_2 - \omega}{\Omega_2} \\
n_3 &= \frac{N_3}{\Omega_3} = \frac{kW_3 - \omega}{\Omega_3} \\
q_1 &= \frac{\sqrt{n_1^2 - 4}}{n_1} \\
q_2 &= \frac{\sqrt{n_2^2 - 4}}{n_2} \\
q_3 &= \frac{\sqrt{n_3^2 - 4}}{n_3}
\end{aligned}
\qquad (4.55)
$$

When the surface tension is considered, $I_{21}^*, I_{22}^*, K_{21}^*$ and K_{22}^* in eq. (4.55) are replaced by

$$
\begin{aligned}
I_{21}^* &= \alpha_{21}\beta_{21}{}^2[(n_2{}^2 - 4) + \{\frac{q_2K_1I_0{}'(q_2K_1)}{I_0(q_2K_1)}\}\{1 + T_{21}(1 - K_1{}^2)\}]I_0(q_2K_1) \\
I_{22}^* &= [(n_2{}^2 - 4) + \{\frac{q_2K_2I_0{}'(q_2K_2)}{I_0(q_2K_2)}\}\{1 + T_{22}(1 - K_2{}^2)\}]I_0(q_2K_2) \\
K_{22}^* &= [(n_2{}^2 - 4) + \{\frac{q_2K_2K_0{}'(q_2K_2)}{K_0(q_2K_2)}\}\{1 + T_{22}(1 - K_2{}^2)\}]K_0(q_2K_2) \\
K_{21}^* &= \alpha_{21}\beta_{21}{}^2[(n_2{}^2 - 4) + \{\frac{q_2K_1K_0{}'(q_2K_1)}{K_0(q_2K_1)}\}\{1 + T_{21}(1 - K_1{}^2)\}]K_0(q_2K_1)
\end{aligned}
\qquad (4.56)
$$

When eq. (4.55) is changed into asymptotic expansions , eq. (4.55) becomes

$$
\begin{aligned}
&-\alpha_{21}\beta_{21}{}^2\alpha_{32}\beta_{32}{}^2\sqrt{q_1K_1/q_2K_1}\sqrt{q_2K_2/q_3K_2}\ \exp^{(q_2K_1 - q_2K_2)} \\
&[n_2{}^2 - 4 + q_2K_1](n_3{}^2 - 4 - q_3K_2) \\
&-\alpha_{21}\beta_{21}{}^2\alpha_{32}\beta_{32}{}^2\sqrt{q_1K_1/q_2K_1}\sqrt{q_2K_2/q_3K_2}\ \exp^{(q_2K_2 - q_2K_1)} \\
&[n_2{}^2 - 4 - q_2K_1](n_3{}^2 - 4 - q_3K_2) \\
&+\alpha_{21}\beta_{21}{}^2\sqrt{q_1K_1/q_2K_1}\sqrt{q_3K_2/q_2K_2}\ \exp^{(q_2K_1 - q_2K_2)}
\end{aligned}
$$

$$
\begin{aligned}
&[n_2^{\,2}-4+q_2K_1][n_2^{\,2}-4-q_2K_2]\\
&-\alpha_{21}\beta_{21}{}^2\sqrt{q_1K_1/q_2K_1}\sqrt{q_3K_2/q_2K_2}\,\exp^{(q_2K_2-q_2K_1)}\\
&[n_2^{\,2}-4+q_2K_2][n_2^{\,2}-4-q_2K_1]\\
&+\alpha_{32}\beta_{32}{}^2\sqrt{q_2K_1/q_1K_1}\sqrt{q_2K_2/q_3K_2}\,\exp^{(q_2K_1-q_2K_2)}\\
&(n_1^{\,2}-4+q_1K_1)(n_3^{\,2}-4-q_3K_2)\\
&-\alpha_{32}\beta_{32}{}^2\sqrt{q_2K_1/q_1K_1}\sqrt{q_2K_2/q_3K_2}\,\exp^{(q_2K_2-q_2K_1)}\\
&(n_1^{\,2}-4+q_1K_1)(n_3^{\,2}-4-q_3K_2)\\
&-\sqrt{q_2K_1/q_1K_1}\sqrt{q_3K_2/q_2K_2}\,\exp^{(q_2K_1-q_2K_2)}\\
&[n_2^{\,2}-4-q_2K_2](n_1^{\,2}-4+q_1K_1)\\
&-\sqrt{q_2K_1/q_1K_1}\sqrt{q_3K_2/q_2K_2}\,\exp^{(q_2K_2-q_2K_1)}\\
&[n_2^{\,2}-4+q_2K_2](n_1^{\,2}-4+q_1K_1)=0
\end{aligned}
\qquad (4.57)
$$

When the surface tension is considered, eq. (4.66) becomes

$$
\begin{aligned}
&-\alpha_{21}\beta_{21}{}^2\alpha_{32}\beta_{32}{}^2\sqrt{q_1K_1/q_2K_1}\sqrt{q_2K_2/q_3K_2}\,\exp^{(q_2K_1-q_2K_2)}\\
&[n_2^{\,2}-4+q_2K_1\{1+T_{21}(1-K_1^{\,2})\}](n_3^{\,2}-4-q_3K_2)\\
&-\alpha_{21}\beta_{21}{}^2\alpha_{32}\beta_{32}{}^2\sqrt{q_1K_1/q_2K_1}\sqrt{q_2K_2/q_3K_2}\,\exp^{(q_2K_2-q_2K_1)}\\
&[n_2^{\,2}-4-q_2K_1\{1+T_{21}(1-K_1^{\,2})\}](n_3^{\,2}-4-q_3K_2)\\
&+\alpha_{21}\beta_{21}{}^2\sqrt{q_1K_1/q_2K_1}\sqrt{q_3K_2/q_2K_2}\,\exp^{(q_2K_1-q_2K_2)}\\
&[n_2^{\,2}-4+q_2K_1\{1+T_{21}(1-K_1^{\,2})\}][n_2^{\,2}-4-q_2K_2\{1+T_{22}(1-K_2^{\,2})\}]\\
&-\alpha_{21}\beta_{21}{}^2\sqrt{q_1K_1/q_2K_1}\sqrt{q_3K_2/q_2K_2}\,\exp^{(q_2K_2-q_2K_1)}\\
&[n_2^{\,2}-4+q_2K_2\{1+T_{22}(1-K_2^{\,2})\}][n_2^{\,2}-4-q_2K_1\{1+T_{21}(1-K_1^{\,2})\}]\\
&+\alpha_{32}\beta_{32}{}^2\sqrt{q_2K_1/q_1K_1}\sqrt{q_2K_2/q_3K_2}\,\exp^{(q_2K_1-q_2K_2)}\\
&(n_1^{\,2}-4+q_1K_1)(n_3^{\,2}-4-q_3K_2)
\end{aligned}
$$

$$
\begin{aligned}
&-\alpha_{32}\beta_{32}{}^{2}\sqrt{q_2K_1/q_1K_1}\sqrt{q_2K_2/q_3K_2}\ \exp^{(q_2K_2-q_2K_1)}\\
&(n_1{}^2-4+q_1K_1)(n_3{}^2-4-q_3K_2)\\
&-\sqrt{q_2K_1/q_1K_1}\sqrt{q_3K_2/q_2K_2}\ \exp^{(q_2K_1-q_2K_2)}\\
&[n_2{}^2-4-q_2K_2\{1+T_{22}(1-K_2{}^2)\}](n_1{}^2-4+q_1K_1)\\
&-\sqrt{q_2K_1/q_1K_1}\sqrt{q_3K_2/q_2K_2}\ \exp^{(q_2K_2-q_2K_1)}\\
&[n_2{}^2-4+q_2K_2\{1+T_{22}(1-K_2{}^2)\}](n_1{}^2-4+q_1K_1)=0
\end{aligned}
\tag{4.58}
$$

For non-axisymmetric disturbances (m≠ 0), eq. (4.35) becomes

$$
I_{11}=[\frac{q_1K_1I_m{}'(q_1K_1)}{I_m(q_1K_1)}+\frac{2m}{n_1}]I_m(q_1K_1)
$$

$$
I_{21}=[\frac{q_2K_1I_m{}'(q_2K_1)}{I_m(q_2K_1)}+\frac{2m}{n_2}]I_m(q_2K_1)
$$

$$
I_{22}=[\frac{q_2K_2I_m{}'(q_2K_2)}{I_m(q_2K_2)}+\frac{2m}{n_2}]I_m(q_2K_2)
$$

$$
K_{21}=[\frac{q_2K_1K_m{}'(q_2K_1)}{K_m(q_2K_1)}+\frac{2m}{n_2}]K_m(q_2K_1)
$$

$$
K_{22}=[\frac{q_2K_2K_m{}'(q_2K_2)}{K_m(q_2K_2)}+\frac{2m}{n_2}]K_m(q_2K_2)
$$

$$
K_{32}=[\frac{q_3K_2K_m{}'(q_3K_2)}{K_m(q_3K_2)}+\frac{2m}{n_3}]K_m(q_3K_2)
$$

$$
\begin{aligned}
I_{11}{}^{*}&=[(n_1{}^2-4)+\{\frac{q_1K_1I_m{}'(q_1K_1)}{I_m(q_1K_1)}+\frac{2m}{n_1}\}]I_m(q_1K_1)\\
I_{21}{}^{*}&=\alpha_{21}[(n_2{}^2-4)+\{\frac{q_2K_1I_m{}'(q_2K_1)}{I_m(q_2K_1)}+\frac{2m}{n_2}\}]I_m(q_2K_1)\\
I_{22}{}^{*}&=[(n_2{}^2-4)+\{\frac{q_2K_2I_m{}'(q_2K_2)}{I_m(q_2K_2)}+\frac{2m}{n_1}\}]I_m(q_2K_2)
\end{aligned}
\tag{4.59}
$$

$$K_{21}^{*} = \alpha_{21}[(n_2^2 - 4) + \{\frac{q_2 K_1 K_m^{'}(q_2 K_1)}{K_m(q_2 K_1)} + \frac{2m}{n_2}\}]K_m(q_2 K_1)$$

$$K_{22}^{*} = [(n_2^2 - 4) + \{\frac{q_2 K_2 K_m^{'}(q_2 K_2)}{K_m(q_2 K_2)} + \frac{2m}{n_2}\}]K_m(q_2 K_2)$$

$$K_{32}^{*} = \alpha_{32}[(n_3^2 - 4) + \{\frac{q_3 K_2 K_m^{'}(q_3 K_2)}{K_m(q_3 K_2)} + \frac{2m}{n_3}\}]K_m(q_3 K_2)$$

when the surface tension is considered, $I_{21}^{*}, I_{22}^{*}, K_{21}^{*}$ and K_{22}^{*} in eq. (4.59) are replaced by

$$I_{21}^{*} = [(n_2^2 - 4) + \{\frac{q_2 K_1 I_m^{'}(q_2 K_1)}{I_m(q_2 K_1)} + \frac{2m}{n_2}\}\{1 + \Gamma_{21}(1 - m^2 - K_1^2)\}]I_m(q_2 K_1)$$

$$I_{22}^{*} = [(n_2^2 - 4) + \{\frac{q_2 K_2 I_m^{'}(q_2 K_2)}{I_m(q_2 K_2)} + \frac{2m}{n_2}\}\{1 + \Gamma_{22}(1 - m^2 - K_2^2)\}]I_m(q_2 K_2)$$

$$K_{21}^{*} = [(n_2^2 - 4) + \{\frac{q_2 K_1 K_m^{'}(q_2 K_1)}{K_m(q_2 K_1)} + \frac{2m}{n_2}\}\{1 + \Gamma_{21}(1 - m^2 - K_1^2)\}]K_m(q_2 K_1) \qquad (4.60)$$

$$K_{22}^{*} = [(n_2^2 - 4) + \{\frac{q_2 K_2 K_m^{'}(q_2 K_2)}{K_m(q_2 K_2)} + \frac{2m}{n_2}\}\{1 + \Gamma_{22}(1 - m^2 - K_2^2)\}]K_m(q_2 K_2)$$

where

$$n_1 = \frac{N_1}{\Omega_1} = \frac{kW_1 + m\Omega_1 - \omega}{\Omega_1}$$

$$n_2 = \frac{N_2}{\Omega_2} = \frac{kW_2 + m\Omega_2 - \omega}{\Omega_2}$$

$$n_3 = \frac{N_3}{\Omega_3} = \frac{kW_3 + m\Omega_3 - \omega}{\Omega_3}$$

$$q_1 = \frac{\sqrt{n_1^2 - 4}}{n_1}$$

$$q_2 = \frac{\sqrt{n_2^2 - 4}}{n_2}$$

$$q_3 = \frac{\sqrt{n_3^2 - 4}}{n_3}$$

4.2.3.2 Azimuthally periodic perturbations (m ≠ 0 and k = 0)

When eq. (4.37) is expressed in asymptotic expansion forms, eq. (4.37) becomes

$$
\begin{aligned}
&\alpha_{21}\beta_{21}{}^{2}\alpha_{32}\beta_{32}{}^{2}(m+\frac{2m}{n_1})(-m+\frac{2m}{n_2})[n_2{}^{2}-4+(m+\frac{2m}{n_2})]\\
&(n_3{}^{2}-4-m+\frac{2m}{n_3})\left(\frac{R_1}{R_2}\right)^{2m}\\
&-\alpha_{21}\beta_{21}{}^{2}\alpha_{32}\beta_{32}{}^{2}(m+\frac{2m}{n_1})(m+\frac{2m}{n_2})[n_2{}^{2}-4+(-m+\frac{2m}{n_2})]\\
&(n_3{}^{2}-4-m+\frac{2m}{n_3})\\
&-\alpha_{21}\beta_{21}{}^{2}(m+\frac{2m}{n_1})(-m+\frac{2m}{n_3})[n_2{}^{2}-4+(m+\frac{2m}{n_2})]\\
&[n_2{}^{2}-4+(-m+\frac{2m}{n_2})]\left(\frac{R_1}{R_2}\right)^{2m}\\
&\\
&\alpha_{21}\beta_{21}{}^{2}(m+\frac{2m}{n_1})(-m+\frac{2m}{n_3})[n_2{}^{2}-4+(m+\frac{2m}{n_2})]\\
&[n_2{}^{2}-4+(-m+\frac{2m}{n_2})]\\
&-\alpha_{32}\beta_{32}{}^{2}(m+\frac{2m}{n_2})(-m+\frac{2m}{n_2})(n_1{}^{2}-4+m+\frac{2m}{n_1})\\
&(n_3{}^{2}-4-m+\frac{2m}{n_3})\left(\frac{R_1}{R_2}\right)^{2m}\\
&\alpha_{32}\beta_{32}{}^{2}(m+\frac{2m}{n_2})(-m+\frac{2m}{n_2})(n_1{}^{2}-4+m+\frac{2m}{n_1})\\
&(n_3{}^{2}-4-m+\frac{2m}{n_3})\\
&[n_2{}^{2}-4+(-m+\frac{2m}{n_2})]\left(\frac{R_1}{R_2}\right)^{2m}\\
&-(-m+\frac{2m}{n_2})(-m+\frac{2m}{n_3})(n_1{}^{2}-4+m+\frac{2m}{n_1})
\end{aligned}
\tag{4.61}
$$

$$[n_2^2 - 4 + (m + \frac{2m}{n_2})] = 0$$

When the surface tension is considered, eq. (4.61) becomes

$$\alpha_{21}\beta_{21}{}^2\alpha_{32}\beta_{32}{}^2(m + \frac{2m}{n_1})(-m + \frac{2m}{n_2})[n_2^2 - 4 + (m + \frac{2m}{n_2})\{1.+T_{21}(1-m^2)\}]$$

$$(n_3^2 - 4 - m + \frac{2m}{n_3})\left(\frac{R_1}{R_2}\right)^{2m}$$

$$-\alpha_{21}\beta_{21}{}^2\alpha_{32}\beta_{32}{}^2(m + \frac{2m}{n_1})(m + \frac{2m}{n_2})[n_2^2 - 4 + (-m + \frac{2m}{n_2})\{1.+T_{21}(1-m^2)\}] \qquad (4.62)$$

$$(n_3^2 - 4 - m + \frac{2m}{n_3})$$

$$-\alpha_{21}\beta_{21}{}^2(m + \frac{2m}{n_1})(-m + \frac{2m}{n_3})[n_2^2 - 4 + (m + \frac{2m}{n_2})\{1.+T_{21}(1-m^2)\}]$$

$$[n_2^2 - 4 + (-m + \frac{2m}{n_2})\{1.+T_{22}(1-m^2)\}]\left(\frac{R_1}{R_2}\right)^{2m}$$

$$\alpha_{21}\beta_{21}{}^2(m + \frac{2m}{n_1})(-m + \frac{2m}{n_3})[n_2^2 - 4 + (m + \frac{2m}{n_2})\{1.+T_{22}(1-m^2)\}]$$

$$[n_2^2 - 4 + (-m + \frac{2m}{n_2})\{1.+T_{21}(1-m^2)\}]$$

$$-\alpha_{32}\beta_{32}{}^2(m + \frac{2m}{n_2})(-m + \frac{2m}{n_2})(n_1^2 - 4 + m + \frac{2m}{n_1})$$

$$(n_3^2 - 4 - m + \frac{2m}{n_3})\left(\frac{R_1}{R_2}\right)^{2m}$$

$$\alpha_{32}\beta_{32}{}^2(m + \frac{2m}{n_2})(-m + \frac{2m}{n_2})(n_1^2 - 4 + m + \frac{2m}{n_1})$$

$$(n_3^2 - 4 - m + \frac{2m}{n_3})$$

$$(m + \frac{2m}{n_2})(-m + \frac{2m}{n_3})(n_1^2 - 4 + m + \frac{2m}{n_1})$$

$$[n_2^2 - 4 + (-m + \frac{2m}{n_2})\{1.+T_{22}(1-m^2)\}]\left(\frac{R_1}{R_2}\right)^{2m}$$

$$-(-m + \frac{2m}{n_2})(-m + \frac{2m}{n_3})(n_1^2 - 4 + m + \frac{2m}{n_1})$$

$$[n_2^2 - 4 + (m + \frac{2m}{n_2})\{1.+T_{22}(1-m^2)\}] = 0$$

4.2.3.3 Helical disturbances ($m \neq 0$ and $k \neq 0$)

Equation (4.37) expressed in asymptotic form is

$$\alpha_{21}\beta_{21}{}^2\alpha_{32}\beta_{32}{}^2 \exp^{(q_2K_1 - q_2K_2)}(q_1K_1 + \frac{2m}{n_1})(-q_2K_2 + \frac{2m}{n_2})(n_3^2 - 4 - q_3K_2 + \frac{2m}{n_3})$$

$$[n_2^2 - 4 + (q_2K_1 + \frac{2m}{n_2})]$$

$$-\alpha_{21}\beta_{21}{}^2\alpha_{32}\beta_{32}{}^2 \exp^{(q_2K_2 - q_2K_1)}(q_1K_1 + \frac{2m}{n_1})(q_2K_2 + \frac{2m}{n_2})(n_3^2 - 4 - q_3K_2 + \frac{2m}{n_3})$$

$$[n_2^2 - 4 + (-q_2K_1 + \frac{2m}{n_2})]$$

$$-\alpha_{21}\beta_{21}{}^2 \exp^{(q_2K_1 - q_2K_2)}(q_1K_1 + \frac{2m}{n_1})(-q_3K_2 + \frac{2m}{n_3})[n_2^2 - 4 + (q_2K_1 + \frac{2m}{n_2})]$$

$$[n_2^2 - 4 + (-q_2K_2 + \frac{2m}{n_2})]$$

$$\alpha_{21}\beta_{21}{}^2 \exp^{(q_2K_2 - q_2K_1)}(q_1K_1 + \frac{2m}{n_1})(-q_3K_2 + \frac{2m}{n_3})[n_2^2 - 4 + (q_2K_2 + \frac{2m}{n_2})]$$

$$[n_2^2 - 4 + (-q_2K_1 + \frac{2m}{n_2})]$$

$$-\alpha_{32}\beta_{32}{}^2 \exp^{(q_2K_1 - q_2K_2)}(q_2K_1 + \frac{2m}{n_2})(-q_2K_2 + \frac{2m}{n_2})(n_1^2 - 4 + q_1K_1 + \frac{2m}{n_1})$$

$$[n_2^2 - 4 + (q_2K_2 + \frac{2m}{n_2})] = 0$$

$$
\begin{aligned}
&+\alpha_{32}\beta_{32}{}^{2}\exp^{(q_2K_2-q_2K_1)}(q_2K_2+\frac{2m}{n_2})(-q_2K_1+\frac{2m}{n_2})(n_1{}^{2}-4+q_1K_1+\frac{2m}{n_1})\\
&(n_3{}^{2}-4-q_3K_2+\frac{2m}{n_3})\\
&+\exp^{(q_2K_1-q_2K_2)}(q_2K_1+\frac{2m}{n_2})(-q_3K_2+\frac{2m}{n_3})(n_1{}^{2}-4+q_1K_1+\frac{2m}{n_1})\\
&[n_2{}^{2}-4+(-q_2K_2+\frac{2m}{n_2})]\\
&-\exp^{(q_2K_2-q_2K_1)}(-q_2K_1+\frac{2m}{n_2})(-q_3K_2+\frac{2m}{n_3})(n_1{}^{2}-4+q_1K_1+\frac{2m}{n_1})\\
&[n_2{}^{2}-4+(q_2K_2+\frac{2m}{n_2})]=0
\end{aligned}
\tag{4.63}
$$

When the surface tension is considered, eq. (4.37) becomes

$$
\begin{aligned}
&\alpha_{21}\beta_{21}{}^{2}\alpha_{32}\beta_{32}{}^{2}\exp^{(q_2K_1-q_2K_2)}(q_1K_1+\frac{2m}{n_1})(-q_2K_2+\frac{2m}{n_2})(n_3{}^{2}-4-q_3K_2+\frac{2m}{n_3})\\
&[n_2{}^{2}-4+(q_2K_1+\frac{2m}{n_2})\{1+T_{21}(1-m^{2}-K_1{}^{2})\}]\\
&-\alpha_{21}\beta_{21}{}^{2}\alpha_{32}\beta_{32}{}^{2}\exp^{(q_2K_2-q_2K_1)}(q_1K_1+\frac{2m}{n_1})(q_2K_2+\frac{2m}{n_2})(n_3{}^{2}-4-q_3K_2+\frac{2m}{n_3})\\
&[n_2{}^{2}-4+(-q_2K_1+\frac{2m}{n_2})\{1+T_{21}(1-m^{2}-K_1{}^{2})\}]\\
&-\alpha_{21}\beta_{21}{}^{2}\exp^{(q_2K_1-q_2K_2)}(q_1K_1+\frac{2m}{n_1})(-q_3K_2+\frac{2m}{n_3})[n_2{}^{2}-4+(q_2K_1+\frac{2m}{n_2})\\
&\{1+T_{21}(1-m^{2}-K_1{}^{2})\}][n_2{}^{2}-4+(-q_2K_2+\frac{2m}{n_2})\{1+T_{22}(1-m^{2}-K_2{}^{2})\}]\\
&\alpha_{21}\beta_{21}{}^{2}\exp^{(q_2K_2-q_2K_1)}(q_1K_1+\frac{2m}{n_1})(-q_3K_2+\frac{2m}{n_3})[n_2{}^{2}-4+(q_2K_2+\frac{2m}{n_2})\\
&\{1+T_{22}(1-m^{2}-K_2{}^{2})\}][n_2{}^{2}-4+(-q_2K_1+\frac{2m}{n_2})\{1+T_{21}(1-m^{2}-K_1{}^{2})\}]\\
&-\alpha_{32}\beta_{32}{}^{2}\exp^{(q_2K_1-q_2K_2)}(q_2K_1+\frac{2m}{n_2})(-q_2K_2+\frac{2m}{n_2})(n_1{}^{2}-4+q_1K_1+\frac{2m}{n_1})
\end{aligned}
$$

$$
\begin{aligned}
&(n_3{}^2 - 4 - q_3K_2 + \frac{2m}{n_3}) \\
&+\alpha_{32}\beta_{32}{}^2 \exp^{(q_2K_2 - q_2K_1)}(q_2K_2 + \frac{2m}{n_2})(-q_2K_1 + \frac{2m}{n_2})(n_1{}^2 - 4 + q_1K_1 + \frac{2m}{n_1}) \\
&(n_3{}^2 - 4 - q_3K_2 + \frac{2m}{n_3}) \\
&+\exp^{(q_2K_1 - q_2K_2)}(q_2K_1 + \frac{2m}{n_2})(-q_3K_2 + \frac{2m}{n_3})(n_1{}^2 - 4 + q_1K_1 + \frac{2m}{n_1}) \qquad (4.64) \\
&[n_2{}^2 - 4 + (-q_2K_2 + \frac{2m}{n_2})\{1 + T_{22}(1 - m^2 - K_2{}^2)\}] \\
&-\exp^{(q_2K_2 - q_2K_1)}(-q_2K_1 + \frac{2m}{n_2})(-q_3K_2 + \frac{2m}{n_3})(n_1{}^2 - 4 + q_1K_1 + \frac{2m}{n_1}) \\
&[n_2{}^2 - 4 + (q_2K_2 + \frac{2m}{n_2})\{1 + T_{22}(1 - m^2 - K_2{}^2)\}] = 0
\end{aligned}
$$

CHAPTER 5
THE VALIDATION OF NUMERICAL FORMULATION

The validity of the previous numerical formulations is investigated in this chapter. There are three known analytical solutions available to be compared. Rayleigh (1879)'s mathematical theory for stationary flow assumes an inviscid fluid core with surface tension surrounded by a light inviscid fluid. Reshotko and Monnin (1965)'s mathematical theory for rotating flow assumes a heavy inviscid fluid core with rotation surrounded by a light inviscid fluid with rotation. Fung (1983)'s mathematical theory for rotating flow assumes a heavy inviscid annular sheet with rotation exposed to a light inviscid fluid with rotation. The computer code was tested against these known solutions. In addition, Fung (1983)'s mathematical theory for the azimuthally periodic mode ($m \neq 0$ and $k = 0$) with no surface tension was compared with the derivation of this dissertation, eq. (4.37). After the computer code is validated, it will then be extended to the analysis of the inviscid, rotational and axial flow with or without surface tension.

5.1 Rayleigh's Stationary Jet with Surface Tension

Rayleigh (1879) made a mathematical analysis of the instability of a non-viscous jet. He considered a laminar liquid flow with a velocity potential where the jet was only

under the influence of surface tension forces. Although the conditions considered by Rayleigh do not exist in an actual jet, the general conclusions of Rayleigh's work regarding jet instability have been accepted. In his analysis, the surface waves grow as $e^{\omega t}$, where

$$\omega^2 = \frac{\sigma}{R^3\rho} kR \frac{I_1(kR)}{I_0(kR)}[1 - k^2R^2] \tag{5.1}$$

σ is the surface tension, ρ is the density of liquid, R is the undisturbed radius of the jet, k is the wave-number and I_0, I_1 are the modified Bessel functions. The dispersion curve of ω versus k shows a maximum growth rate at $kR = 0.697$ or $\lambda = \frac{2\pi}{k} = 9.02R$. It is verified if the computer code shows the maximum growth rate at $k = \frac{0.697}{R}$. This verification is shown in figure 7. In figure 7, the results from the computer code shows that the maximum growth rate occurs at $k = \frac{0.697}{R}$.

5.2 Reshotko and Monnin's Two-Wheel Flows with No Surface Tension

Reshotko and Monnin (1965) investigated the instability for the two-fluid wheel flow of a heavy density core surrounded by a lighter fluid. The geometry of such a flow is shown in figure 6. The flow is considered to be only azimuthal and solely a function of the radial coordinate. In Reshotko and Monnin's two wheel flows, the instability of two layers with the same rotational velocity and different density was investigated. The inner fluid density is greater than the outer fluid density. For a heavy fluid core surrounded by

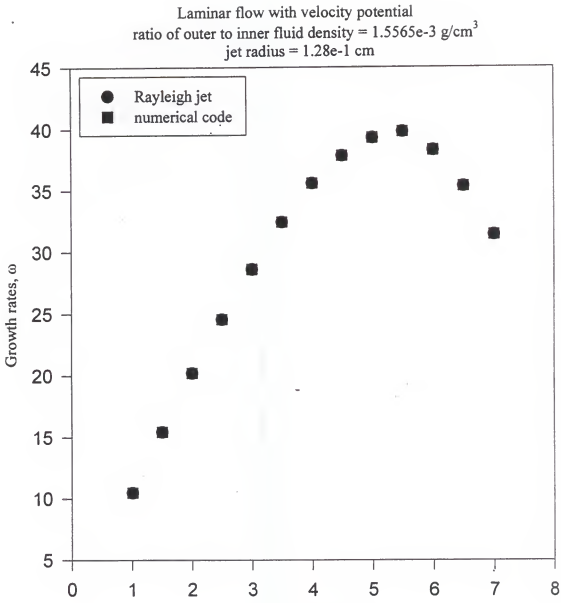

Figure 7. The effects of surface tension on Rayleigh jet

a light fluid, the inertial nature of the instability is apparent from the pressure distribution for $\rho_1 > \rho_2$. The heavy fluid encounters a pressure gradient inadequate for radial balance on penetrating the interface and the element of heavy fluid will continue its motion outward. This behavior is characteristic of Rayleigh-Taylor instabilities.

5.2.1 Axisymmetric Disturbances (m = 0)

The computed results using eq. (4.17) and eq. (4.18) are compared with the results presented in figure 8 of Reshotko and Monnin (1965)'s technical note. For m = 0, the growth rate seems to quadradically increase as axial wave number K increases. It is shown that the computational results match Reshotko and Monnin's results very well.

5.2.2 Non-axisymmetric disturbances (m ≠ 0)

Reshotko and Monnin's results in figure 9 are compared with this works solutions to eqs. (4.24) to (4.25) in figure 10. In figure 9, the growth rate at m = 1 seems to increase linearly as the axial wave number K increases. However, the growth rate for m =2 to m = 5 seems to be independent of K when K is equal to 1 or less than 1. The growth rate increases very slowly as m increases and K increases beyond K = 1. At large K, growth rate seems to converge into a specific value independent of m.

In figure 10, the computational results are shown. The growth rate at m =1 and K = 0 is slightly below Reshotko and Monnin's result while the growth rate for m = 2 to 5

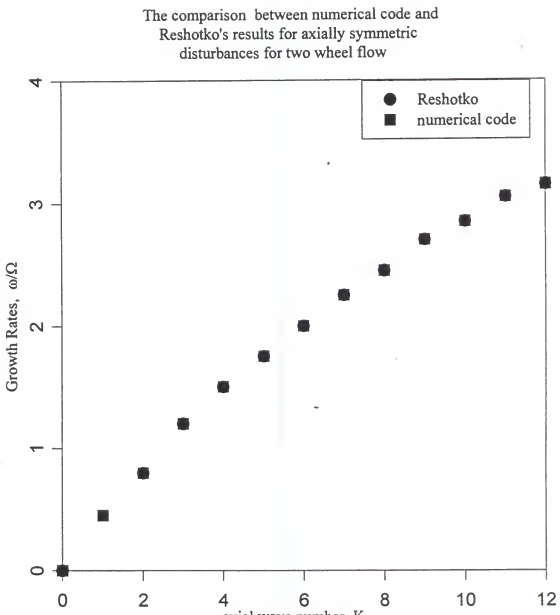

Figure 8. The growth rates on m = 0

case : two wheel flow

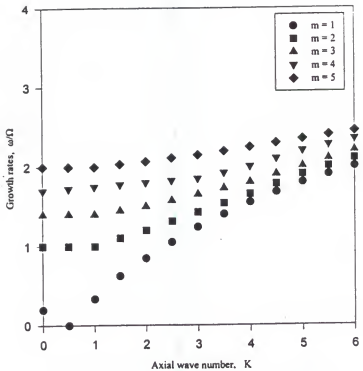

Figure 9. Reshotko's results on m variations

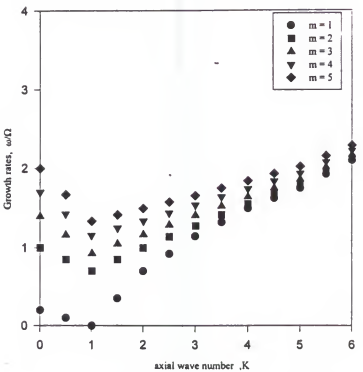

Figure 10. computational results on m variations

and K = 0 is similar to Reshotko and Monnin's results. As K increases, the growth rate decreases until K approaches 1. However, the growth rate increases as K increases over 1. There are some differences between the computation code and Reshotko and Monnin's results for K = 0 to K = 1. But, there are similar trends between the computation code and Reshotko and Monnin's results beyond K = 1. Theoretically, the growth rate is expected to increase as K increases.

For K = 0 to K = 1 in Reshotko and Monnin's results, the growth rate does not seem to be correct because the growth rate seems to be constant. On the other hand, the growth rate shown in figure 10 does not seem to be correct in the theoretical aspect because the growth rate decreases in that same region. In private communications with both Dr. Reshotko and Dr. Monnin, co-authors of Reshotko and Monnin's results, neither had a clear statement of how different results were obtained when their equations and those used in this dissertation are the same. The computer code of the series expression of Bessel fuction was testified to verify the validation of the asymptotic approach. However, the computational results are not produced enough to validate the asymptotic approach. Despite these differences at small K between Reshotko and Monnin's work and the present work, it will be assumed that the computer code is valid.

The extension of Reshotko and Monnin's work to include surface tension was derived in section 4.1.3 of this dissertation. The prediction of the effects of surface tension in Reshotko and Monnin's equations will be discussed in Chapter 6.

5.3 Fung's Equation for Azimuthally Periodic Perturbations (m ≠ 0 and k = 0) with No Surface Tension

Fung (1983) established the general dispersion equation for three rotating layers of fluids as following:

$$\frac{n_1(n_1-2)-\alpha_{21}\beta_{21}{}^2 n_2(n_2-2)+m(1-\alpha_{21}\beta_{21}{}^2)}{n_1(n_1-2)+\alpha_{21}\beta_{21}{}^2 n_2(n_2+2)+m(1-\alpha_{21}\beta_{21}{}^2)}\left(\frac{R_1}{R_2}\right)^{2m} -$$

$$\frac{n_2(n_2-2)+\alpha_{32}\beta_{32}{}^2 n_3(n_3+2)+m(1-\alpha_{32}\beta_{32}{}^2)}{n_2(n_2+2)-\alpha_{32}\beta_{32}{}^2 n_3(n_3+2)-m(1-\alpha_{32}\beta_{32}{}^2)}=0, \qquad (5.2)$$

where $n_s = m - \dfrac{\omega}{\Omega_s}$, $\alpha_{ts} = \dfrac{\rho_t}{\rho_s}$ and $\beta_{ts} = \left(\dfrac{\Omega_t}{\Omega_s}\right)^2$.

This can be compared with eq. (4.50) in section 4.2.2 which is derived with swirling flow. Equation (4.50) is exactly the same as eq. (5.2) which Fung (1983) obtained. Equation (4.50) is one of several solutions to be derived in this dissertation and is obtained by omitting both axial annular jet and surface tension. This validates the derivation of the equations used in current computer code. Therefore, it is assumed that it will valid when the current code will be extended to investigate the instability of the helical flow annular jet.

CHAPTER 6
RESULTS AND DISCUSSION

Although the surface tension was not included in Reshotko and Monnin's mathematical approach, the effect of surface tension has a significant effect on the degree of instability between interfaces of two different fluids. The computational results for the effect of surface tension will be discussed.

The main objective in this dissertation is to investigate the instability of an annular fuel sheet with axial and tangential velocity surrounded by the air with axial and tangential velocity.

The computed results for 4 cases will be discussed in the following order:

1. The effects of the surface tension using the extension of Reshotko and Monnin's equations
2. Annular fuel sheet with axial velocity and surrounding gas with axial velocity
3. Annular fuel sheet with tangential velocity and surrounding gas with tangential velocity
4 The annular sheet with axial and tangential velocity moving through the surrounding gas with axial and tangential velocity

6.1 The Effects of the Surface Tension Using the Extension of Reshotko and Monnin's Equations

The inner denser layer and outer layer rotate in a clockwise direction at the same speed. Equation (4.22) is being solved. Figure 11 shows that the growth rate first increases and later decreases with increasing axial wave number K. It is predicted as the surface tension in the inner layer gets higher, the growth rate increases at very smaller K and then decreases. This predicts that the disintegration of the inner layer fluid by aerodynamic forces is more difficult with higher surface tension. This can be explained from the relationship between the pressure difference, surface tension and curvature radius at the interface of different phases in eq. (3.2.20). The wave length is the inverse of the wave number. The radius of curvature is large when the wave length is large. When the curvature radius is large, the effect of the surface tension is relatively small. Therefore pressure difference predominantly depends on the centrifugal force of the inner core region is higher than that of the outer region. The instability grows at the interface. That phenomena leads to the increase of growth rate.

However, the effect of the surface tension is relatively large when the axial wave number is large and the curvature radius is small. Pressure distribution depends on the difference between the centrifugal force and surface tension force; therefore the degree of instability is balanced between the centrifugal force and surface tension force. The growth rates decrease and the disintegration of the inner layer fluid gets more difficult. Thus, the growth rate increases around the small wave number, later it decreases around the large wave number. Maximum growth rate is formed at a specific axial wave number

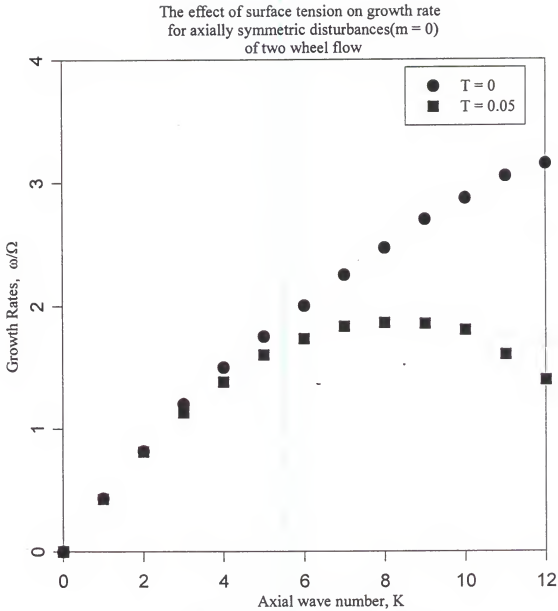

Figure 11. The effect of surface tension

as shown in figure 11. When the surface tension increases, the maximum growth is formed at smaller axial wave number since the growth rate increases until smaller axial number and decreases right after as axial wave number increases.

6.2 Axial Flow Annular Jet

The annular sheet was injected in the axial direction at a speed different from the surrounding gas. The principal cause of instability is due to the relative velocity between the sheet and the surrounding gas. The sheet interacts with the surrounding gas whereby rapidly growing waves are imposed on the sheet just after the nozzle from the atomizer exit of the gas turbine combustor. The velocity jump at both inner interface and outer interface of the annular fuel sheet for step-wise approximations of continuous functions yields the Kelvin-Helmholtz instabilities for even small wave lengths. This instability is due to the strong shearing rates existing in the sharp shear layer created at the vortex sheet. Instabilities produced by the Kelvin-Helmholtz effects due to the relative motion at interfaces are very strong and cause the fuel sheet to be severely unstable. Disintegration occurs when the wave amplitude reaches a critical value and fragments of annular fuel sheet are torn off. The fragments rapidly contract into drops under the action of surface tension. Equation (4.42) is solved for no surface tension, eq. (4.43) is solved for the effects of surface tension.

In figure 12, the effect of surface tension in the annular axial jet is shown. There is a significant effect of reducing growth rate at high values of surface tension.

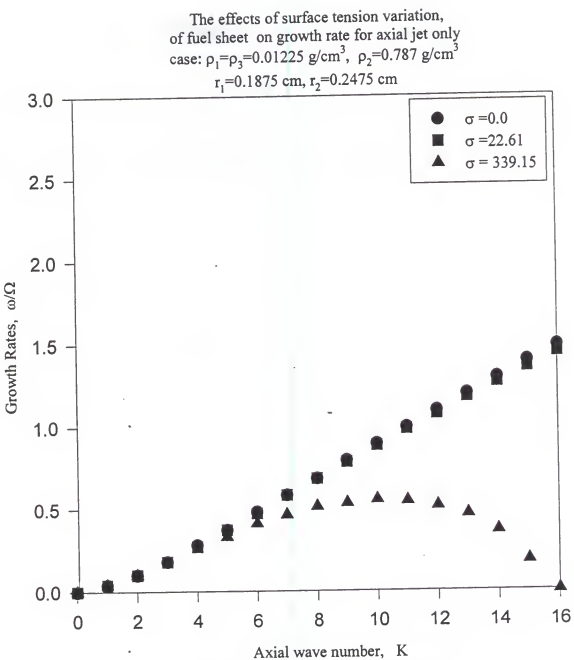

Figure 12. The effect of surface tension

Therefore, the growth rate first increases and decreases later as axial wave number K increases and involves much larger surface tension. When the typical value of surface tension is applied to the analysis of instability, the growth rate decreases little from the zero viscosity case.

In figure 13, the effect of fuel density change for the annular axial jet is shown. It is shown that the growth rate increases as the axial wave number increases at the typical value of surface tension and the growth rate decreases as the density of the annular axial jet increases. It tells that the mechanism of annular denser sheet disintegration should be affected to some extent by a change in annular fuel sheet density. It is predicted that it is harder for denser annular sheet moving in the axial direction to be broken up. For the annular fuel sheet of high density, more resistance and inertial effect to disintegration at the atomizing edge is expected to occur.

In figure 14, the effects of thickness variation for the annular axial jet is shown. It is shown that the growth rate decreases as the thickness of annular fuel sheet increases but the growth rate did not decrease any more beyond a certain thickness of the annular fuel sheet. This similar phenomena is described in J. Meyer and D. Weihs (1987). This result shows that there is a critical penetration thickness. It seems that the annular fuel jet behaves like a full liquid jet when the annular thickness is greater than the critical thickness of fuel sheet and the growth rate is independent of thickness. When the annulus thickness is less than the critical thickness, the jet behaves like a two-dimensional liquid sheet and the growth rate increases as the jet thickness decreases. Therefore, an annular

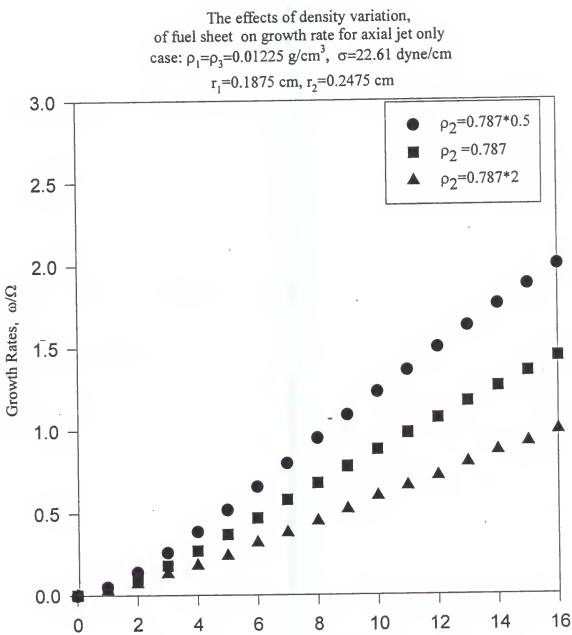

Figure 13. The effects of density variations

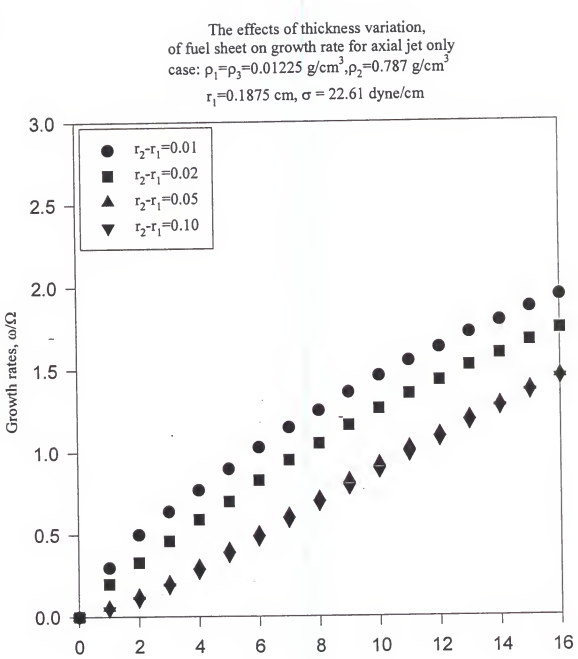

Figure 14. The effects of thickness variations

fuel sheet with a sufficiently small ring thickness is expected to disintegrate into drops much faster than a thicker fuel jet disintegrates into drops.

In figure 15, the effects of the axial velocity variation of the annular fuel sheet is shown. It is shown that the degree of instability is increased as the axial velocity of the annular fuel sheet is increased. That is, the growth rate is increased as the axial velocity of the annular fuel sheet is increased. It is expected that the higher the relative axial velocity between the annular fuel sheet and the surrounding gas is, the faster the aerodynamic forces cause the annular fuel sheet break into spherical shells with exponentially increasing amplitude.

In summary, faster breakup of the annular fuel sheet moving in the axial direction might be implemented by the decrease of density or decrease of thickness or increase of the axial velocity of the annular fuel sheet.

6.3 Rotating Flow Annular Jet

The flow which is now considered has centrifugal instability. This is analogous to the Rayleigh-Taylor instability under which Reshotko and Monnin's two wheel flow is classified. There is the annular fuel sheet exposed to the surrounding gas. The annular sheet is rotated with the angular velocity different from that of the surrounding gas. The flow regions consist of three layers which include an inner gas cylinder, an annular fuel sheet and an outer annular surrounding gas layer. However, the angular velocity in the outer annular gas layer is considered as almost zero because the distance from the center

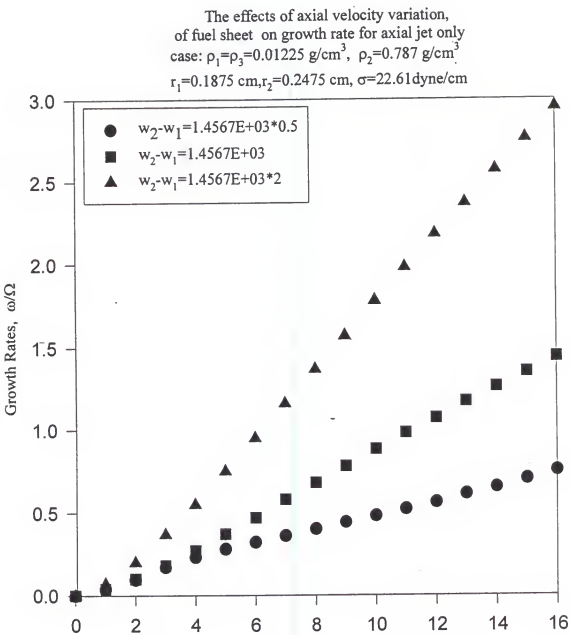

Figure 15. The effect of axial velocity variation

of the combustor to the outer layer radius and there is no angular velocity in most of the outer layer region. Eq. (4.48) for m = 0 and K ≠ 0, eq. (4.50) for m ≠ 0 and K = 0, eq. (4.52) for m ≠ 0 and K ≠ 0 are solved for no surface tension. Eq. (4.49) for m = 0 and K ≠ 0, eq. (4.51) for m ≠ 0 and K = 0, eq. (4.53) for m ≠ 0 and K ≠ 0 are solved for the effects of surface tension. Figure 16 and 17 show that surface tension does not affect the growth rate. That is, the swirling flow in annular fuel sheet in a rotating surrounding gas reacts like the inviscid flow without the surface tension. However, the effects of surface tension are small compared to the effect of the swirling flow in annular sheet. The effects of surface tension are significant in Reshotko and Monnin's two-wheel flow. However, the growth rate does not continually increase as the axial wave number increases, as in Reshotko's two wheel flows without surface tension, but begins to decrease regardless of surface tension. This result is worthy of notice. Regardless of whether surface tension exists or not, maximum growth rate at K = 0.6 is shown in figure 16 and 17. The maximum growth rate occurs at small axial wave number and high azimuthal wave number. Because of the limitation of the computational capability on CRAYC90, the azimuthal wave number beyond m = 20 could not be investigated. It seems that the growth rate increases as m increases in those figures. But, the difference of growth rate between m = 0 and m = 5 is larger than the difference of growth rate between m = 5 and m = 10. When the extrapolation beyond m = 20 at K = 0 is made based on the decreasing rate of the growth rate between m = 0 and m = 20, it is predicted from this trend that the growth rate at K = 0 may decrease around m = 60 as m increases even though the computation of that prediction is not available.

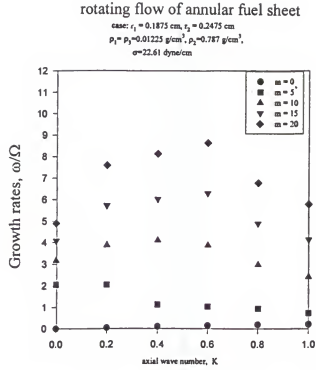

Figure 16. The effect of small surface tension

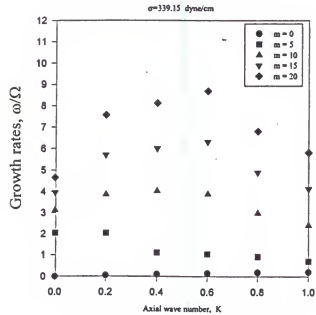

Figure 17. The effect of large surface tension

Notice the magnitude of growth rate when comparing the axial annular jet as shown in figure 12 and the rotating flow of figure 16. This tremendous increase in growth rate magnifies the impact of swirling flow of the annular fuel sheet on fuel atomization. In figure 18, the contour plot of growth rate is shown to make figure 16 and 17 more understandable. The phenomena that the tremendous maximum growth rate occurs at small K such as K = 0.6 shows that predominent instability due to centrifugal force effect has an immediate impact on the breakup of fuel sheet.

In figure 19, the effect of density increase in annular fuel sheet in the rotating surrounding gas is investigated. The maximum growth rate occurs at K = 0.2. The growth rate slowly decreases as K increases beyond K = 0.2. This shows that the effect of density increase exist to some extent over small K. However, the effect of density increase of the annular sheet causes the shift of axial wave number for the maximum growth rate to take place and the growth rate within small K to slowly change. The phenomena that the maximum growth rate occurs not at K = 0.6 but at K = 0.2 by density increase of the annular fuel sheet tells that the more severe breakup of the annular fuel sheet occurs at larger density of the annular sheet than at the typical density of annular fuel sheet. That prediction is expected in terms of pitch angle $\tan\theta = \frac{m}{rk}$. The inclined degree of θ shows the intensity ratio of swirling disturbance with respect to axial disturbance for maximum growth rate. The pitch angle is steeper when axial wave number k for maximum growth rate decreases. One noticeable point is that the

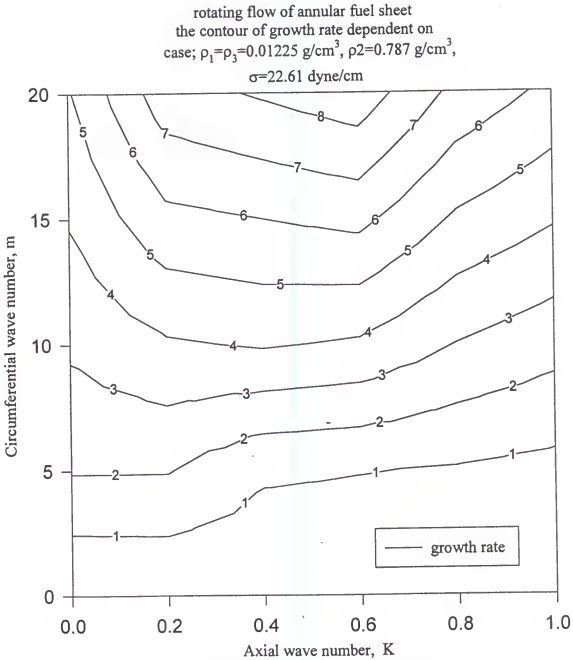

Figure 18. Typical model for small K

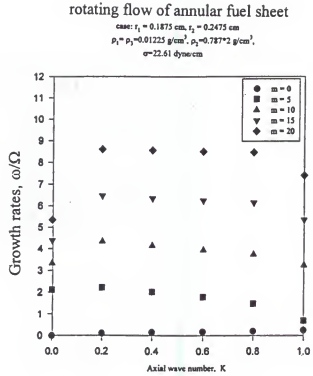

Figure 19. The effects of density increase

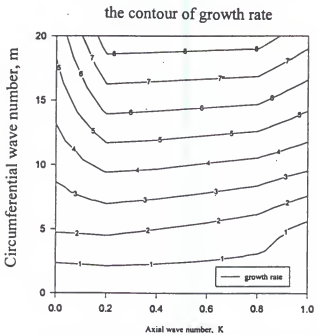

Figure 20. The effect of density increase

Magnitude of the maximum growth rate at K = 0.6 increases a little as the density of annular sheet increases and growth rates increase large at small K except K = 0.6.

The reason the maximum growth rate does not significantly increase, is hypothesized as a result of the cohesive nature of increased density counteracting the accelerating effect of density of annular fuel sheet in disintegration by centrifugal force. The phenomena of the density increase causing the growth rate to decrease has been shown and explained for the axial annular sheet jet in figure 13. Such a phenomena is thought to occur in the similar characteristic for even swirling flow of annular fuel sheet. In figure 20 compared to figure 18, the contour plot for the effect of density increase is shown to help elucidate this concept.

In figure 21, the effects of thickness decrease in annular fuel sheet is shown. The growth rate remarkably increases as the thickness decreases. In comparison with figure 16 of typical thickness, the growth rate increases substantially as the thickness decreases. A similar phenomena was shown for the axial annular jet in figure 14. Also, the maximum growth rate occurs at K = 0.2 as that occurs at K = 0.2 for the density increase of the annular fuel sheet. The pitch angle θ for thickness decrease is steeper than θ for the typical thickness. It is predicted that thinner fuel sheet disintegrates much faster into drops. This highlights the importance of presence of the thinner sheet for good atomization quality. The annular fuel sheet thickness may therefore be of crucial importance to the eventual drop sizes. The contour plot of the effects of thickness is shown in figure 22.

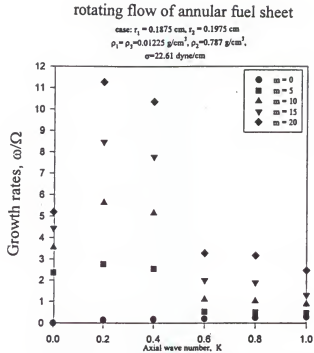

Figure 21. The effect of thickness decrease

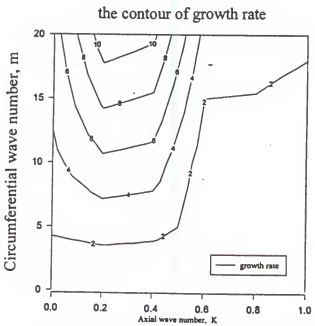

Figure 22. The effects of thickness decrease

In figure 23, the effect of angular velocity increase in annular fuel sheet is shown. the growth rate increases a little as the angular velocity increases in comparison with figure 16. When angular velocity increases in annular fuel sheet, the number of azimuthal mode(m) is increased. This phenomenon is shown in figure 137 of Van Dyke (1980)'s album of fluid motion. The increase of the number of azimuthal mode(m) cause the tangential wave number of figure 5 to increase. It promote the breakup of the annular sheet to many fine sizes. The reason the maximum growth rate does not significantly increase is an unknown priori. The contour plot of the effects of thickness is shown in figure 24.

For large axial wave numbers, the growth rates continually decrease as K increases beyond K = 1. In figure 25, the growth rate is shown for the typical model at large K. The growth rate at K = 0 and m = 20 or m = 15 are less than those at K = 1 and m = 20 or m = 15. On the other hand, the growth rates at K = 0 and m = 10 or m = 5 are larger than those at K = 1 and m = 10 or m = 5. The growth rates of m seem to converge as K increases. Therefore, the growth rates at m = 15 or m = 20 rapidly decrease to converge at K = 7 or larger K. In figure 26, the contour plot for the growth rates is shown for the typical model at large K. In figure 27, the growth rate at K = 1 for density increase is higher than the growth rate at K = 1 for the typical model shown in figure 25. Also, the growth rates regardless of m converge at K = 9 or larger. Therefore, the growth rate gradually decrease as K increases beyond K = 1 and approaches 9. The growth rate for density increase in figure 27 is higher than the growth rate for typical model in figure 25 as K approaches 9. In figure 28, the contour plot for the growth rate is shown for density

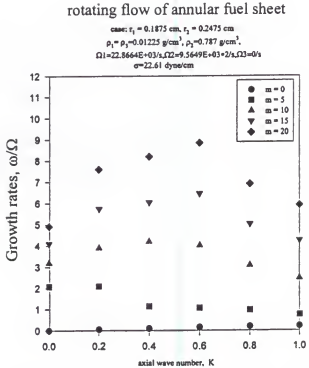

Figure 23. The effect of angular velocity increase

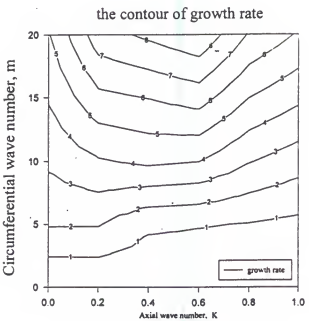

Figure 24. The effect of angular velocity increase

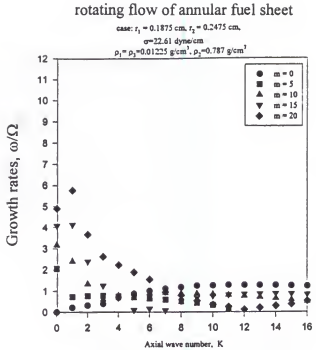

Figure 25. Typical model for large K

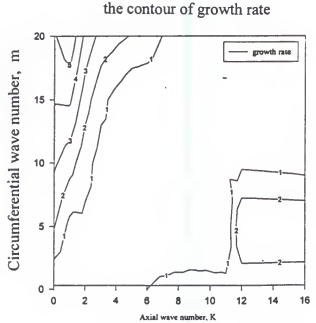

Figure 26. Typical model for large K

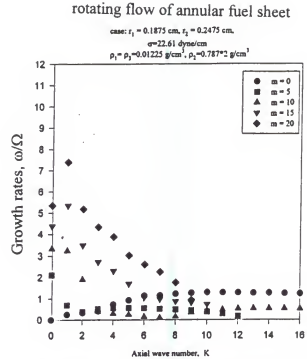

Figure 27. The effects of density increase

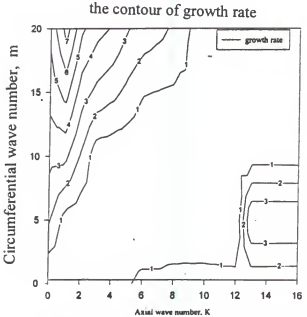

Figure 28. The effects of density increase

increase. In figure 29, the growth rate at K = 0 for thickness decrease is much higher than the growth rate at K = 1. This is due to the very steep decrease of the growth rate as K approaches 1 in figure 21. Also, the growth rates regardless of m converge at K = 2 or larger. Therefore, the growth rate rapidly decreases as K approaches 2. The growth rate for thickness decrease in figure 29 is lower than the growth rate of typical model in figure 25 as K approaches 2. In figure 30, the contour plot for the growth rate is shown. In figure 31, the growth rate is shown for the effect of angular velocity increase at large K. The growth rates at K = 0 and K = 1 are higher than the growth rate of typical model in figure 25. The growth rates of the rest of m seem to converge as K increases. In figure 26, the contour plot for the growth rate is shown.

6.4 Helical Flow Annular Jet

The investigation of the instability of the annular fuel sheet both moving in the axial direction and swirling in the circumferential direction in a rotating surrounding gas has been done. Equation (4.57) for $m = 0$ and $K \neq 0$, eq. (4.61) for $m \neq 0$ and $K = 0$, eq. (4.63) for $m \neq 0$ and $K \neq 0$ are solved for no surface tension. Equation (4.58) for $m = 0$ and $K \neq 0$, eq. (4.62) for $m \neq 0$ and $K = 0$, eq. (4.64) for $m \neq 0$ and $K \neq 0$ are solved for the effect of surface tension.

In figure 33, the growth rate of the typical model for small K is shown. It shows that there seems to be no difference between figure 16 for the typical model of swirling flow and figure 33. This tells that the degree of instability of the annular swirling sheet

rotating flow of annular fuel sheet

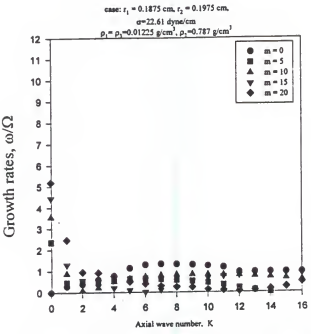

Figure 29. The effects of thickness decrease

the contour of growth rate

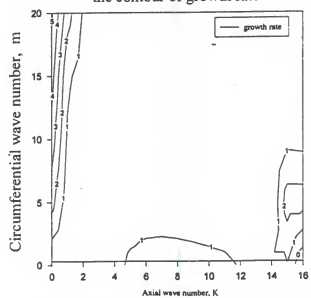

Figure 30. The effects of thickness decrease

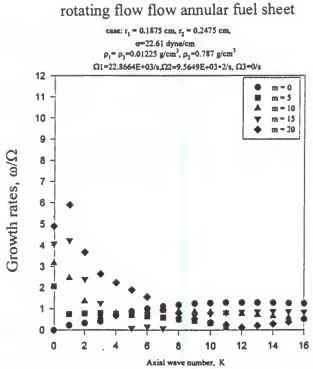

Figure 31. The effects of angular velocity increase for large K

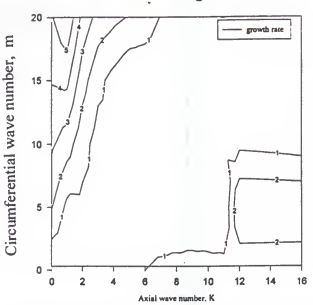

Figure 32. The effects of angular velocity for large K

in a rotating surrounding gas is almost the same as that of the instability of the combination of annular axial jet and annular swirling sheet in a rotating surrounding gas. In figure 34, the effects of density increase are shown. In figure 35, the effect of thickness decrease is shown. In figure 36, the effect of angular velocity increase is shown. Comparing figure 34 with figure 19 and figure 35 with figure 21 and figure 23 with figure 36, it is shown that there is no difference between the instability of annular swirling fuel sheet and the instability of the combination of annular fuel sheet moving axially and swirling circumferentially in a rotating environment. In addition, even the increase of axial velocity increase for the combination of the annular sheet axially moving and swirling circumferentially does not affect the growth rate as shown in figure 37. For the annular axial jet , there is increase of growth rate in figure 15 when the axial velocity in the annular axial sheet increases. However, this phenomena is not shown at all in the combination of annular fuel sheet axially moving and swirling circumferentially in a rotating surrounding gas.

Finally, it can be said that the swirling motion of annular fuel sheet in the rotating gas encroaches upon relative effects of annular sheet moving in the axial direction. It causes strong centrifugal instability to take place. Therefore, strong centrifugal instability contributes to much faster breakup into drops from the annular fuel sheet as soon as the annular fuel sheet is exposed to the rotating surrounding gas in gas turbine combustor.

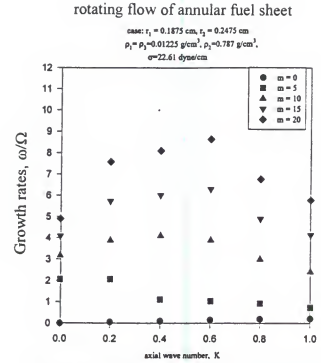

Figure 16. The effect of small surface tension

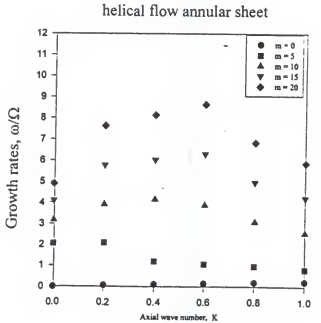

Figure 33. Typical model for small K

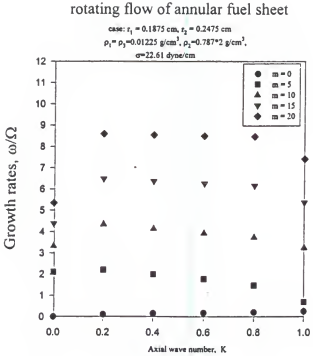

Figure 19. The effects of density increase

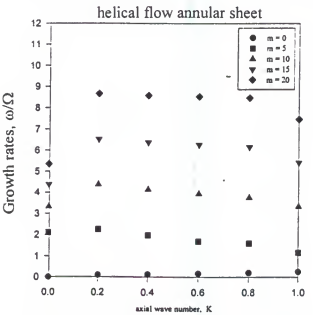

Figure 34. The effects of density increase

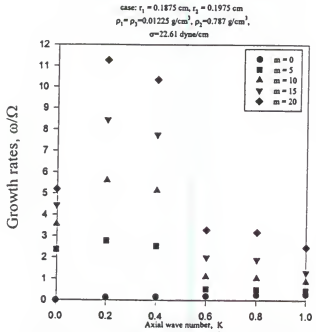

Figure 21. The effect of thickness decrease

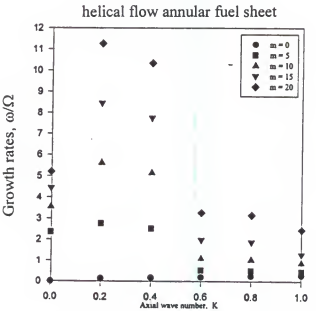

Figure 35. The effect of thickness decrease

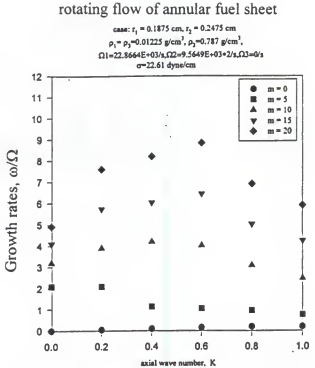

Figure 23. The effect of angular velocity increase

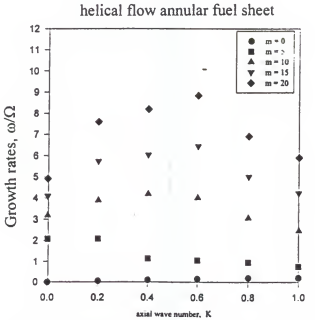

Figure 36. The effect of angular velocity increase

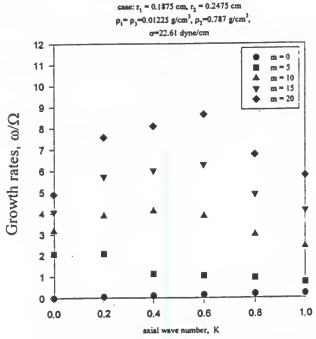

Figure 33. Typical model for small K

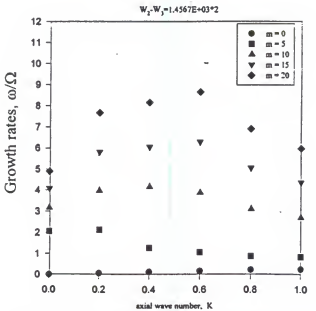

Figure 37. The effects of axial velocity increase

CHAPTER 7
CONCLUSION

Due to the increasing application of airblast atomizers in modern gas turbine engines, all the variables which may have some effect on the process of atomization should be investigated. So far very little has been done mathematically concerning the mechanism of disintegration of annular fuel sheet exposed to the rotating surrounding gas in gas turbine combustor.

The degree of disintegration of annular fuel sheet is due in part to the intensity of the instability of the annular fuel. This process of disintegration is completed just after the nozzle tip as shown in the experiment photographs. The variables which effect the instability growth rate are surface tension, density, fuel sheet thickness, axial velocity and tangential velocity.

7.1 Axial Flow Annular Jet

1. The instability growth rate decreases at a much larger value of surface tension than is typical of liquid fuel.
2. The growth rate decreases as the density increases.
3. The growth rate increases as the fuel sheet thickness decreases.

4. The growth rate increases as the axial velocity increases.

7.2 Rotating Flow Annular Jet

1. The role of surface tension is insignificant. The growth rate for rotating flow annular jet is much higher than that for axial flow annular jet.
2. The role of density increase is to increase the centrifugal effects by the increase of the centrifugal force of the annular fuel sheet. Also, increased density provides more resistance to disintegration of the annular fuel sheet. Therefore, the growth rate does not increase much but does increase as the density increases.
3. The growth rate increases as the fuel sheet thickness decreases.
4. The growth rate is slightly higher as the angular velocity increases. The reason the growth rate does not greatly increase, is not known.

7.3 Helical Flow Annular Jet

Items 1, 2, 3, and 4 in section 7.2 also apply. The instability growth rate showed no difference between rotating flow annular jet and helical flow annular jet. The axial velocity increase does not change of the growth rate. The growth rate for helical flow annular jet is much larger at small wave numbers than that of the axial flow annular jet. Also, the growth rate for the helical sheet increases with angular wave number while the

growth rate for the helical sheet increases only at very small axial wave numbers and then decreases. These results seem to be enough to explain the phenomena of sudden fuel sheet breakup just after the nozzle tip.

The swirling effect of annular fuel sheet in rotating environment has one of the greatest impacts on strong helical breakup of annular fuel sheet in gas turbine combustor. The effect of an annular fuel sheet thickness decrease and angular velocity increase are relatively strong in comparison with other effects. They are the best candidates to be used in the design of atomizers.

In future, better asymptotic expressions of Bessel functions in the dispersion equation are required to obtain accurately computational results after solving the dispersion equation. Mathematical formulation including nonlinear higher order terms is desirable to research for a more physical approach to actual breakup phenomena. Also, instability analysis considering viscosity is desirable to research for the other types of atomizers in which viscosity effect may be important.

APPENDIX
COMPUTATIONAL SOLUTION METHODOLOGY

The dispersion equations derived in Chapter 4 are the two types of

$$F(\omega, \frac{H'(iKq)}{H(iKq)}, \frac{J'(iKq)}{J(iKq)}, \frac{\rho_2}{\rho_1}) = 0 \text{ or}$$

$$F(\omega, Kq\frac{I'(Kq)}{I(Kq)}, Kq\frac{K'(Kq)}{K(Kq)}, \frac{\rho_2}{\rho_1}, \frac{\Omega_2}{\Omega_1}, \frac{\rho_3}{\rho_2}, \frac{\Omega_3}{\Omega_2}) = 0.$$

These equations are very difficult solve directly on a supercomputer since they include Bessel functions and the complex arguments are in Bessel functions. It is possible to get the asymptotic solutions for these types of equations by changing the dispersion equation into asymptotic expression. When the absolute magnitudes of the arguments in Bessel functions are toward either 0 or infinity, the asymptotic expressions are available.

When $Kq \to 0$, $\frac{J_m'(iKq)}{J_m(Kq)} = m + \ldots.$, $\frac{H_m'(iKq)}{H_m(Kq)} = -m + \ldots$,

$$Kq\frac{I_m'(Kq)}{I_m(Kq)} = m + \ldots, \text{ and } Kq\frac{K'_m(Kq)}{K_m(Kq)} = -m + \ldots.$$

When $Kq \to \infty$ and $m = 0$, $i\frac{J_0(iKq)}{J_1(Kq)} = 1 + \frac{1}{2Kq}\ldots,$

$$-i\frac{J_0(iKq)}{J_1(Kq)} = 1 - \frac{1}{2Kq}\ldots,$$

$$Kq\frac{I_0'(Kq)}{I_0(Kq)} = 1 - \frac{1}{2Kq}\ldots, \text{ and } Kq\frac{K_0'(Kq)}{K_0(Kq)} = -1 - \frac{1}{2Kq}\ldots.$$

When $Kq \to \infty$ and $m \neq 0$, $\frac{J_m'(iKq)}{J_m(Kq)} = Kq(1 - \frac{1}{2Kq} + \ldots)$,

$$\frac{H_m'(iKq)}{H_m(Kq)} = -Kq(1 + \frac{1}{2Kq} + \ldots) ,$$

$$Kq\frac{I_m'(Kq)}{I_m(Kq)} = Kq + \ldots,$$

and $$Kq\frac{K'_m(Kq)}{K_m(Kq)} = -Kq + \ldots.$$

When the above asymptotic forms are substituted into the dispersion equations in Chapter 4, the dispersion equations are solvable. The disadvantage of this asymptotic approach seems that the asymptotic form does not depend on K when $Kq \to 0$. Therefore, the asymptotic solution independent on K is obtained when $Kq \to 0$. The asymptotic solution dependent on K is only obtained when $Kq \to \infty$. For this reason, the asymptotic solution for $Kq \to 0$ is regarded as the asymptotic solution at $K = 0$. Also, the asymptotic solution for $Kq \to \infty$ is regarded as the asymptotic solution at $K \neq 0$.

The Flowchart for the computer code to validate the asymptotic approach in comparision with Reshotko and Monnin's results is as follows:

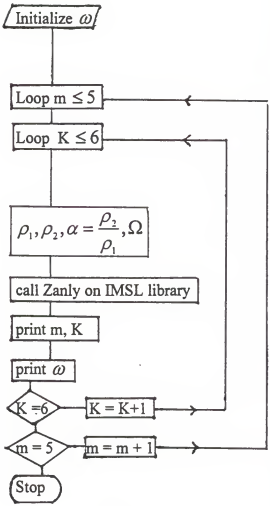

Subroutine Zanly

$$n = \frac{\omega}{\Omega} - m$$

if K = 0

$$\left(\frac{1}{\alpha} - 1\right)\left(m - \frac{2m}{n}\right)\left(m + \frac{2m}{n}\right) + (n^2 - 4)\left[\frac{1}{\alpha}\left(m + \frac{2m}{n}\right) + \left(m - \frac{2m}{n}\right)\right] = 0$$

if K > 0

$$\left(n^2-4\right)-\left[\ -\frac{qK}{(1+\alpha)}(1-\alpha)+\left(\frac{1-\alpha}{1+\alpha}\right)^2\left(\frac{1}{2}+\frac{2m}{n}\right)+\right.$$
$$\left(\frac{1-\alpha}{1+\alpha}\right)\frac{1}{qK}\left[\frac{1}{4}+\frac{2m}{n}+\left(\frac{2m}{n}\right)^2+\frac{1}{128}(32m^4-8m^2+18)\right]-$$
$$\left.\left(\frac{1}{qK}\right)^2\left(\frac{1-\alpha}{1+\alpha}\right)^2\left(\frac{1}{2}+\frac{2m}{n}\right)\left[\frac{1}{64}(32m^4-8m^2+18)+\frac{1}{4}+\frac{2m}{n}+\left(\frac{2m}{n}\right)^2\right]\ \right]=0$$

The Flowchart for the rotating flow annular jet is shown to investigate the instability growth rate as follows:

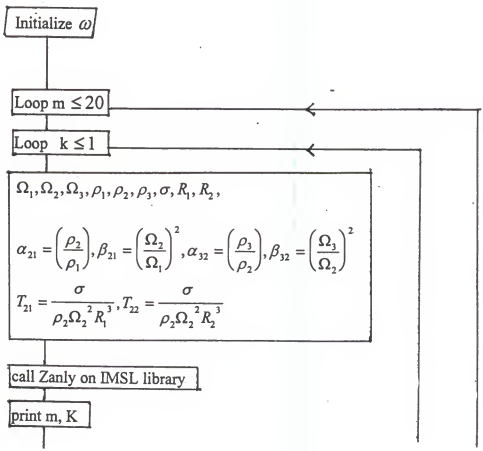

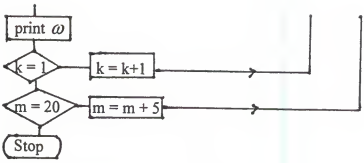

Subroutine Zanly

$$n_1 = \frac{N_1}{\Omega_1} = \frac{m\Omega_1 - \omega}{\Omega_1}$$

$$n_2 = \frac{N_2}{\Omega_2} = \frac{m\Omega_2 - \omega}{\Omega_2}$$

$$n_3 = \frac{N_3}{\Omega_3} = \frac{m\Omega_3 - \omega}{\Omega_3}$$

$$q_1 = \frac{\sqrt{n_1^2 - 4}}{n_1}$$

$$q_2 = \frac{\sqrt{n_2^2 - 4}}{n_2}$$

$$q_3 = \frac{\sqrt{n_3^2 - 4}}{n_3}$$

if k = 0

$$\alpha_{21}\beta_{21}^2\alpha_{32}\beta_{32}^2(m+\frac{2m}{n_1})(-m+\frac{2m}{n_2})[n_2^2 - 4 + (m+\frac{2m}{n_2})\{1.+T_{21}(1-m^2)\}]$$

$$(n_3^2 - 4 - m + \frac{2m}{n_3})\left(\frac{R_1}{R_2}\right)^{2m}$$

$$-\alpha_{21}\beta_{21}{}^{2}\alpha_{32}\beta_{32}{}^{2}(m+\frac{2m}{n_1})(m+\frac{2m}{n_2})[n_2{}^{2}-4+(-m+\frac{2m}{n_2})\{1.+T_{21}(1-m^2)\}]$$

$$(n_3{}^{2}-4-m+\frac{2m}{n_3})$$

$$-\alpha_{21}\beta_{21}{}^{2}(m+\frac{2m}{n_1})(-m+\frac{2m}{n_3})[n_2{}^{2}-4+(m+\frac{2m}{n_2})\{1.+T_{21}(1-m^2)\}]$$

$$[n_2{}^{2}-4+(-m+\frac{2m}{n_2})\{1.+T_{22}(1-m^2)\}]\left(\frac{R_1}{R_2}\right)^{2m}$$

$$\alpha_{21}\beta_{21}{}^{2}(m+\frac{2m}{n_1})(-m+\frac{2m}{n_3})[n_2{}^{2}-4+(m+\frac{2m}{n_2})\{1.+T_{22}(1-m^2)\}]$$

$$[n_2{}^{2}-4+(-m+\frac{2m}{n_2})\{1.+T_{21}(1-m^2)\}]$$

$$-\alpha_{32}\beta_{32}{}^{2}(m+\frac{2m}{n_2})(-m+\frac{2m}{n_2})(n_1{}^{2}-4+m+\frac{2m}{n_1})$$

$$(n_3{}^{2}-4-m+\frac{2m}{n_3})\left(\frac{R_1}{R_2}\right)^{2m}$$

$$\alpha_{32}\beta_{32}{}^{2}(m+\frac{2m}{n_2})(-m+\frac{2m}{n_2})(n_1{}^{2}-4+m+\frac{2m}{n_1})$$

$$(n_3{}^{2}-4-m+\frac{2m}{n_3})$$

$$(m+\frac{2m}{n_2})(-m+\frac{2m}{n_3})(n_1{}^{2}-4+m+\frac{2m}{n_1})$$

$$[n_2{}^{2}-4+(-m+\frac{2m}{n_2})\{1.+T_{22}(1-m^2)\}]\left(\frac{R_1}{R_2}\right)^{2m}$$

$$-(-m+\frac{2m}{n_2})(-m+\frac{2m}{n_3})(n_1{}^{2}-4+m+\frac{2m}{n_1})$$

$$[n_2{}^{2}-4+(m+\frac{2m}{n_2})\{1.+T_{22}(1-m^2)\}]=0$$

if k > 0

$$\alpha_{21}\beta_{21}{}^{2}\alpha_{32}\beta_{32}{}^{2}\exp^{(q_2K_1-q_1K_2)}(q_1K_1+\frac{2m}{n_1})(-q_2K_2+\frac{2m}{n_2})(n_3{}^{2}-4-q_3K_2+\frac{2m}{n_3})$$

$$[n_2{}^{2}-4+(q_2K_1+\frac{2m}{n_2})\{1+T_{21}(1-m^{2}-K_1{}^{2})\}]$$

$$-\alpha_{21}\beta_{21}{}^{2}\alpha_{32}\beta_{32}{}^{2}\exp^{(q_2K_2-q_1K_1)}(q_1K_1+\frac{2m}{n_1})(q_2K_2+\frac{2m}{n_2})(n_3{}^{2}-4-q_3K_2+\frac{2m}{n_3})$$

$$[n_2{}^{2}-4+(-q_2K_1+\frac{2m}{n_2})\{1+T_{21}(1-m^{2}-K_1{}^{2})\}]$$

$$-\alpha_{21}\beta_{21}{}^{2}\exp^{(q_1K_1-q_2K_2)}(q_1K_1+\frac{2m}{n_1})(-q_3K_2+\frac{2m}{n_3})[n_2{}^{2}-4+(q_2K_1+\frac{2m}{n_2})$$

$$\{1+T_{21}(1-m^{2}-K_1{}^{2})\}[n_2{}^{2}-4+(-q_2K_2+\frac{2m}{n_2})\{1+T_{22}(1-m^{2}-K_2{}^{2})\}]$$

$$\alpha_{21}\beta_{21}{}^{2}\exp^{(q_1K_2-q_2K_1)}(q_1K_1+\frac{2m}{n_1})(-q_3K_2+\frac{2m}{n_3})[n_2{}^{2}-4+(q_2K_2+\frac{2m}{n_2})$$

$$\{1+T_{22}(1-m^{2}-K_2{}^{2})\}][n_2{}^{2}-4+(-q_2K_1+\frac{2m}{n_2})\{1+T_{21}(1-m^{2}-K_1{}^{2})\}]$$

$$-\alpha_{32}\beta_{32}{}^{2}\exp^{(q_2K_1-q_1K_2)}(q_2K_1+\frac{2m}{n_2})(-q_2K_2+\frac{2m}{n_2})(n_1{}^{2}-4+q_1K_1+\frac{2m}{n_1})$$

$$(n_3{}^{2}-4-q_3K_2+\frac{2m}{n_3})$$

$$+\alpha_{32}\beta_{32}{}^{2}\exp^{(q_2K_1-q_1K_2)}(q_2K_2+\frac{2m}{n_2})(-q_2K_1+\frac{2m}{n_2})(n_1{}^{2}-4+q_1K_1+\frac{2m}{n_1})$$

$$(n_3{}^{2}-4-q_3K_2+\frac{2m}{n_3})$$

$$+\exp^{(q_2K_1-q_1K_2)}(q_2K_1+\frac{2m}{n_2})(-q_3K_2+\frac{2m}{n_3})(n_1{}^{2}-4+q_1K_1+\frac{2m}{n_1})$$

$$[n_2{}^{2}-4+(-q_2K_2+\frac{2m}{n_2})\{1+T_{22}(1-m^{2}-K_2{}^{2})\}]$$

$$-\exp^{(q_2K_2-q_1K_1)}(-q_2K_1+\frac{2m}{n_2})(-q_3K_2+\frac{2m}{n_3})(n_1{}^{2}-4+q_1K_1+\frac{2m}{n_1})$$

$$[n_2{}^{2}-4+(q_2K_2+\frac{2m}{n_2})\{1+T_{22}(1-m^{2}-K_2{}^{2})\}]=0$$

REFERENCE LIST

Aigner, M. and Wittig, S. (1987) "Swirl and counterswirl effects in prefilming airblast atomizers," 87-GT-204.

Batchelor, G. K. (1963) "Analysis of the stability of the axisymmetric jets," J. of Fluid Mech., Vol. 14, pp. 529-551.

Castleman, R. A. (1931) "The mechanism of atomization of liquids," Bureau of Standards Journal of Research, Vol. 6, No. 281, pp. 369-376.

Chuech, S. G. and Singhal, A. K. (1991) "Numerical modeling for primary atomization of liquid jets," AIAA Journal of Propulsion and Power, Vol. 7, No. 6, pp. 879-886.

Dombrowski, N. and Johns, W. R. (1963) "The aerodynamic instability and disintegration of viscous liquid sheets," Chem. Eng. Sci., Vol. 18, pp. 203-214.

Fung, Y. T., and Kurzweg, U. H. (1975) "Stability of swirling flows with radius-dependent density," J. Fluid Mech., Vol. 72, pp. 243-255.

Fung, Y. T. (1974) "Stability of heterogeneous swirling flows," Ph.D Dissertation, University of Florida.

Fung, Y. T. (1983) "Non-axisymmetric instability of a rotating layer of fluid," J. Fluid Mech. Vol. 127, p. 83.

Giffen, E., and Muraszew, A. (1953) "The atomization of liquid fuels," Chapman & Hall Ltd., London.

Hanratty, T. J. (1983) "Interfacial instabilities caused by airflow over a thin liquid layer," Proceedings of a Symposium Conducted by the Mathematics Research Center, the University of Wisconsin-Madison, pp. 221-259.

Holroyd, H. B. (1933) "On the atomization of liquid jets," J. Franklin Inst., Vol. 215, p. 93.

Kurzweg, U. H. (1970) "Helical modes of instability in swirling flow between concentric cylinders," J. of Appl. Math. Phys., Vol. 21, pp. 260-265.

Lefebvre, A. H. (1972) "Effects of fuel injection method on gas turbine combustor emissions," Proceedings of the Symposium on Emissions from Continuous Combustion Systems, General Motors Research Laboratory, Warren, Michigan, pp. 255-278.

Lefebvre, A. H. (1992) "Energy considerations in twin-fluid atomization," ASME Journal of Engineering for Gas Turbines and Power, Vol. 114, pp. 89-96.

Lin, S. P. and Kang, D. J. (1987) "Atomization of a liquid jet," Phys. Fluids 30, pp. 2000-2006.

Lin, S. P. and Zhou, Z. W (1992) "Effects of compressibility on the atomization of liquid jets," AIAA Journal of Propulsion and Power, Vol. 8, No. 4, pp. 736-740.

McDonell, V. G. and Samuelsen, G. S. (1990) "Gas and drop behavior in reacting and non-reacting airblast atomizer sprays," AIAA Journal of Propulsion and Power Vol. 7, No. 5, pp. 684-691.

Meyer, M. and Weihs, D. (1987) "Capillary instability of an annular liquid jet, " J. Fluid Mech. Vol. 179, p. 531.

Ranz, W. E. (1956) "On sprays and spraying," Dept. Engng. Res. Penn State University Bulletin 65.

Rayleigh, L. (1879) "On the instability of jets," London Mathematical Society Proc.Vol. 10, p. 4.

Reitz, R. D. (1987) "Modeling atomization processes in high pressure vaporizing sprays," Atomization and Spray Technology 3, pp. 303-337.

Reshotko, Eli and Monnin, C. F. 1965) "Stability of two-fluid wheel flows," NASA-TN D-2696, Lewis Research Center, Cleveland, Ohio.

Rizk, N. K. (1977) "Studies on liquid sheet disintegration in airblast atomizers," Ph.D Dissertation, Cranfield Institute of Technology, England.

Rizk, N. K. and Mongia, H. C. (1991) "Low NO_x rich-lean combustion concept application," AIAA-91-1962.

Rupe, J. H. (1962) "On the dynamic charateristics of free-liquid jets and a partial correlation with orifice geometry," J. P. L., Tech. Report, No. 32, p. 207.

Samuelsen, G. S. and Stapper, B. E. (1992) "Internal flow effects in prefilming airblast atomizers," ASME Journal of Engineering for Gas Turbines and Power, Vol. 114, pp. 39-45.

Sattelmayer, T. and Wittig, S. "Internal flow effects in prefilming airblast atomizers: Mechanisms of atomization and droplet spectra," ASME Journal of Engineering for Gas Turbines and Power, Vol. 108, pp. 465-472.

Schweitzer, P. H. (1937) " Mechanism of disintegration of liquid jets," J. Appl. Physics, Vol. 8, pp. 193-202.

Shkadov, V. Ya (1970) "Wave formation on the surface of a viscous liquid due to tangential stress," Fluid Dynamics, Vol. 5, p. 473.

Taylor, G. I. (1940) "Generation of ripples by wind blowing over a viscous fluid," Collected Works of G. I. Taylor, Vol. 3, pp. 244-254.

Van Dyke, M. (1980) "An album of fluid motion," The Parabolic Press, Stanford, CA.

BIOGRAPHICAL SKETCH

Insoo Cho was born November 29, 1958, in Seoul, Korea. He received his high school diploma in 1977. In March, 1977, he enrolled in the Mechanical Engineering Department of HanYang University (HYU), Seoul, Korea, and received his bachelor's degree in 1981. Then he worked for the military army and some companies in Korea for a few years. In May, 1985, he enrolled in the Mechanical Engineering Department, Florida Institute of Technology in Melbourne, Florida.

In May, 1989, he received his master's degree in the Mechanical Engineering Department, Florida Institute of Technology. Then he enrolled in the Aerospace Engineering Department , University of Florida. in August, 1989. Two years later, he moved to the Mechanical Engineering Department at the same university.

I certify that I have read this study and that in my opinion it conforms to acceptable standards of scholarly presentation and is fully adequate, in scope and quality, as a dissertation for the degree of Doctor of Philosophy.

E. C. Hansen

E. C. Hansen, Chairman
Assistant Professor of
Mechanical Engineering

I certify that I have read this study and that in my opinion it conforms to acceptable standards of scholarly presentation and is fully adequate, in scope and quality, as a dissertation for the degree of Doctor of Philosophy.

A. E. S. Green

A. E. S. Green
Graduate Research Professor
of Mechanical Engineering

I certify that I have read this study and that in my opinion it conforms to acceptable standards of scholarly presentation and is fully adequate, in scope and quality, as a dissertation for the degree of Doctor of Philosophy.

W. E. Lear

W. E. Lear
Assistant Professor of
Mechanical Engineering

I certify that I have read this study and that in my opinion it conforms to acceptable standards of scholarly presentation and is fully adequate, in scope and quality, as a dissertation for the degree of Doctor of Philosophy.

U. H. Kurzweg

U. H. Kurzweg
Professor of Aerospace Engineering,
Mechanics and Engineering
Science

I certify that I have read this study and that in my opinion it conforms to acceptable standards of scholarly presentation and is fully adequate, in scope and quality, as a dissertation for the degree of Doctor of Philosophy.

J. D. Abbitt
Assistant Professor of Aerospace Engineering, Mechanics and Engineering Science

This dissertation was submitted to the Graduate Faculty of the College of Engineering and to the Graudate School, and was accepted as partial fulfillment of the requirements for the degree of Doctor of Philosophy.

May, 1996

Winfred M. Phillips
Dean, College of Engineering

Karen A. Holbrook
Dean, Graduate School